INFORMATION TO USERS

This manuscript has been reproduced from the microfilm master. UMI films the text directly from the original or copy submitted. Thus, some thesis and dissertation copies are in typewriter face, while others may be from any type of computer printer.

The quality of this reproduction is dependent upon the quality of the copy submitted. Broken or indistinct print, colored or poor quality illustrations and photographs, print bleedthrough, substandard margins, and improper alignment can adversely affect reproduction.

In the unlikely event that the author did not send UMI a complete manuscript and there are missing pages, these will be noted. Also, if unauthorized copyright material had to be removed, a note will indicate the deletion.

Oversize materials (e.g., maps, drawings, charts) are reproduced by sectioning the original, beginning at the upper left-hand corner and continuing from left to right in equal sections with small overlaps.

Photographs included in the original manuscript have been reproduced xerographically in this copy. Higher quality 6" x 9" black and white photographic prints are available for any photographs or illustrations appearing in this copy for an additional charge. Contact UMI directly to order.

ProQuest Information and Learning
300 North Zeeb Road, Ann Arbor, MI 48106-1346 USA
800-521-0600

Supramolecular Architecture:

"Formation and Characterization of Multi-Porphyrin Arrays."

by

Fotis Nifiatis

A dissertation submitted to the Graduate Faculty in Chemistry in partial fulfillment of the requirements for the degree of Doctor of Philosophy, The City University of New York

2001

Bell & Howell Information and Learning Company
300 North Zeeb Road
P.O. Box 1346
Ann Arbor, MI 48106-1346

This manuscript has been read and accepted for the Graduate Faculty in Chemistry in satisfaction of the dissertation requirement for the degree of Doctor of Philosophy.

4-27-01
Date

Chair of Examining Committee

4-27-01
Date

Executive Officer

C.M. Drain

L. Francesconi

K. Grohmann

A. Couzis
Supervisory Committee

THE CITY UNIVERSITY OF NEW YORK

Abstract

Supramolecular Architecture

"Formation and Characterization of Multi-Porphyrin Arrays."

by

Fotis Nifiatis

Adviser: Professor C.M. Drain

The beauty of micro- and nanoscopic words relies on the marriage of chemistry and symmetry. Our contribution to nanoscopic materials has been the formation of multiporphyrin square arrays and tapes by both coordination chemistry and H-bonding.

Meso pyridyl porphyrins and *cis*-Pt(II) or *trans*-Pd(II) complexes have been utilized for the formation of the metal mediated square arrays and tapes. Linear tapes were formed by interaction of 180° coordinating dipyridyl porphyrin and the terminal monopyridyl porphyrin to *trans*-Pd(II) complex. The more rigid planar tapes were derived from a solution of 90° coordinating (L-shaped) dipyridyl porphyrin and the X-shaped tetrapyridyl porphyrin upon addition of the *cis*-Pt(II) complex. The more complicated square array was derived from the stoichiometrically "correct" mixture of X, T, and L-coordinating (tetrapyridyl, tripyridyl and *cis*-dipyridyl) porphyrins upon the addition of the *trans*-Pd(II) complex. The last array consists of 9 porphyrins and 12 Pd atoms that come together to form a 5x5 nm^2 array.

Similar square and tapes were the desired supramolecular structures for our hydrogen-bonded multiporphyrins arrays. The shape and organization was directed by hydrogen bonding between the 3,5-diacetoamido-4'-pyridyl and 1-butyluracyl patterns at the *meso* positions of the porphyrins.

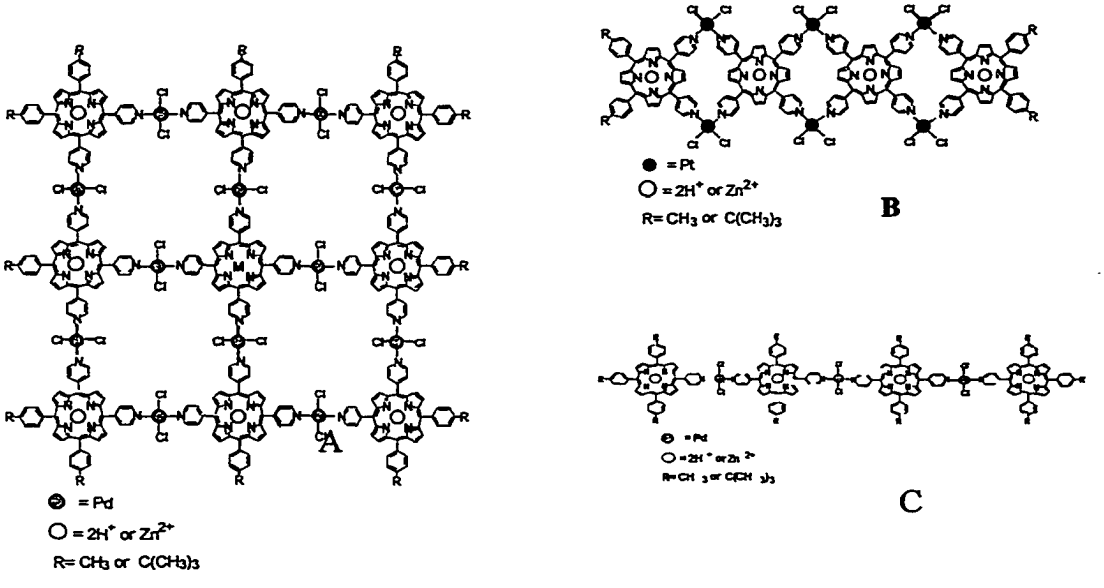

Supramolecular materials self-assembled by metal coordination to exocyclic pyridyl ligands to form:
A. *planar squares with Pd*
B. *planar tapes with Pt*
C. *linear tapes with Pd*

Dedicated
to the memory of my father and
to my mother.

Acknowledgment

I would like to thank the people who have made it possible for me to reach this stage of my life. First and foremost, Professor Charles Michael Drain for being such a wonderful advisor. I have learned a great deal thanks to his knowledge and kind guidance. I am amazed by his energy and enthusiasm towards chemistry...thanks a lot, boss!!!

The Drain group members, past and present, deserve my heart-felt gratitude. They have been invaluable to me during my years at Hunter. I will always remember Xianchang Gong (with or without his goggles), Xinxu Shi, Tatjana Milic, Dr. Isabelle Sylvain, and Xin Chen (even though she hasn't had health insurance for Mimi all these years, but I still love her). I would like to thank them for their discussions about chemistry, their suggestions on my experiments and their emotional support at difficult moments. I would like to thank all the undergraduate students that passed through our lab, Vanessa, Suhel, Vinita, Anna, Margaretta, as well as so many other summer students, for creating a loving and pleasant working environment. I would like to thank the undergraduates Alexander Vasenko, Vinita Tiwari, and Suhel Ahmed for their work in my project.

I am very grateful to Dr. Clifford Soll for his help with mass spec and to Dr. Michael Blumenstein for his help and answers to questions about NMR. Also, I would like thank Dr. Alexander Couzis and Dr. James Batteas for their help on the ellipsometry and AFM experiments.

On a personal note, it would never be too late to acknowledge the support and affection of my family. Without their generous sacrifices I could not have come to this country and you would not be holding this thesis in your hands.

Table of Contents

List of Tables

Table of Figures

Chapter 3: Formation and Characterization of Multiporphyrin Arrays.

Chapter 4: Photophysical Properties of Multiporphyrin Arrays

Appendix

Abbreviations

$OEPH_2$	2,3,7,8,12,13,17,18octaethyl porphyrin
$TPPH_2$	5,10,15,20tetraphenyl porphyrin
$TPCH_2$	5,10,15,20tetraphenyl chlorin
$TPyPH_2$	5,10,15,20tetrakis(4-pyridyl) porphyrin
$T(tbuPh)PH_2$	5,10,15,20tetrakis(4-*tert*-butylphenyl) porphyrin
$5Py10,15,20(tbuPh)PH_2$	5mono(4- pyridyl)10,15,20tris(4-*tert*-butylphenyl) porphyrin
$5,10Py15,20(tbuPh)PH_2$	5,10bis(4- pyridyl)15,20bis(4-*tert*-butylphenyl) porphyrin
5,10Py15,20(tbuPh)PZn	5,10bis(4- pyridyl)15,20bis(4-*tert*-butylphenyl) porphyrinato Zinc
$5,15Py10,20(tbuPh)PH_2$	5,15bis(4- pyridyl)10,20bis(4-*tert*-butylphenyl) porphyrin
5,10,15Py20(tbuPh)PH2	5,10,15tris(4- pyridyl)20mono(4-*tert*-butylphenyl) porphyrin
$5U10,15,20(tbuPh)PH_2$	5mono(1'-butyl-6'-uracyl)10,15,20tris(4-*tert*-butylphenyl) porphyrin
5U10,15,20(tbuPh)PZn	5mono(1'-butyl-6'-uracyl)10,15,20tris(4-*tert*-butylphenyl) porphyrinato Zinc
$5,10U15,20(tbuPh)PH_2$	5,10bis(1'-butyl-6'-uracyl)15,20bis(4-*tert*-butylphenyl) porphyrin
5,10U15,20(tbuPh)PZn	5,10bis(1'-butyl-6'-uracyl)15,20bis(4-*tert*-butylphenyl) porphyrinato Zinc
$5AA10,15,20(tbuPh)PH_2$	5mono(3,5-di(acetamido)-4-pyridyl)10,15,20tris(4-*tert*-butylphenyl) porphyrin
5AA10,15,20(tbuPh)PZn	5mono(3,5-di(acetamido)-4-pyridyl)10,15,20tris(4-*tert*-butylphenyl) porphyrinato Zinc
$5,10AA15,20(tbuPh)PH_2$	5,10bis(3,5-di(acetamido)-4-pyridyl)15,20bis(4-*tert*-butylphenyl) porphyrin

5,10AA15,20(tbuPh)PZn	5,10bis(3,5-di(acetamido)-4-pyridyl)15,20bis(4-*tert*-butylphenyl) porphyrinato Zinc
Bpy	Bipyridine
M	Metal
PDT	Photodynamic Therapy
ET	Energy Transfer
eT	electron Transfer
CR	Charge Recombination
IC	Internal Conversion
ISC	Inter-System Crossing

CHAPTER 1

INTRODUCTION

Chemistry has been the bridge between the simple and the complex, between the laws of physics and the rules of life, between the basic and the applied. Since 1828, the synthesis of urea by Friedrich Wöhler,[1.1] molecular chemistry has developed a vast number of sophisticated and powerful methods for the construction of complex molecular structures by using covalent bonds to control the connection of atoms.

Fairly we can say that molecular chemistry has established its power over the covalent bond. The time has come to do the same with non-covalent intermolecular forces. This is the object and the goal of supramolecular chemistry, to go beyond the molecular chemistry, and gain understanding and control over the intermolecular bonds.[1.2] Supramolecular chemistry is concerned with the next step in complexity beyond the molecule - towards the supermolecule – expressed as organized polymolecular systems held together by non-covalent interactions. The non-covalent interactions define the action or organization of the molecular individuals, and detect the stability of the association the ability to recognize other subunits, and the dynamics of the system[1.2].

Because of the varied nature of intermolecular forces, it involves organic chemistry and the synthetic methods for the formation of molecules, coordination chemistry and metal ion-ligand complexes, physical chemistry and the experimental and theoretical studies of interactions, biochemistry and the biological processes that start with substrate binding and recognition, and material science including the mechanical properties of solids. Its roots reach back to Paul Ehrinch who recognized that molecules do not act if they do not bind,[1.3] to Emil Fisher (1894) who presented the "lock and key" image implying

complementarity,[1.4] of a receptor to its ligand (the basis of molecular recognition), and to Alfred Werner (1893) who recognized that selective fixation requires interaction or affinity between partners,[1.5] (coordination chemistry). In modern times, synthetic supramolecular chemistry is represented by the selective binding of alkali metal cations to natural and synthetic ligands,[1.6] to crown ethers,[1.7] and to cryptands.[1.8]

Supramolecular species have well defined structural, conformational, thermodynamic, kinetic, and dynamic properties. Although, the interactions between molecules are determined by their electronic properties, we nominally classify these intermolecular forces as: metal ion coordination, electrostatic forces, hydrogen bonding, Van der Waals interactions, etc. For the most part, the weak character of the intermolecular forces, compared to covalent bonds, makes supramolecular species thermodynamically less stable, kinetically more labile, and dynamically more flexible than covalent molecules. It can be said that supramolecular chemistry represents a "soft chemistry" introducing new terms that can better describe classes of compounds and types of properties.

Recognition, information, and complementarity are significant components of supramolecular chemistry. Molecular recognition is expressed by the energy and information involved in binding and selection of substrates by a given receptor. Mere binding is not recognition. Recognition is binding with a purpose and it is defined by a set of structurally well-defined intermolecular interactions showing geometrical and interactional complementarity.[1.2]

Information is stored in the architecture of both the receptor, and the ligand. The architecture of the receptor can be described by its size, shape, conformation, chirality, etc. The binding sites of the receptor are also characterized by electronic properties, like charge, polarity, Van der Waals forces, and etc. The ligand is complementary in shape, size, and electronics. In addition, the medium plays a very important role in the stability and selectivity of supramolecular species, which results from a balance between solvation (of both ligand and acceptor) and complexation (inherent molecular solvation of the acceptor by the ligand). The read out of the information is the rate of formation and dissociation of the supermolecule.[1,2] In short, supramolecular chemistry is a chemical information science were the information is stored in the molecules while the reading and the process of information is through the structural and interactional features of the molecules in the supermolecules.[1,2] A vast variety of receptors have been designed for recognition of different types of substrates, different in size, shape, charge, nature, and etc.[1,2]

Molecular devices are structurally organized and functionally integrated chemical systems built into supramolecular architectures.[1,9] The function of the device may be due to a molecular component(s) or to the ensemble. One may speak of photonic, electronic, or ionic devices depending on whether its components are photoactive, electroactive, or ionoactive.[1,9]

The theoretical basis of the supramolecular photonics is that the formation of supramolecular species can change the photophysical properties of the individual

components. The formation of the supramolecular entity may change the ground and/or the excited state properties of the individual components. Several processes can be observed in supramolecular systems like: excitation energy migration, photoinduced charge separation by electron or energy transfer, photo regulations of the binding sites perturbation of optical transitions, etc. Photophysical and photochemical changes of supramolecular species can take place only if the correct selective binding of the complementary components takes place, and results in the correct molecular geometry.

Supramolecular photonic devices require high organization of their components to provide photosignals through energy transfer (ET) or electron transfer (eT). Luminescent species (fig. 1.1) absorb and emit light at different wavelengths. The minimum requirement for an ET/eT system is that there is a donor (D) and an acceptor (A). Light absorption also may cause intra- or intermolecular electron transfer resulting electron-hole separation (fig. 1.2). The system may also contain a photosensitizer (PS), in addition to the donor (D), and acceptor (A). Absorption of light by the photosensitizer can lead to an electron transfer from the donor (D) to the electron acceptor (A), if the redox properties of the photosensitizer (PS) at the ground and excited state are suitable, to yield the separated charges D^{+}-PS-A^{-} (fig. 1.2). Organic and inorganic compounds, with large polarizabilities, can have remarkable non-linear properties that first depend on molecular

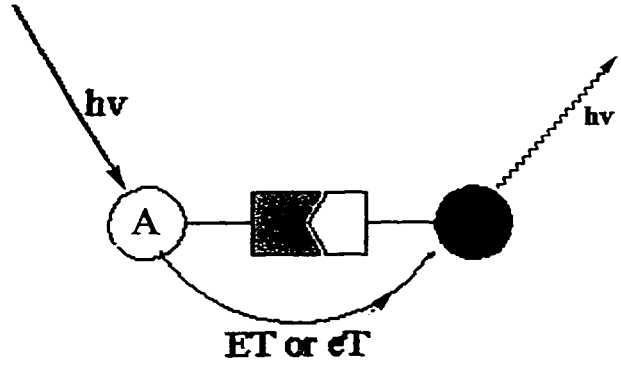

Figure 1.1 *Luminescent photoactive devices.*

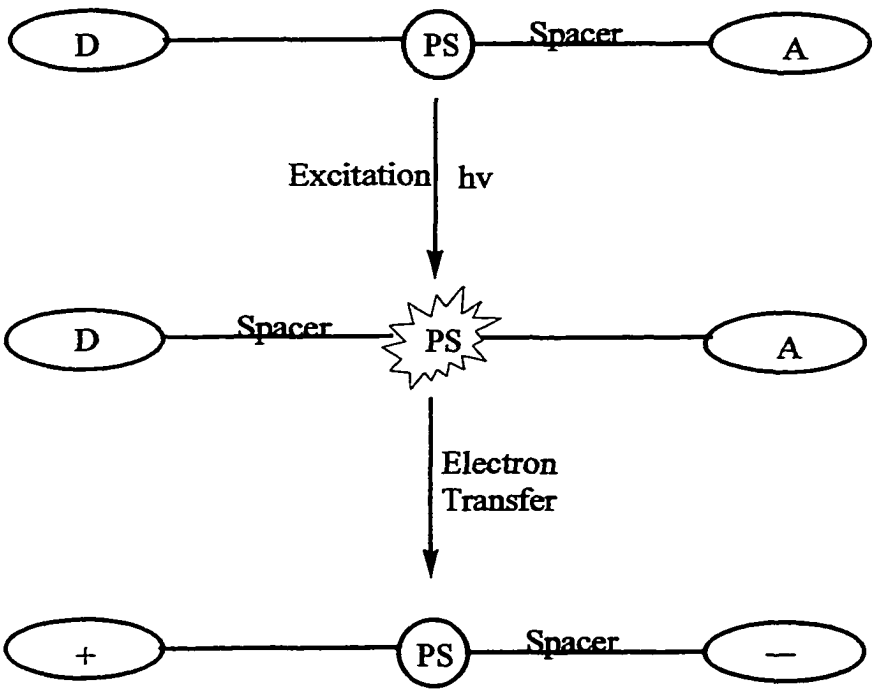

Figure 1.2 *Photoinduced electron transfer in photoactive devices.*

features,[1.10] but materials from these molecules are highly dependent on the supramolecular geometry,[1.11] *i.e.*, the non-linear optical properties of a material are defined by those of its components and their arrangement in the material, *e.g.*, D-PS-A systems, because of their ability to produce charged separated species can exhibit non-linear optical properties.[1.11]

Porphyrins and metallo-porphyrins have broad applications as field-responsive materials, particularly for optoelectronic applications.[1.12] The porphyrin ligands can be used in order to introduce desirable properties to the molecule and the material. Porphyrins and metalloporphyrins can interact with applied electric and magnetic fields as well as with chemical species.[1.13] They have greater thermal stability, compared to typical organic

chromophores,[1.14] and their extended π-conjugated macrocyclic ring gives high NLO effects.[1.15] Their field- and chemo-sensitivity make them very popular as sensors.[1.13]

CHAPTER 2

INDIVIDUAL PORPHYRINS

2.1 Introduction

Porphyrins and metallo-porphyrins have received a lot of attention over the last decades. Great motivation for their studies arises from their importance in biological systems,[2.1] their use as industrial pigments,[2.2] as solid state devices,[2.3] as solar energy transducers,[2.4] as photo- and electro-chemical catalysts,[2.5] and as dye laser materials.[2.6] Studies on the photophysical properties of the porphyrins started as early as in 1834 after emission from chlorophyll was observed.[2.7] Since then a large number of synthetic and naturally occurring porphyrins have been extensively studied. Model systems give us the control over the porphyrin composition so structural, electronic and vibrational properties can be tuned to serve our needs.[2.7]

The basic porphyrin unit is shown in figure 2.1.A the electronic "heart" of the free-base porphyrin is a 18-membered ring with 18 π-electrons. This porphyrin ring is responsible for the characteristic optical spectra of the porphyrin which is "perturbed" to a greater or lesser extent by various chemical modifications of the basic structure at any of the peripheral positions by functional groups.[2.7] The dianionic porphyrin macromocycle can coordinate a central metal ion or two protons to give metallo- or free-base porphyrin, respectively (fig. 2.1 B and C). The porphyrins have characteristic optical spectra with a very strong π-π^* transition around 400nm (Soret band) and usually four other bands, in the visible region two Q-bands if it is metalated.

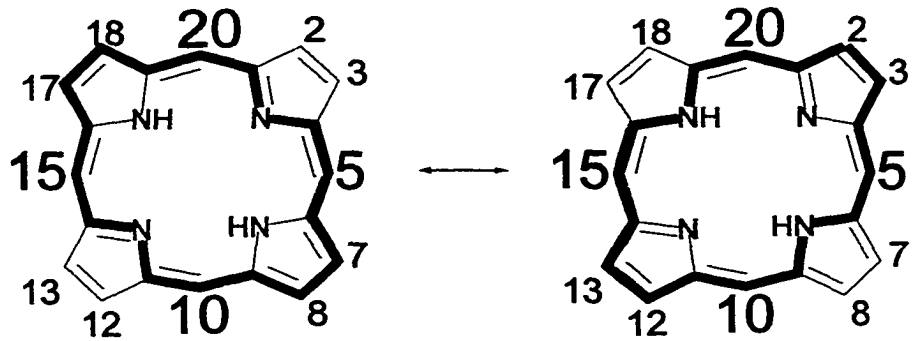

A

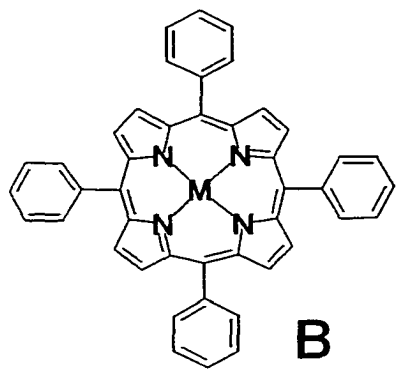

B

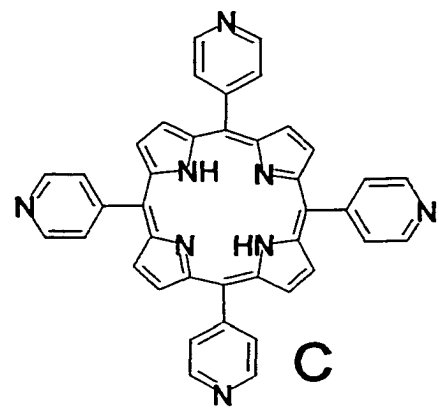

C

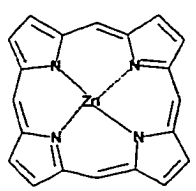

D. Porphyrin

Q(1,0) at 585nm

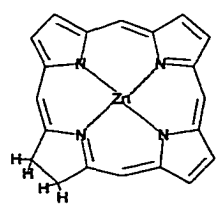

E. Chlorin

Q(1,0) at 610nm

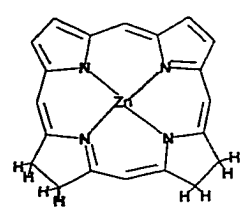

F. Isobacteriochlorin

Q(1,0) at 602nm

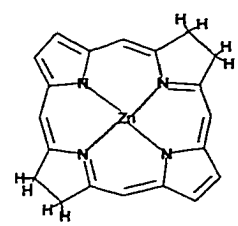

G. Bacteriochlorin

Q(1,0) at 755nm

Figure 2.1

A. 18-Annulene ring (free-base porphyrin).
B. General structure of a metallo- TPP (M=metal).
C. $TPyPH_2$ (tetrapyridyl porphyrin) free-base porphyrin.
D. Zinc Porphyrin.[2,8]
E. Zinc Chlorin.[2,8]
F. Zinc Isobacteriochlorin.[2,8]
G. Zinc Bacteriochlorin.[2,8]

As can be seem from figure 2.1.A that not all the peripheral double bonds in the pyrrolic rings are required to maintained aromaticity. Reduction of one or two of these peripheral double bonds gives chlorins or bacteriochlorins respectively (fig. 2.1 E, F and G). Proceeding from porphyrin to metallo-porphyrin (D), to reduced metallo-porphyrins (D, E and G) the change in symmetry and energetics results a red shift (bathochemical shift) of the optical spectra, the porphyrins have higher extinction coefficients (ε).[2.7, 2.9] Nature uses these optical properties of the reduced porphyrins to harvest solar energy for photosynthesis by using both chlorophylls and bacteriochlorophylls as both antenna and reaction-center pigments.[2.10] The long wavelength absorption of these natural occurring chromophores may make them useful as photosensitizers in photodynamic therapy (PDT).[2.11]

2.2 Porphyrin Synthesis

Both symmetrical and unsymmetrical 5,10,15,20-tetra(kis)arylporphyrins can be synthesized conveniently from pyrroles and aromatic aldehydes in "one-" or "two-" step reactions. The one-stage reaction involves mixing the suitable aldehydes in refluxing media under oxidizing conditions.[2.12] Frequently, the porphyrin percipitates out of the reaction mixture, making isolation easy. The two-step, reaction involves condensation of the pyrrole with the aldehydes at low temperature, until a maximum yield of porphyrinogen is obtained, and then the mixture is oxidized with an oxidation agent such as 2,3-dichloro-5,6-dicyanobenzoquinone (DDQ).[2.13] As with most experimental procedures for these compounds, the isolated yields are lower than those determined spectroscopically by UV-Vis. analysis. The best reaction conditions and work up vary from porphyrin to porphyrin depending on the substituents on the porphyrin macrocycle, and there is no best method for all porphyrins. Many reported yields are based on estimates from UV-Vis spectroscopy and the reaction mixture. Although the extinction coefficient of the Soret band varies from porphyrin to porphyrin. Further complications in these spectroscopic estimates of yields are due to the absorption of chlorins, and other isomers that have some absorption in the Soret region. Even if the reduced porphyrins are in small amounts in the reaction mixture, their contribution to the Soret band can be important since they have eight to fifteen times higher extinction coefficient (ε) than that of the fully oxidized porphyrins.[2.13]

In 1939, Rothemund, synthesized aromatic and aliphatic porphyrins by mixing pyrrole with the aromatic aldehydes in pyridine at 200°C under anaerobic conditions.[2.14] The yield was about 5%. The resulting porphyrin was contaminated with a significant amount of chlorin. Later Calvin[2.15] was able to oxidize tetraphenylchlorin (TPC) to the corresponding porphyrin ($TPPH_2$) and to reduce $TPPH_2$ to $TPCH_2$. Adler[2.12] showed that the porphyrin yield is greater than that obtained by the Rothemund synthesis when the reaction was carried in acidic media, by using acetic acid or propionic acid, and was open to the air. The Adler method gives 10-20% yield. MacDonald[2.16] formed porphyrins by coupling of the dipyrroles in 10-20% yield. The Lindsey method[2.13] involves anaerobic condensation to form a porphyrinogen followed by oxidation to the porphyrin (yield 10-60%). The method does not require high temperatures and that makes it suitable for unstable aldehydes. Recently Drain[2.17] formed porphyrins in a solventless (yield 7-23%). The advantage of the last method is the easy purification of the product.

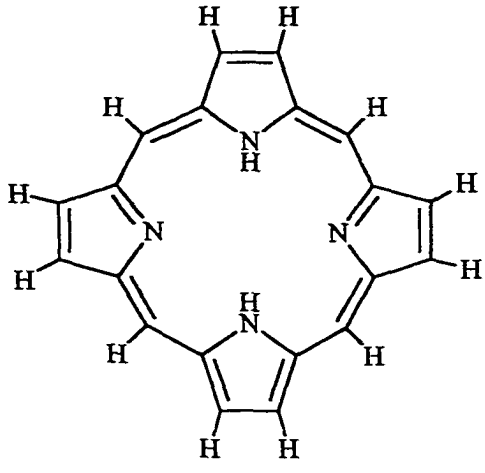

Figure 2.2 *Porphin. (parent compound)*

The most difficult porphyrin to be prepared is the parent compound, porphin fig. 2.2. Models show that alkyl or aryl groups substitution, at the 3- or 4- position on the pyrrole starting material, indroduces beneficial steric effect. The β-pyrrole substitution favors cyclization since the induced steric effect forces the growing polypyrryl chain to coil with the N-atoms towards the center.[2.18] Additionally, since the β-position is blocked,

aldehyde-pyrrole condensation takes place at the a-pyrrole position that leads to the desired product. *Meso* substitution has beneficial effect on the porphyrin formation as well since the substituent inhibits sterically condensation of the β-pyrrole position.[2.18]

For use in the metal mediated assemblies, we formed two series of porphyrins according to Adler's method starting from the commercially available benzaldehydes and pyrrole. Pyrrole was passed over a basic alumina column before addition to the reaction flask.

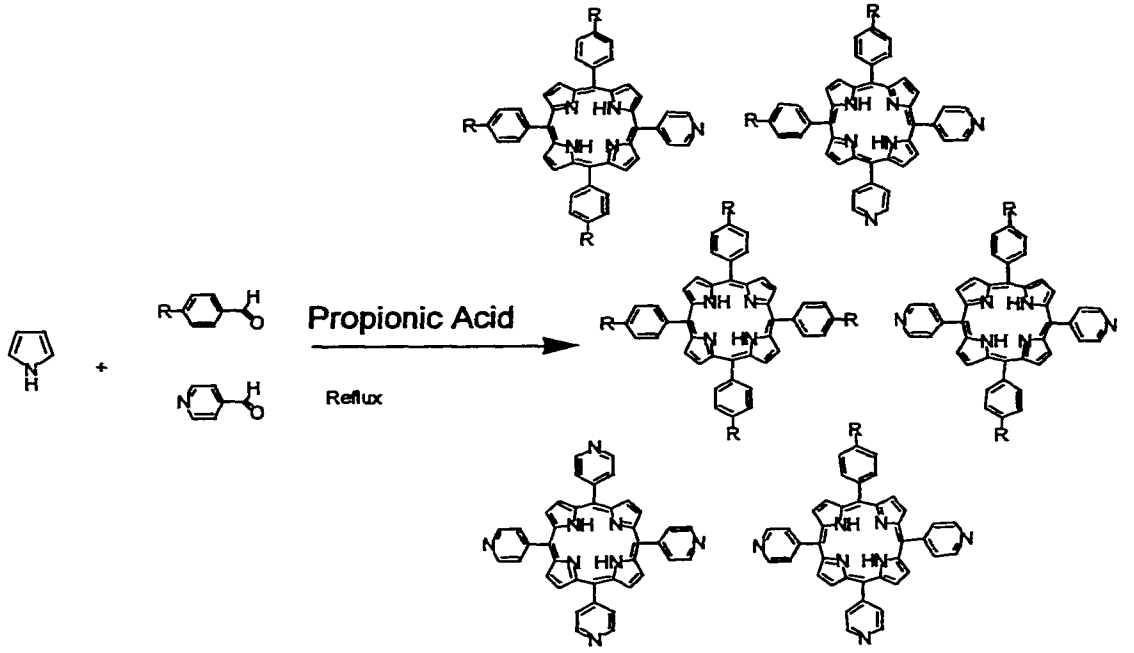

Figure 2.3 *Porphyrin synthesis. (Adler's method)*

The synthetic scheme is shown in figure 2.3. The statistical mixture of porphyrins was separated by column chromatography of increasing polarity. Flash silica gel was used as the stationary phase while the column was eluted with a toluene-dioxane gradient.

2.3 Characterization

The (4-pyridyl)$_{x=1\ to\ 4}$ (4-*tert*-butylphenyl)$_{y=4-x}$ porphyrins were characterized by ^{1}H-NMR, ^{13}C-NMR and ESI-MS.

2.3.1 ^{1}H-NMR

A major problem with earlier ^{1}H-NMR studies was that a high concentration of porphyrin was required in order good spectra to be obtained. At high concentrations the porphyrins aggregate making the NMR spectra less accurate. Modern NMR instruments have much higher sensitivity making possible to obtain a ^{1}H-NMR at concentrations between 10-1000 μM were aggregation effects can be less important. Although, porphyrin chemical shifts should be considered less accurate than these of other organic compound.[2.19] In order to increase sensitivity a larger pulse angle and/or a shorter relaxation delay can be used by taking advantages of the short T_1 times (0.25-1.0 sec)[2.20] of the porphyrins with respect to the other organic molecules.

The proton chemical shifts in porphyrins are highly dependent on the distance and orientation from the delocalized π-electrons of the porphyrin ring. Protons above or inside the porphyrin ring are in the shielded region of the ring current effect and they are upfield shifted (high energy region) in the spectra. Protons at the porphyrin periphery are in the deshielded area and they are down field shifted (low energy region) in the spectra. The ^{1}H-NMR is utilized to characterize the individual porphyrins as well as porphyrin

assemblies and aggregates. Intermolecular and intramolecular interactions, such as axial coordination of metallo-porphyrins, aggregation, and hydrogen bonding can also be monitored by ^{1}H-NMR.

In the case of differentially substituted porphyrins the pattern of resonances, combined with TLC data, can be used to unambiguously assign the structures. In the following discussion, a pyrrole proton refers to a proton bonded to the β-pyrrole carbon and the proton associated with the pyrrole nitrogen will be referred as a pyrrole N-H or internal proton. Figures 2.4 and 2.5 summarize the assignments of the ^{1}H-NMR spectra while from B1 through B5 are the actual spectra of all the (4-pyridyl)$_{x=1\ to\ 4}$ (4-*tert*-butylphenyl)$_{y=4-x}$ porphyrins.

All substituents at the *meso* position have characteristic chemical shifts: tbuPh gives two doublets at about 7.6 and 8.2ppm (J_{H-H}=8.1Hz) and one singlet at about 1.48 and 1.63ppm (tbu protons); Py gives two doublets at about 8.0 and 9.1. The ^{1}H-NMR spectrum of a 4-pyridyl ring is strictly an AA'BB' type which is usually too complex to be analyzed for J values.[2.21] However the spectra of tbuPh appears as AB type with significant coupling between only the 2 and 3 and the 5 and 6 protons.

The assignments of the coupled signals for the *meso* substituents are achieved simply by comparisons with related spectra. For instance, a comparison of the spectrum of the T(tbuPh)PH_2 **(1)** to that of 5Py(tbuPh)PH_2 **(2)** shows that porphyrin **2** has a new set of

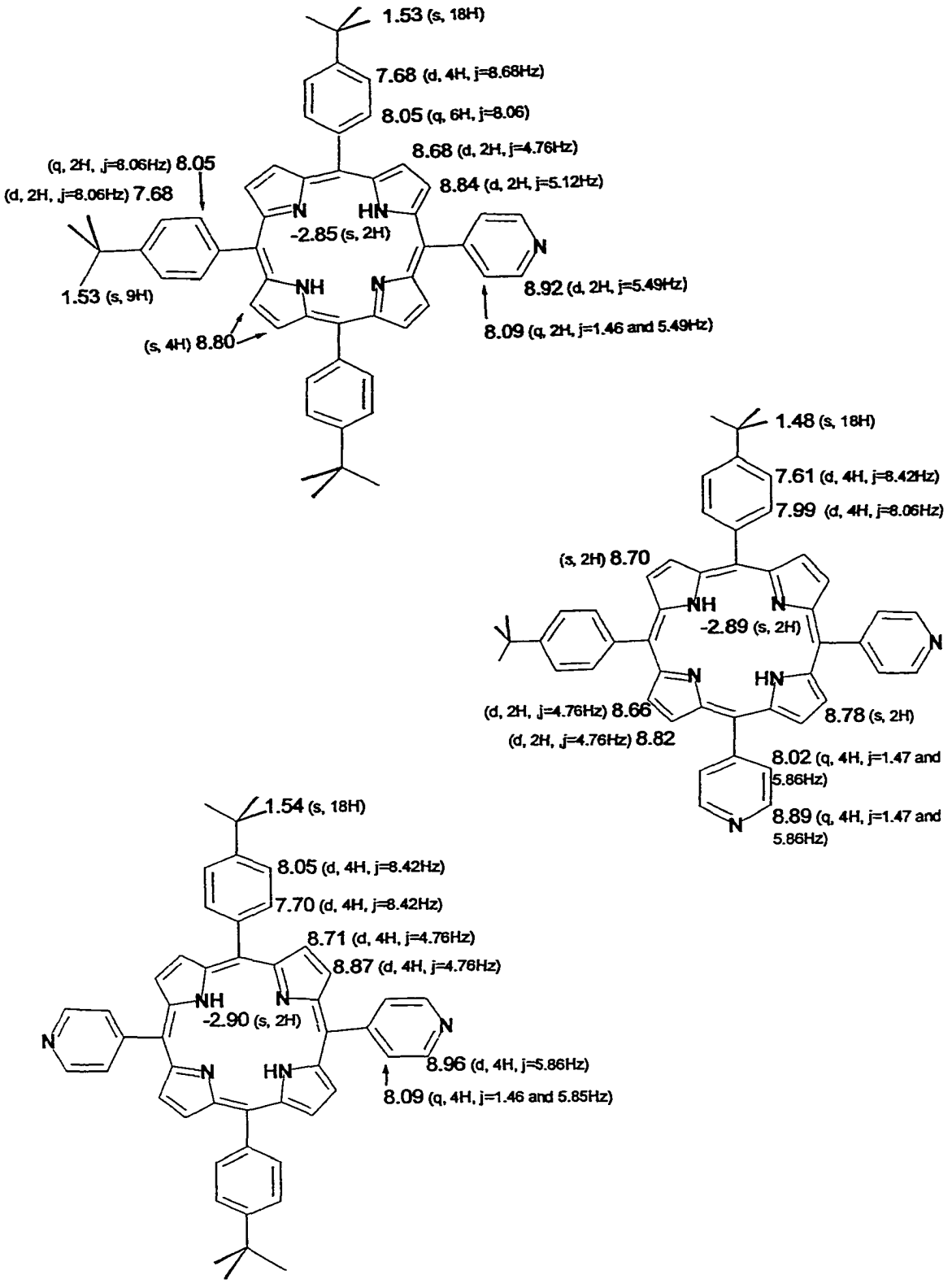

Figure 2.4 ^{1}H *chemical shifts for the (4-pyridyl) (4-tert-butylphenyl) porphyrins in* $CDCl_3$. *(j=±0.5Hz).*

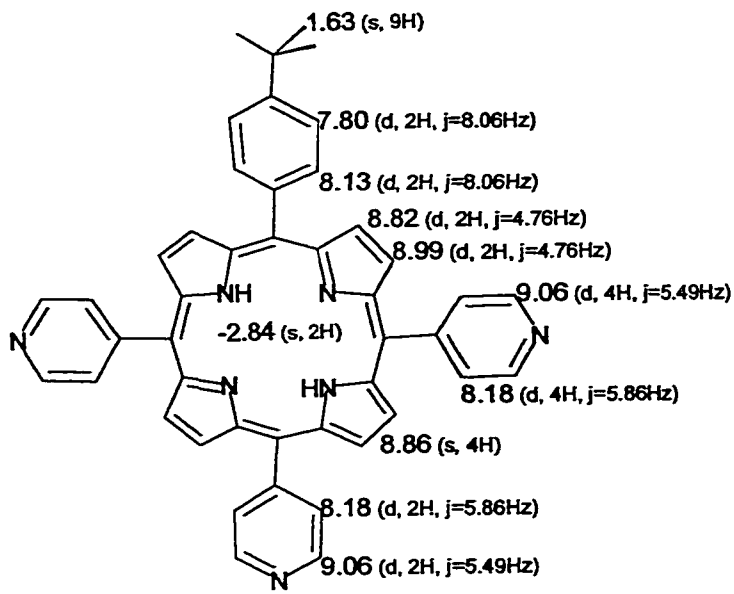

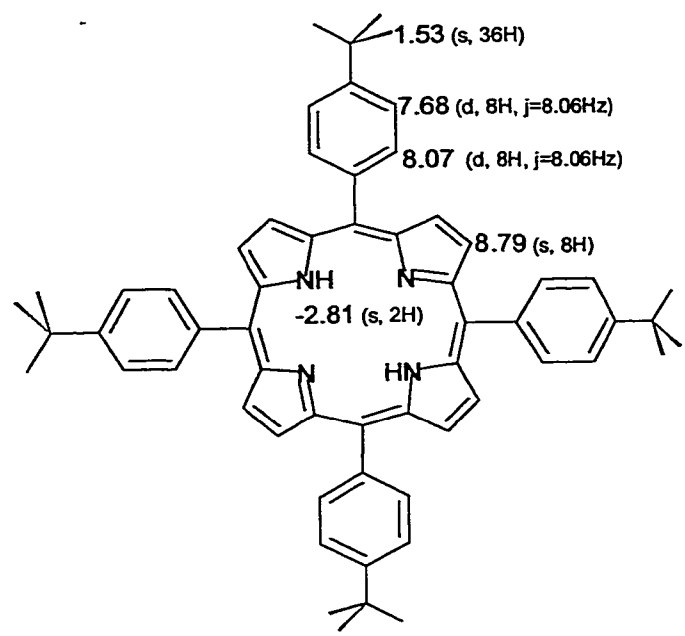

Figure 2.5 *^1H chemical shifts for the (4-pyridyl) (4-tert-butylphenyl) porphyrins in $CDCl_3$. (j=±0.5).*

signals at 8.09 and 8.92ppm, for the pyridyl group, while the phenyl signals, at 7.68 and 8.07ppm, reduce in from 6H, for each one, and the β-pyrrole signals of porphyrin **1** at 8.79ppm splits into two doublets and one singlet; the internal proton signal at –2.81ppm scarcely changes to –2.85ppm.

The signals for the phenyl protons (2,6 and 3,5) in the spectrum of $T(tbuPh)PH_2$ are easily assigned by consideration of their intensities and their distances of the protons from the porphyrin ring, which provide deshielding effects.[2.22] The pyridyl protons were assigned based on the same principle.

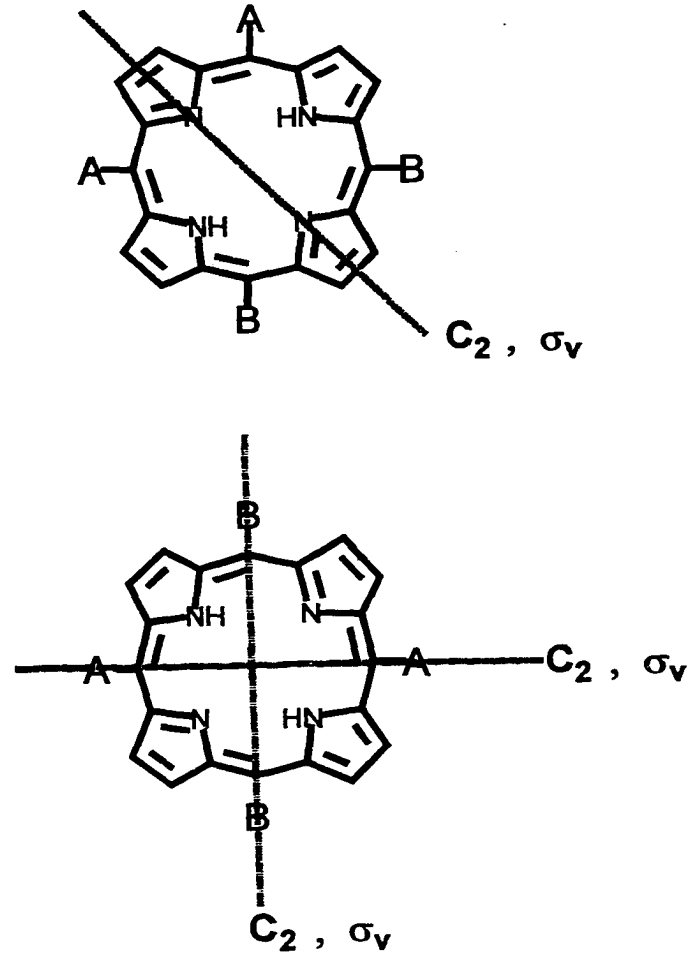

Figure 2.6 *The C_2 and σ_v symmetry elements of cis and trans A_2B_2P type porphyrin.*

The ^{1}H-NMR spectral pattern of the pyrrole protons readily distinguishes between *cis* and *trans* isomers. Figure 2.6 shows the C_2 and σ symmetry elements of the two isomers of the $A_2B_2PH_2$ type. The symmetry difference of the (*cis*) 5,15 and (*trans*) 5,15 isomers cannot be seen at the pyrrole N-H protons because there is fast tautomeric interconversion at room temperature in organic solvents.

For the *cis* isomer, the four types of pyrrole protons give rise to two singlets and two doublets, while the two types of pyrrole protons of the *trans* isomer give two doublets for any pair of adjacent protons. B3 and B4 show the spectra of *cis* and *trans* diPy(tbuPh)PH_2.

Solov'ev and co-workers[2.23] showed that the chemical shift pyrrole protons in porphin is 9.74 ppm and that of the pyrrole N-H, in the same porphyrin, is –3.76ppm. Our chemical shifts for the pyrrole protons on the (4-pyridyl) (4-*tert*-butyl phenyl) porphyrins, as it can be seen in fig. 2.4 and 2.5, are about 8.6 and 9.0ppm. The internal protons are about –2.9 and –2.8ppm. The data show decrease of the ring current with substitution at the *meso* positions of the macrocycle. The effects are similar whether pyridyl of *tert*-butyl group is attached to the *meso* position. According to Gouterman's four orbital model[2.24] pyrrole substitution is not expected to have such a profound effect on the ring current and consequently on the chemical shifts. The internal protons experience the largest current shift, since they are in the middle of the ring, and they can be used for its measurement.[2.7]

2.3.2 ^{13}C-NMR

Figures 2.7 and 2.8 introduce the assignments of the ^{13}C-NMR of the (4-pyridyl) (4-*tert*-butylphenyl) porphyrins, while the actual ^{1}H-decoupled spectra are shown form B10 through B15. Due to the well-assigned ^{1}H-NMR spectra of the porphyrins, carbon atoms that have hydrogen atom(s) can be directly assigned from the multiplicity of their coupled, or the intensity of their ^{1}H-decoupled spectra.

The assignment of the quaternary carbons in porphyrins were a major challenge, especially since the chemical shifts of these carbons can give valuable information that are unavailable from the ^{1}H-NMR. The quaternary carbons are differentiated by their singlet peaks in the ^{1}H-coupled spectra and by their low intensity in the ^{1}H-decoupled spectra. The last effect is due to the longer relaxation times and the small Nuclear Overhouser Enhancement due to the absence of hydrogen. In the ^{13}C-NMR of the porphyrins exchange broadening of the α-pyrrole carbon is observed. This is due to the N-H tautomeric exchange and it is a significant differentiation between α- and β-pyrrole carbons of the ^{13}C-NMR.

Ring current effects on the proton chemical shifts are roughly ± 5-10ppm and that influences significantly the appearance of the proton spectrum since the ranges of the proton signals are slightly greater than the above range. Although ring current effects are of the same absolute magnitude for ^{1}H and ^{13}C, they contribute less than 10% to the ^{13}C shifts since the signals in the ^{13}C-NMR are spread over a region of about 200ppm.

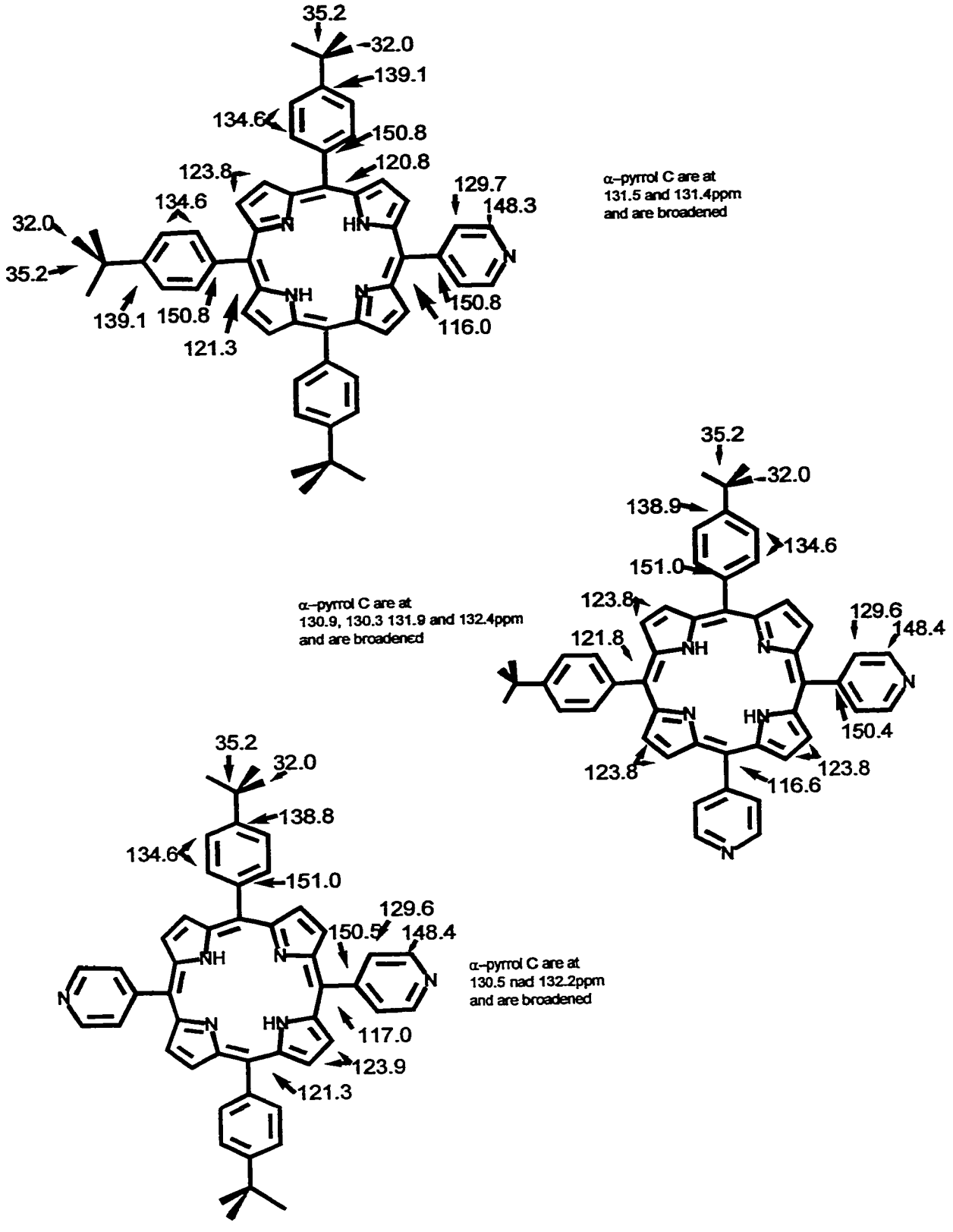

Figure 2.7 ^1H chemical shifts for the (4-pyridyl)$_{x=1\ to\ 4}$ (4-tert-butylphenyl)$_{y=4-x}$ porphyrins in $CDCl_3$..

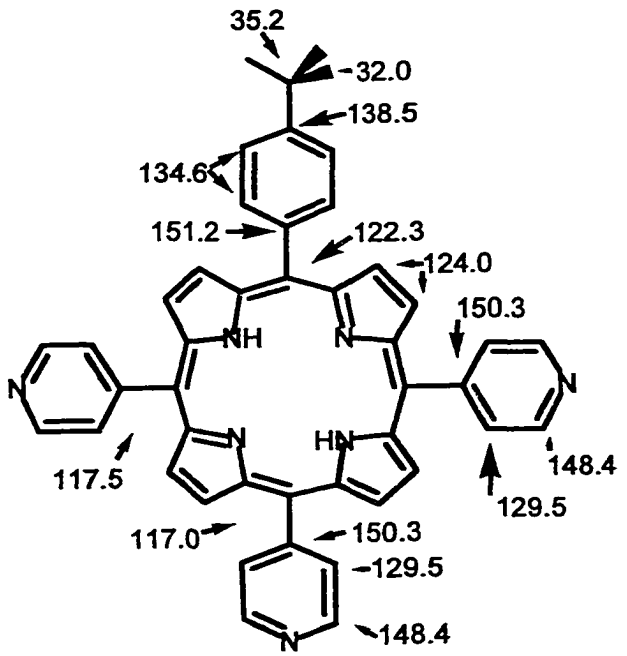

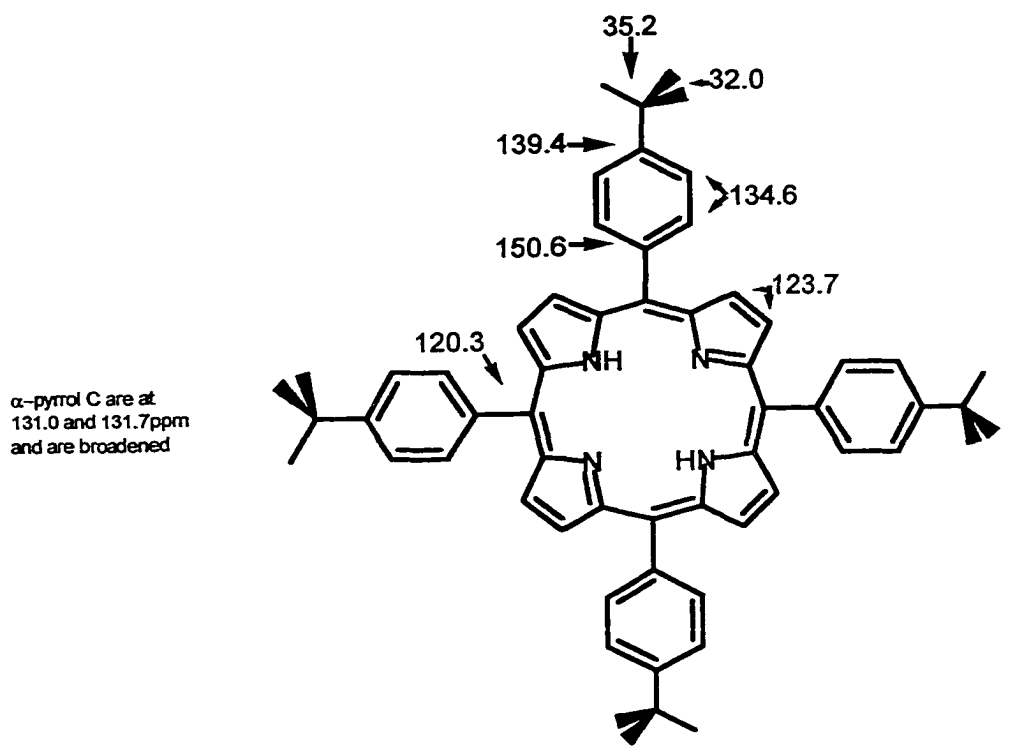

Figure 2.8 *^1H chemical shifts for the (4-pyridyl)$_{x=1\ to\ 4}$ (4-tert-butylphenyl)$_{y=4-x}$ porphyrins in $CDCl_3$..*

The signals of the ^{13}C-NMR spectra of the (4-pyridyl)$_{x=1\ to\ 4}$ (4-*tert*butylphenyl)$_{y=4-x}$ porphyrins can be more of less subdivided into five regions: the aliphatic carbons with chemical shifts in the range ~32-36ppm; the *meso* carbons in the range 115-122ppm; the β-pyrrole carbons in the range 123.5-124ppm; the a-pyrrole carbons in the range 131-132ppm; and the aromatic substituents of the range 130-151ppm. The α- and β-pyrrole carbons are in the range 120-135ppm, a range that olefinic carbons are observed. The later is evidence of an inner (18-annulene) conjugated system that explains the olefinic character of the macrocycle.

It is not shown in the figures but we have observed that after metalation of the porphyrins the difference between the different types of α- and β-pyrrole is less noticeable in the ^{13}C-NMR spectra and the signals are shifted to a lower energy region of the spectra (downfield shift). These effects are due to the redistribution of the charge densities after metalation of the porphyrin.

2.3.3 ESI-MS

Table 2.1 summarizes the data of the mass spectra for the (4-pyridyl) (4-*tert*-butyl phenyl) porphyrins. The major peaks seen are common in porphyrin mass spectra.[2.25]

Porphyrin	*Chemical Formula*	*Calculated*	*Found (Rel. Int.)*
T(tbuPh)PH$_2$	$C_{60}H_{53}N_4$	838	839(100), 840(80), 841(35),842(15)
5Py10,15,20(tbuPh)PH$_2$	$C_{55}H_{53}N_5$	783	784(100), 785(70), 786(20),787(15)
5,10Py15,20(tbuPh)PH$_2$	$C_{50}H_{44}N_6$	728	729(100), 730(58),731(18)
5,15Py10,20(tbuPh)PH$_2$	$C_{50}H_{44}N_6$	728	729(100), 730(58),731(18)
5,10,15Py20(tbuPh)PH$_2$	$C_{45}H_{35}N_7$	673	674(100), 675(50), 676(15)

Table 2.1 *ESI-MS of (4-pyridyl)$_{x=1\ to\ 4}$ (4-tertbutylphenyl)$_{y=4-x}$ porphyrins in $CHCl_3/CH_3CN$ (1/9) with 1% TFA.*

2.4 Steady-state photophysical properties of porphyrins

The foundation for the study of the optical properties of the porphyrins lies on a theoretical framework developed by Gouterman.[2.24] The four orbital model describes the lowest excited states of regular porphyrins as mixtures of configurations arising from one electron promotions from the two porphyrin ring π HOMOs (highest occupied molecular orbitals) to the two ring π* LUMOs (lowest unoccupied molecular orbitals). Metalloporphyrins with D_{4h} (square planar) symmetry have nearly degenerate HOMOs and strictly degenerate LUMOs. Configuration interactions between the electronic promotions of the form ($a_{1u}e_g$) and ($a_{2u}e_g$) give rise to the singlet ground state (S_0) absorption spectra containing a strong near-UV band (B or Soret) and a weak Q-band absorption in the red region of the spectrum (fig. 2.9 and 2.10). The higher energy

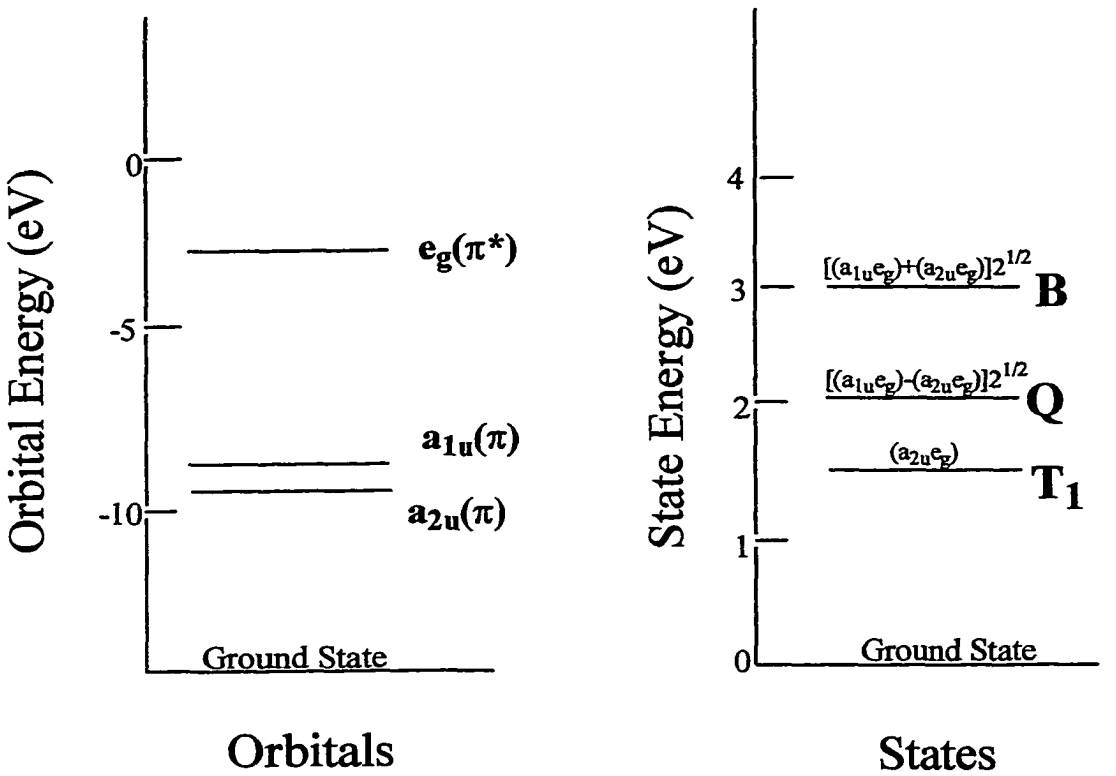

Figure 2.9 (Left figure) Relative energies of HOMOs (a_{1u} *and* a_{2u}) *and LUMOs* (e_g).
(Right figure) Energies of the two lowest in energy excited states and their respectiveterms in the four-orbital model of porphyrin spectroscopy.[2.26]

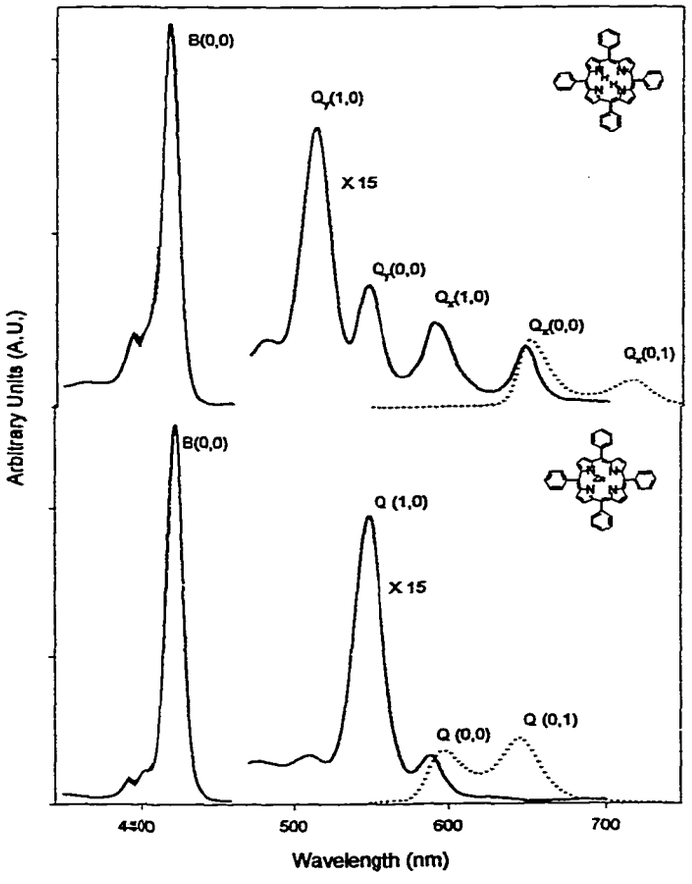

Figure 2.10 *Ground state absorption (solid lines) and fluorescence (dashed lines) spectra of a metallo-porphyrin (TPPZn) and that of a free-base porphyrin ($TPPH_2$) in toluene.*

absorption represents an $S_0 \rightarrow S_2$ transition while the lower energy Q state represents a $S_0 \rightarrow S_1$, where S_2 and S_1 correspond to the second and first excited states, respectively. In addition to the electronic bands, Q(0,0) and B(0,0), porphyrin absorption spectra typically contain bands at ~400nm, higher in energy that the (0,0) bands, which arise from vibrational transitions coupled to electronic transitions (Fig. 2.10). These general comments give a general picture of the ground electronic state of the porphyrin systems.

PORPHYRIN 2 PORPHYRIN 1

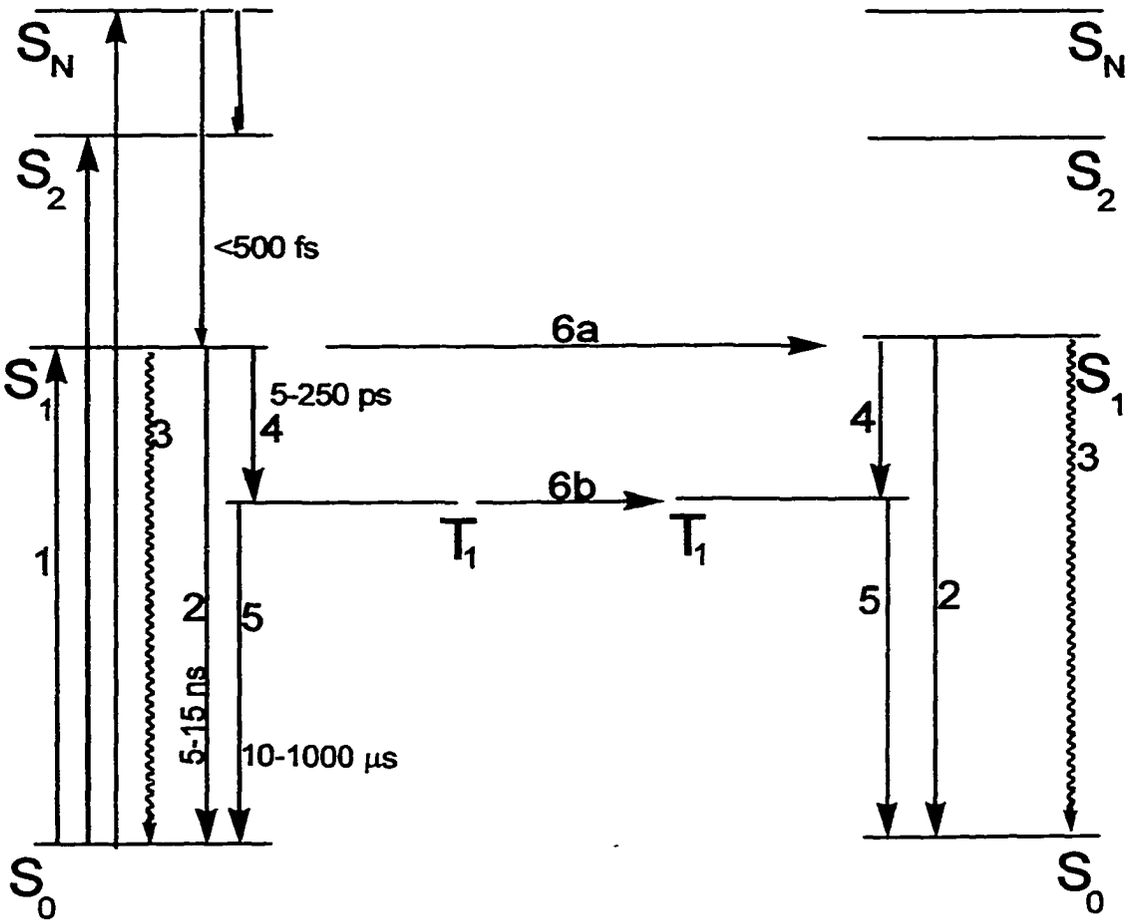

***Figure 2.11** Modified jablonski diagram*
1. *Absorption of light.*
2. *Fluorescence.*
3. *Internal conversion (IC).*
4. *Inter-system crossing (ISC).*
5. *Phosphorescence.*

6a. Electron or energy transfer (singlet to singlet).
6b. Electron or energy transfer (triplet to triplet).

Following optical excitation, porphyrins like other organic molecules, can follow a variety of decay channels, some intramolecular and some intermolecular. The excited state dynamic properties are normally introduced with a Jablonski diagram (fig. 2.11).

photoexcitation to either the S_1 or S_2 state of the macrocycle leads to rapid ($<10^{-12}$ sec) relaxation to the lowest vibrational level of the S_1 state. From here, the system may relax to the ground state S_0 radiatevely by fluorescence or nonradiatevely by internal conversion (IC) with rate constants K_F and K_{IC} respectively. Also, from S_1, intersystem crossing (ISC) to the lowest triplet state (T_1) may occur with rate K_{ISC}. From T_1, the molecule may decay radiatevely by phosphorescence, with rate K_P, or nonradiatevely, with rate K_I, to the ground state. Metalloporphyrins with open-shell metal configurations may relax from S_1 to T_1 through metal states such as (d,d) states where the excitation becomes localized on the metal, or (d,π^*) states, where the metal transfers an electron to the porphyrin ring. In the case of porphyrins porphyrins bonded to an electron acceptor such as quinone, electron transfer (eT) may cause the production of a porphyrin cation/acceptor anion (P^+A^-) state which then returns to the ground sate through charge recombination (CR).

2.4.1 Optical Absorption Studies

The (4-pyridyl) (4-*tert*-butylphenyl) porphyrins (table 2.2) show typical optical spectra consisting of a dominant Soret band around 420nm and four visible bands (from 510-650nm). Of the types of spectra classified as etio, rhodo, oxorhodo and phyllo, according to the relative intensities of the four visible bonds,[2.26] the (4-pyridyl) (4-*tert*-butylphenyl) porphyrins give etio spectra (Qy(1,0)>Qy(0,0)>Qx(1,0)>Qx(0,0).

Porphyrin	*Soret B(0,0)*	$Q_y(1,0)$	$Q_y(0,0)$	$Q_x(1,0)$	$Q_x(0,0)$	$Q(0,0)^{a'}$	$Q(1,0)^{b'}$	$\frac{Q(0,0)}{Q(1,0)}$
$TPPH_2$	418.4 (448.1)	514.4 (22.9)	548.5 (10.8)	591.3 (7.6)	648.1 (4.9)	15.7	30.5	0.515
$T(tbuPh)PH_2$	420.6 (387.9)	516.0 (16.2)	551.0 (8.8)	593.3 (4.6)	649.4 (4.2)	13.0	20.8	0.625
5Py $10,15,20(tbuPh)PH_2$	420.4 (418.2)	515.6 (19.0)	550.5 (9.3)	592.2 (5.5)	648.1 (4.2)	13.5	24.5	0.551
5,10Py $15,20(tbuPh)PH_2$	419.9 (414.0)	514.8 (19.2)	549.2 (8.0)	591.1 (5.6)	647.4 (3.4)	11.4	24.8	0.460
5,15Py $10,20(tbuPh)PH_2$	419.7 (396.0)	514.5 (18.4)	548.8 (7.7)	591.5 (5.4)	647.6 (3.5)	11.2	23.8	0.470
5,10,15Py $(+Ph)PH_2$	419.0 (383.7)	513.8 (18.9)	547.9 (6.5)	590.0 (5.5)	645.6 (2.6)	9.1	24.4	0.373
$TPyPH_2$	418.2 (325.1)	513.0 (16.1)	545.5 (3.9)	589.3 (4.3)	649.4 (1.7)	5.6	20.4	0.274

Table 2.2 *UV-Vis data for the (4'pyridyl) 4-tert-butyl phenyl) porphyrins. 1 μM conc. of porphyrin in toluene at RT. Cuvette 1x1cm. λ_{max} (extinction coefficient ($\varepsilon x\ 10^{-3}$, $M^{-1}\ cm^{-1}$))*

a': $Q(0,0)=Q_x(0,0)+Q_y(0,0)$

b': $Q(1,0)=Q_x(1,0)+Q_y(1,0)$

There is small but consistent blue shift of the Soret band as the number of Py increases. Such shifts are observed on alkylation of pyrrole hydrogen have been attributed to the electron-donor properties of the substituents,[2.24, 2.27] but increasing conjugation on going from Py→tbuPh offers a more general rationalization. The Soret band is sharp, and the ratio of Soret to visible absorbance maxima is relatively normal. Following Gouterman et al.[2.28] the absorbance intensities ratio Q(0,0)/Q(1,0) (eq. 1) is given in the last column of the table 2.2 as a measure of the substituent effect on the absorption properties.

$$Q(0,0)/Q(1,0)=[Qx(0,0) + Qy(0,0)]/[Qx(1,0) + Qy(1,0)] \qquad \text{(eq. 2.1)}$$

2.4.2 Optical Emission Studies

The emission spectra group the porphyrins into normal and perturbed categories. Normal fluorescence behavior includes: 1. A quantum yield comparable to $TPPH_2$ (Φ_f=0.11)[2.29] or $OEPH_2$ (Φ_f =0.16),[2.30] 2. Small (~100cm^{-1}) absorption/emission "Stokes" shifts between the $Q_x(0,0)$ absorption and $Q_x(0,0)$ fluorescence peaks (as in $TPPH_2$ and $OEPH_2$), and 3. Vibronic structures and bandwidths similar to $TPPH_2$ and $OEPH_2$. In contrast, perturbed emission spectra are characterized by 1. Lower quantum yields (<0.01), 2. Larger stokes shifts (~900cm^{-1}) and, 3. Generally only a single, broad (~1500cm^{-1} fwhm) fluorescence band with no clear vibronic structure. Table 2.3 gives the principle emission peaks, the relative intensities of these peaks, the Stokes shift observed between the absorption and emission spectra if each porphyrin, the quantum yield estimates, and the measured lifetimes. The fluorescence quantum yield for each sample was measured using the ratio method, utilizing $TPPH_2$ in toluene as a standard Φ_f=0.11.[2.29] Each solution was excited at such a wavelength so that the absorption of the sample in question and that of the standard was the same. The technique follows the equation, outlined by Parker and Rees.[2.29]

$$\frac{F_2}{F_1} = \frac{Area_2}{Area_1} = \frac{\Phi_2 \varepsilon_2 C_2 d_2}{\Phi_1 \varepsilon_1 C_1 d_1} = \frac{\Phi_2 A_2}{\Phi_1 A_1} \qquad \text{(eq. 2.2)}$$

where F=fluorescence area

Φ=fluorescence quantum yield

ε=extinction coefficient and

A=absorbance

Porphyrin	*Excitation wavelength (nm)*	*Q(0,0)*	*Q(0,1)*	*Q(0,0)/Q(0,1)*	*Q(0,0)*		*Stokes Shift (cm^{-1}) ±20%*	*Quantum Yields Φ_f*	*Life-times[a'] τ_f (ns)*	*Fuoresc. Rate Const.[b'] K_f (ns^{-1})*	*Radiative Life-Time[c'] τ_0 (ns)*
					Abs. (nm)	*Fluoresc. (nm)*					
$TPPH_2$	424.1	651.9	717.8	2.9	648.1	651.9	89	0.11[2.25]	12.2	0.009	110.91
$T(tbuPh)PH_2$	424.1	654.0	720.9	3.6	649.4	654.0	108	0.14	12.05	0.012	86.07
5Py (tbuPh)PH_2	421.0	652.5	717.5	3.6	648.1	652.5	104	0.08	10.8	0.007	135.00
5,10Py (tbuPh)PH_2	421.9	651.0	718.0	2.9	647.4	651.0	85	0.10	12.3	0.008	123.00
5,15Py (tbuPh)PH_2	422.5	652.0	718.2	3.2	647.6	652.0	104	0.10	11.8	0.008	118.00
5,10,15Py (tbuPh)PH_2	421.0	649.7	716.0	2.4	645.6	649.7	97	0.13	12.6	0.010	96.92
$TPyPH_2$	411.7	649.5	714.7	1.6	649.0	652.3	77.9	0.05	11.4	0.088	228.00

Table 2.3 Fluorescence data for the (4-pyridyl) (4-tertbutylphenyl) porphyrin.
1μM conc. of porphyrin in toluene at RT. Cuvette 1x1cm.
a': excitation wavelength 421nm emission 650nm. 1μM solutions, in toluene, were degassed with N_2 for 5 min.
b': Φ_f/τ_f. [2.31]
c': τ_f/Φ_f. [2.31]

The error is ± 5%. The lifetime measurements were obtained using the phase modulation technique and a 10-100Hz frequence. The error is ± 5%.

It has been observed that the fluorescence lifetime, τ_f, increases as the fluorescence quantum, Φ_f, increases.[2.29] This trend is observed in the quantum yields of table 2.3 as well. The radiative lifetimes, τ_0, in table 2.3, were calculated as τ_f/Φ_f, and the fluorescence rate constant, K_f, was calculated as Φ_f/τ_f.[2.31] The radiative lifetime, τ_0, is longer for porphyrins with high number of pyridyl groups, and variation is due, in part, to the degree of porphyrin polymerization. The $TPPH_2$ and T(*tbu*Ph)PH_2 monomers have a slightly shorter τ_0 and on average a higher Φ_f value than the $TPyPH_2$ where there can be a weak hydrogen bonding between the pyridyl groups and the inner protons of the porphyrins and π-stacking. This may be the case with the $TPyPH_2$. The dependence of the emission intensity and of the Stokes shift on the porphyrin concentration (table 2.K) strengthens the above argument.

Gradyusho and coworkers[2.26] developed equation (2.3) as an approximation of porphyrin photophysical behavior

$$\Phi_f+\Phi_p=1 \qquad \text{equation (2.3)}$$

Gouterman[2.23] presented evidence that equation 2.3 generates poor approximation of porphyrin photophysical behavior, by producing sums as low as 0.60. The difference $1-(\Phi_f+\Phi_p)$ is a measure of the Φ_{IC} (the internal conversion yield.) $\Phi_f+\Phi_p$ is close to unity for systems where the internal conversion yield, Φ_{IC}, is very low. Here we will avoid making any assumptions about the Φ_{IC} in order to minimize any possible error.

As can be seen from the steady-state data, the emission of the (4-pyridyl) (4-*tert*-butylphenyl) porphyrins represent examples of normal photophysical behavior. They have similar photophysical properties to those of $TPPH_2$ and when phenyl group is substituted by tbuPh, increased quantum yield and lifetime are observed.

2.5 Metalation of porphyrins

In most cases, the formation of a metallo-porhyrin involves the reaction of the free-base porphyrin (PH_2) with the metal salt MX_2 producing P(M) and the corresponding acid molecule HX (fig. 2.4)

$$PH_2 + MX_2 \underset{b.}{\overset{a.}{\rightleftharpoons}} P(M) + 2HX$$

Figure 2.12 *a. Metalation of PH_2.*
b. Demetalation of P(M).

For our needs the metalated porphyrins were formed. By the acetate method.[2.33]

$$Zn(OAc)_2 + PH_2 \xrightarrow[\text{Reflux}\ 2\ \text{hours}]{CHCl_3/MeOH\ (1/1)} P(Zn) + 2AcOH$$

***Figure 2.13** Porphyrin metalation. (Acetate method)*

10% excess of the Zn salt was used. The porphyrin was dissolved in $CHCl_3$ and the Zn salt in MeOH. Chromatography on alumina was used to separate the metalated porphyrin from the unreacted free base and by products due to chemical alterations of the porphyrin under the reaction conditions. Basic alumina is the stationary phase of the column while

$CHCl_3$ was used to elute the free-base porphyrin and the side products and 5% MeOH in $CHCl_3$ to elute the metalated porphyrin from the column.

Models show that the little too large ionic radii of the Zn(II) (0.74 Å) makes it difficult for the metal to fit nicely in the porphyrin hole. Zinc porphyrin complexes have a strong preference to adapt a somewhat square-pyramidal geometry with the Zn out of the plane of the porphyrin.

CHAPTER 3

Formation and Characterization of Multiporphyrin Arrays

3.1 Introduction

Research in nanostructured materials is motivated by the belief that ability to control the building blocks, or nanostructures, of the materials can result in enhanced properties of the material at macroscale dimensions. For instance increased hardness, catalytic enhancement, selective absorption or higher efficiency electronic or optical behavior has been demostrated with some nanoscaled systems. Synthesis and assembly strategies involve precursors from the liquid, solid, or gas state. Deposition is achieved by chemical or physical approaches that direct the building of the desired material's molecular structure by use of their chemical reactivity or their physical characteristics. The complexity of biological materials is a good example of high structural order accomplished by the self-assembly of organic material. It is worth noticing that many synthetic and self-assembly methods have been inspired by biological systems.

While molecular chemistry is based on covalent reactions, supramolecular chemistry is based the on self-assembly or organization of molecular components. The use of macrocyclic structures was a solution to the need for better control over the geometry and rigidity of molecular receptors. Such a pre-organization has been observed since the design of crown ethers[1.7] and cryptands[1.8].

Self-assembly is a very broad term used for structures that generate chemical systems in equilibrium. It describes a spatial conformation through spontaneous connection of a few or many components that results the formation of discrete or extended species.[1.2] These

can be molecular, covalent, or supramolecular. Self-assembly is a process in which supramolecular organization is achieved by a complex system of components that can have a "key-lock" relationship on a chemical or physical level.

Self-assembly requires molecular components that have two or more interaction sites making them capable of forming multiple associations. When the components are self-complementary, they associate with themselves to form homo-assemblies. When complementary components associate with each other they form hetero-assemblies. Occupation of a given site may lead to a change in the binding strength of the other site(s) making subsequent binding events easier (positive cooperativity) or more difficult (negative cooperativity). Positive cooperativity is a characteristic of the molecular amplification devices since the next step of the assembly process is facilitated by the previous step.[1,2]

By definition self-assembling systems are under equilibrium, which provides the ability for self-healing (self-repearing or annealing) of the system. This is a difference with covalent systems where the non-labile product usually cannot be spontaneously healed and the defects are permanent (mostly in the form of unwanted side-products). These are kinetic products. The mechanism that introduces the organization in the supramolecular complex systems is determined by competing molecular interactions, e.g. Coulombic, hydrogen bonding, Van der Waals, or interactions between hydrophobic and hydrophilic components. Our work focuses on the formation of self-assembled structures by use of coordination chemistry or by hydrogen bonds.

3.2 Metal Mediated Self-Assembly

Inorganic self-assembly involves the formation of well-defined metallo-supramolecular architectures from organic ligands and metal ions. The metal ion acts as cement holding the ligands together and at the same time provides orientation for the ligands and so the desirable geometry for the assembly. Metal ions may also add to the functionality of the system.

The emphasis on supramolecular architecture lies on the design of the ligand and the choice of the metal ion. The metal ions play a very important role in the field of supramolecular chemistry since they provide:

1. a set of coordination geometries,
2. range of binding strengths that controls the formation and dissociation kinetics/energetics making the metal from inert to labile, and
3. a wide spectra of photochemical and electrochemical properties.

Porphyrin-type ligands have been widely used in multi-component covalent arrays to study photoinduced energy and/or electron transfer processes.[3.1, 3.2] The most important reasons for such investigations arise from the interest in mimicking natural photosystems.[3.1] Successful strategies include the attachment of the tetrapyrrolic ring both by covalent[3.1, 3.2, 3.3] or non-covalent[3.4] bonds to suitable molecular components such as electron acceptors. The photoinduced process can be easily detected by optical spectroscopic techniques.[3.4, 3.5]

Various molecular devices based on multiporphyrin arrays have been designed and prepared. Good examples are artificial photosynthetic systems,[3.6] photoinduced picosecond molecular switches,[3.7] optoelectronic gates,[3.8] fluorescence quenching sensors,[3.9] photonic wires,[3.10] and PDT therapy agents.[3.11] The porphyrin array architectures, reported in the literature, include linear chains,[3.12] cyclic oligomers,[3.13] squares, [3.14] sheets, tapes,[3.15] stars,[3.16] and others.

Nevertheless, the challenge remains for the preparations of new porphyrin-containing oligomers with well-defined structure and properties, since the optimal molecular arrangement for various applications has still to be understood. Preparation of porphyrin arrays in high yields and significant quantities is still problematic. One of the major obstacles for porphyrin derivatives is low solubility, which complicates scale-up and characterization of the products. Here I will describe the preparation of well defined multiporphyrin arrays that are reasonably soluble in most organic solvents from readily available, starting materials. These consist of four or nine pyridyl-substituted porphyrins self-assembled with square-planar *trans*-Pd dichloride or *cis*-Pt dichloride complexes. It is worth noting that in one square multiporphyrin array (fig. 3.1) we bring together 21 molecules, of four different types, forming a ~25 nm^2 square assembly.

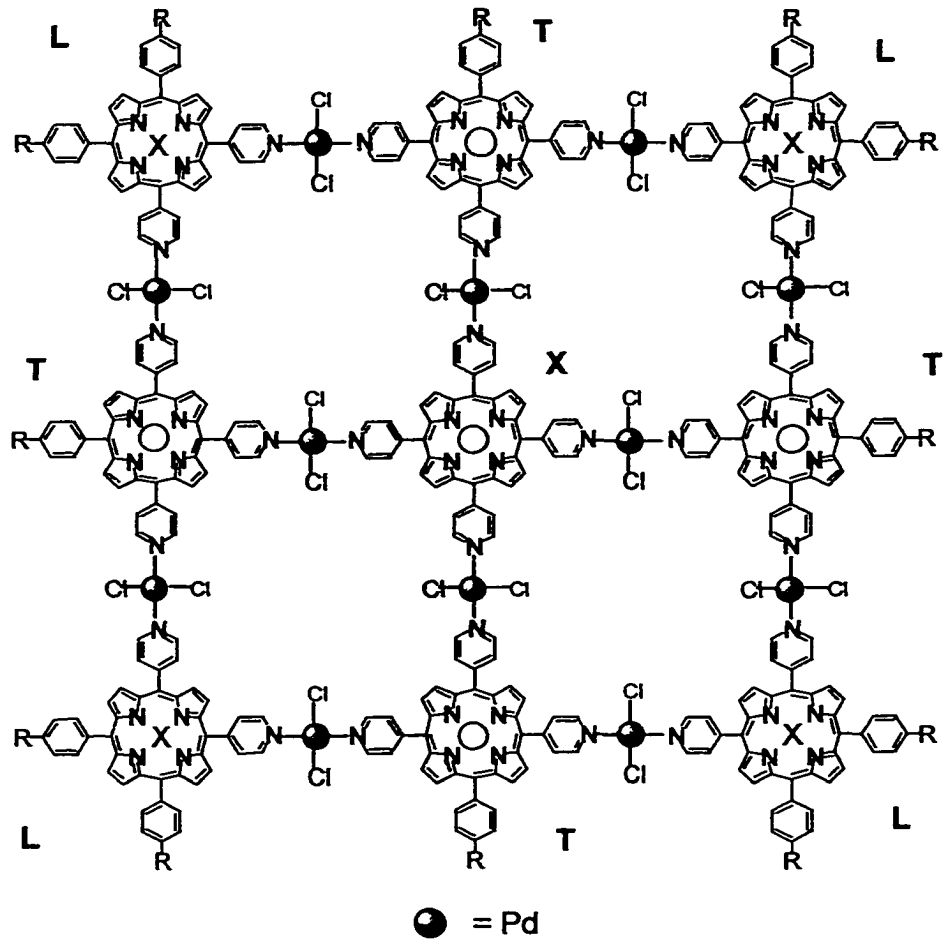

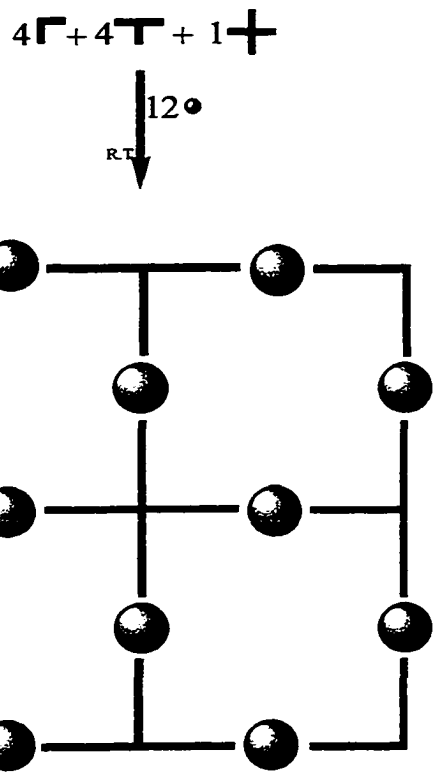

Figure 3.1 *Schematic presentation of nonamer*
3a. R=4-tolyl, O=X=2H^{+}.
3b. R=4-tolyl, O=X=Zn^{2+}.
3c. R=4-tolyl, O=2H^{+}, X=Zn^{2+}.
4a. R=4-tertbutylphenyl, O=X=2H^{+}.
4b. R=4-tertbutylphenyl, O=X=Zn^{2+}.
4c. R=4-tertbutylphenyl, O=2H^{+}, X=Zn^{2+}.

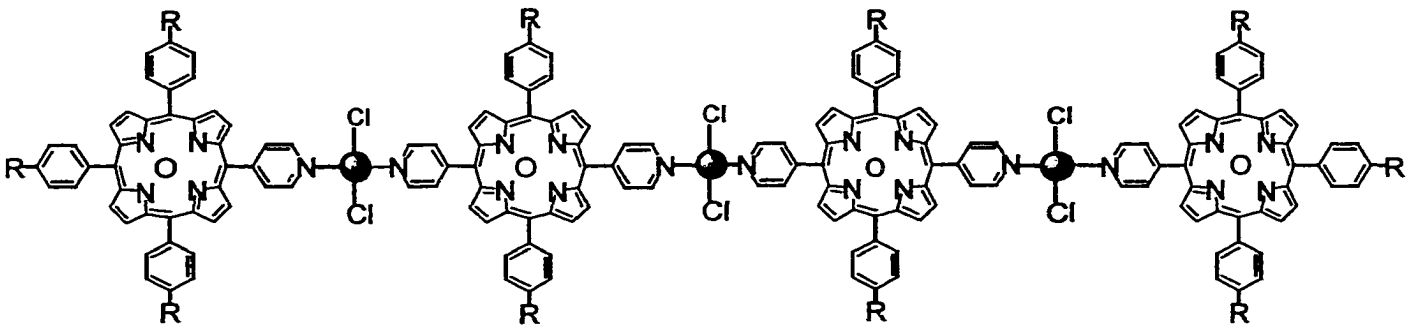

● =Pd

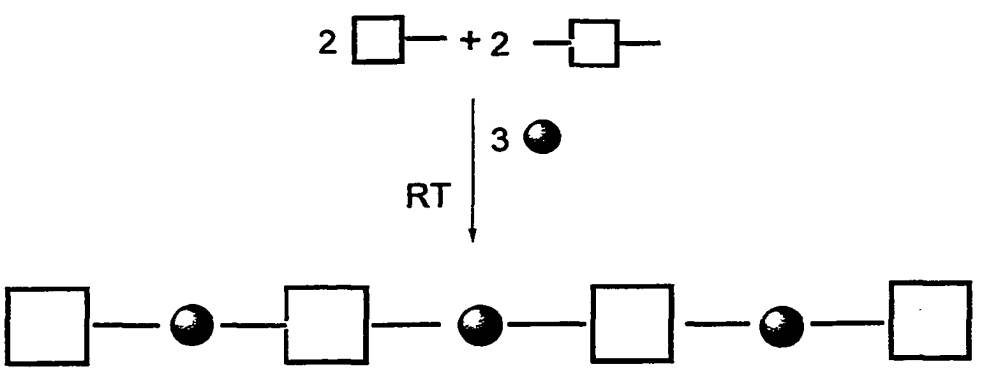

Figure 3.2 *Schematic presentation of Pd-linear tape*
5a. R=4-tolyl, O=2H^{+}.
5b. R=4-tolyl, O=Zn^{2+}.
6a. R=4-tertbutylphenyl, O=2H^{+}.
6b. R=4-tertbutylphenyl, O=Zn^{2+}.

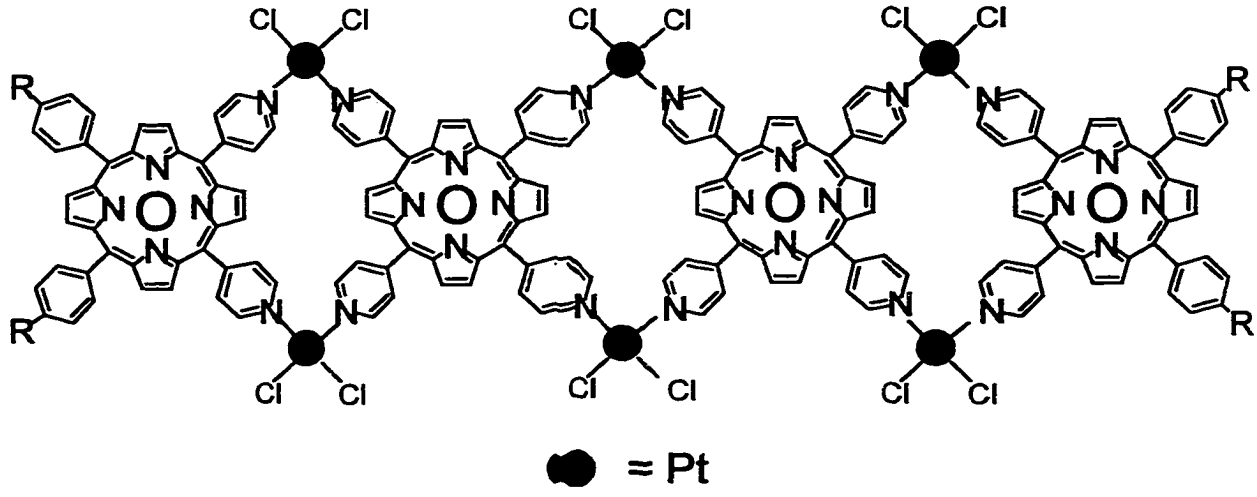

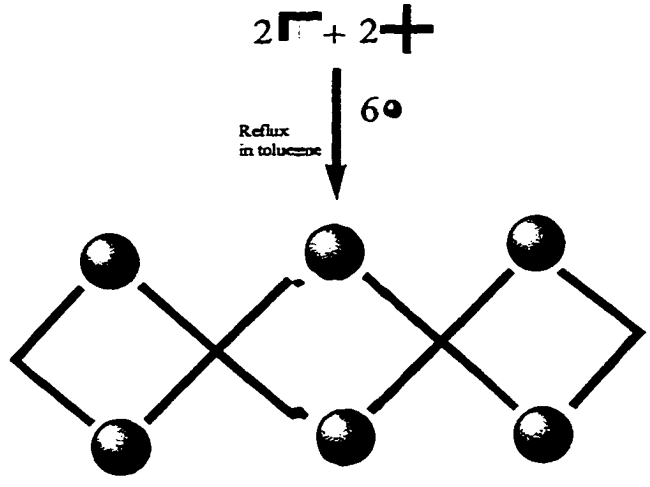

Figure 3.3 *Schematic presentation of Pt-planar tape*
7a. *R=4-tolyyl, O=2H^{+}.*
7b. *R=4-tolyyl, O=Zn^{2+}.*
8a. *R=4-tert-butylphenyl, O=2H^{+}.*
8b. *R=4-tert-butylphenyl, O=Zn^{2+}.*

3.2.1 Formation

The self-assembly of rigid supramolecular macrocycles require well-defined, geometrically rigid, building block precursors. Specifically, the assembly of the square-shaped array required four programmed L-shaped, four T-shaped modules and the one X-shaped (fig. 3.1). Bis(4-pyridyl)porphyrins, substituted at the 5 and 10 positions, tris(4-pyridyl)porphyrins, and tetrakis(4-pyridyl)porphyrins can serve as L-shaped, T-shaped and X-shaped blocks, respectively. As linking blocks, nine *trans*-$(PhCN)_2PdCl_2$ are required.

In the linear-tapes multiporphyrin arrays, (fig. 3.2) **5** and **6**, two of the 5,15 bis(4-pyridyl) porphyrins, and two of the mono(4-pyridyl) porphyrins are required together with three transition metal-based linear units. Finally, six *cis*-Pt(II) linking metals were used to connect two L-shape building blocks with two X-shape building blocks to form the planar-tapes **7** and **8**.

At all case both free base porphyrin (**3a**, **4a**, **5a**, **6a**, **7a**, and **8a**) and zinc porphyrin derivatives (**3b**, **4b**, **5b**, **6b**, **7b**, and **8b**) were formed. Chloroform, toluene and mineral oil were the preferred solvents in most cases but acetone, dichloromethane, and THF were evaluated as a media for the formation of several multiporphyrin arrays. Formation of compounds **3**, **4**, **5**, and **6** took place by stirring the reaction mixture at room temperature for about 15 minutes. Longer reaction times and higher temperatures were applied for the formation of the Pt-containing species (arrays **7** and **8**). This is attributed

to the stronger character of the Pt(II)-pyridine bond in contrast to the labile character of the Pd(II)-pyridine bond.[3.17] All the species were formed at wide range of concentrations ranging from 0.3μM to 100μM in the resulting species. At concentrations higher than ~50μM a purple-red microcrystals were precipitated out of the reaction mixture. The solubility in most organic solvents of the 4-*tert*-butylphenyl arrays (**4**, **6**, and **8**) was greater than that of the 4-tolyl arrays (**3**, **5**, and **7**). Also, increased solubilities for all the resulting species were observed in non-polar solvents like mineral oil and toluene. The free-base multiporphyrins had higher solubilities in organic solvents than the corresponding zinc-metalated multiporphyrins, as was expected.

3.2.2 Characterization

The characterization of non-covalent aggregates has been a challenge that is still only partially met. X-ray crystallography, a very useful technique in characterizing covalent structures, has not been useful with these arrays due to the lack of suitable crystals. Instead, characterization is based on combining inferences from a set of solution phase methods. Individually each method may not give complete information; collectively they make a strong case. Also, there are numerous examples of structure in the solid phase which are different from those found in solution.

3.2.2.1 UV-Vis

Titration of the Pt(II) or Pd(II) complex into solution of the porphyrins in toluene and mineral oil results clear isosbestic points for the B (Soret) and Q-band in the UV-Vis spectra of the porphyrins (fig. 3.4) indicating the formation of only one species in solution.

Array	*In Toluene*		*In Mineral Oil*	
	Starting Material *(nm)*	***Red Shift*** *(nm)*	***Starting Material*** *(nm)*	***Red Shift*** *(nm)*
Nonamer 4a	419.5	8.1	418.9	17.6
Pt-planar tape 8a	419.2	2.4	418.8	15.2
Pd-linear tape 6a	420.1	1.5	419.8	12.2

Table 3.1 *Characteristics of the Soret absorptions in the UV-Vis spectra. 1μM in the resulting supramolular species.*

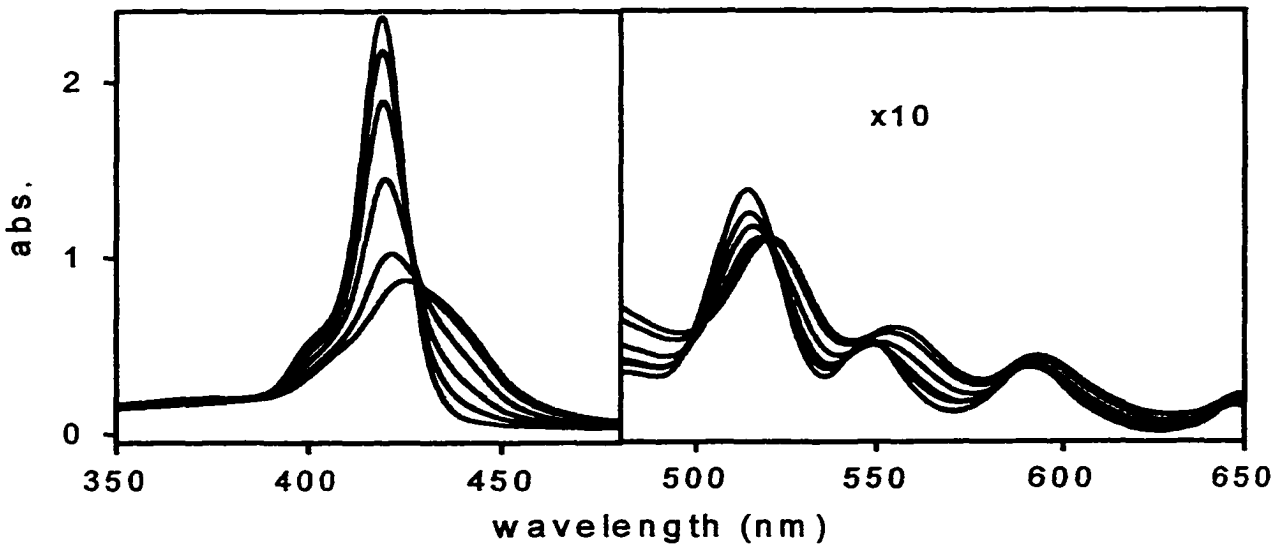

Figure 3.4 *Isosbestic points resulting from titration of $PdCl_2$(benzonitrite)$_2$ into a 4:4:1 stochiometric mixture of free-base porphyrins (5,10Py15,20(tbuPh)PH_2, 5,10,15Py20(tbuPh)PH_2, and TPyPH_2) in mineral oil indicates cooperative formation of nonamer **4a** shown in figure 3.1.*

These red shifts are more pronounced for the nonamer, less for the Pt-containing tapes and the least for the Pd-tape. Analogues but smaller red shifts have been reported for the Pd-square tetramer[3.14a] (fig. 3.5). The formation of the Pd-containing dimer and the square tetramer were repeated and the results are compared with those of the new arrays (Table 3.2) under the same experimental conditions.

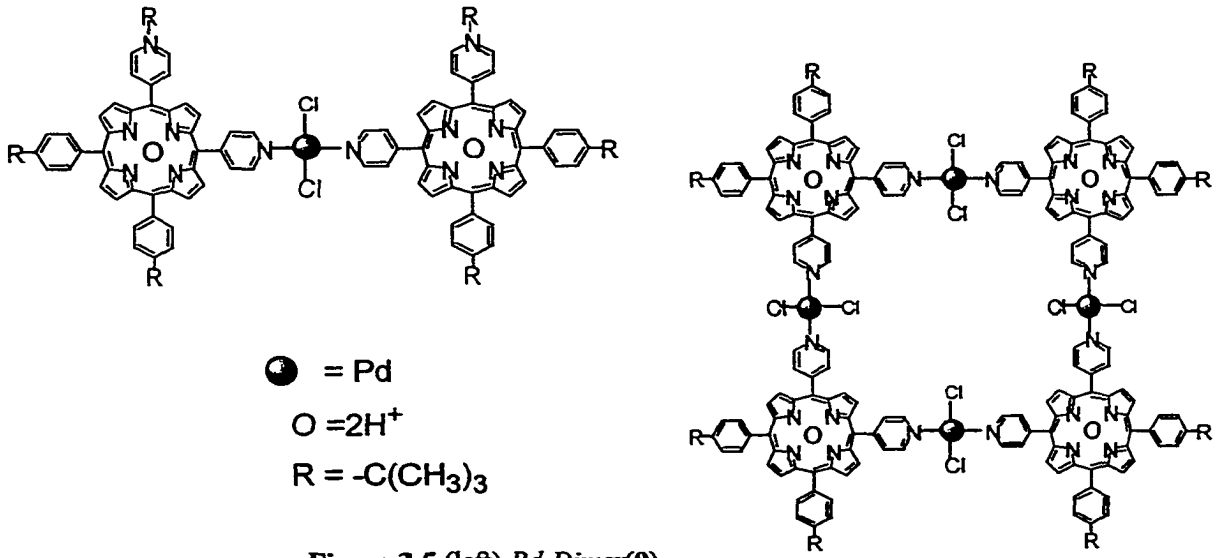

Figure 3.5 (left) *Pd-Dimer*(**9**).
(right) Pd-Square (**10**).

Array	*Red Shift (nm)*	
	Soret	*1st Q-band*
Pd-Dimer (9)	0.6	0.6
Pd-linear Tape (tetramer) (6a)	1.5	0.9
Pd-Square (tetramer) (10)	1.5	1.5
Pt-Planar Tape (tetramer) (8a)	2.4	1.8
Pd-Nonamer (4a)	8.1	6.6

Table 3.2 *Red shifts of the Soret and highest in energy Q-band in the UV-Vis spectra. 1μM conc. for the resulrting species in toluene. tertbutyl phenyl porphyrins were used as building units.*

Still the nonamer exhibits the largest red shift while the dimer the smallest red shift. This is attributed to the number of building units and the existence of intramolecular exciton coupling between the porphyrin chromophores. More extended electronic communication is responsible for the greater red shift observed at the UV-Vis spectra of the nonamer. Among the three tetramers, the largest shift is observed for the Pt-containing array. This is due to the stronger character of the Pt-N bond, compared to the labile character of the Pd-N bond something that has been studied by Fujita[3.17] The greater intramolecular exciton coupling between the porphnyrin of the square tetramer compared to that observed for the Pd-linear tape is also attributed to the geometry of the species. More extended electron communication is observed among the coplanar building units of the square planar Pt-arrays than of the linear Pd-tapes in which the porphyrins can freely rotate around the axis that connects the metal ions.

The UV-Vis spectra of the arrays **3a-8b** reveal the broadening of the Soret band of the resulting species compared to the width of the starting porphyrins. The effect is attributed to the intramolecular exciton coupling between the porphyrin chromophores in the arrays. Also the extinction coefficient (ε) per porphyrin unit decreases upon the formation of each array as a consequence of the electron communication. An interesting observation is that upon formation of the multiporphryin arrays the shoulder on the Soret band, due to the B(0,1) transition, tends to disappears. Peak-fitting analysis of all the Soret regions for the nonamer reveals three bands at 403.5, 420.8 and 438.0nm with relative heights of 1:4.5:2.3. The soret region of the Pd tape is less well resolved, but three peaks are formed here as well. The Pt-tape, on the other hand, showed three Soret bands as well.

3.2.2.2 NMR studies

^{1}H-NMR titrations exhibit similar trends as those observed for other metal-mediated porphyrin arrays.[3.14a,c, 3.16, 3.18] More specifically, there is a highly characteristic shift in the pyridyl protons upon coordination of the metal ion. Compound **4a** was extensively studied and used as a model compound. In the starting stoichiometric mixture of the porphyrins (1X-, 4T-, and 4L-shaped), for the formation of **4a**, there are four sets of protons α to the pyridyl nitrogen atom; each signal should be a doublet, but a complex multiplet at δ=9.051ppm is observed in the ^{1}H-NMR spectrum due to the mixture. As $PdCl_2(PhCN)_2$ is titrated into a 70μM stoichiometric mixture of the porphyrins the peaks at 9.051ppm decreases in intensity as new peaks, at 9.454ppm, grow in (Fig 3.6). The miltiplet observed at 8.13ppm due to the protons β to the pyridyl nitrogen atom, in the ^{1}H-NMR spectrum of the starting porphyrins, (fig. 3.6) is shifted to 8.32ppm after the addition of the $PdCl_2(PhCN)_2$. The signals for the *tert*-butyl protons shift and split from one peak at 1.621ppm to two peaks of 1.627 and 1.634ppm with the excepted ratio of 2:1 (not shown) and broaden slightly. The coexistance of the three peaks (at 1.621, 1.627, and 1.634ppm), in the ^{1}H-NMR of the final product, indicates equilibrium between the starting material and the final product. This is expected for the labile character of the Pd-N bond. The ratio between the three peaks indicates a greater than 70% yield for **4a** in the reaction mixture. Although these new resonances are broader, consistent with the large increase in molecular size and slower tumbling, the line width indicates that the material in solution is of the size expected for **4a**.

The labile character of Pd-N bond leads to an equilibrium for the formation of the Pd-containing arrays, as shown by NMR and UV-Vis experiments. The Pt-planar tape 7 goes to completion as indicated by ^{195}Pt-NMR, and ^{1}H-NMR

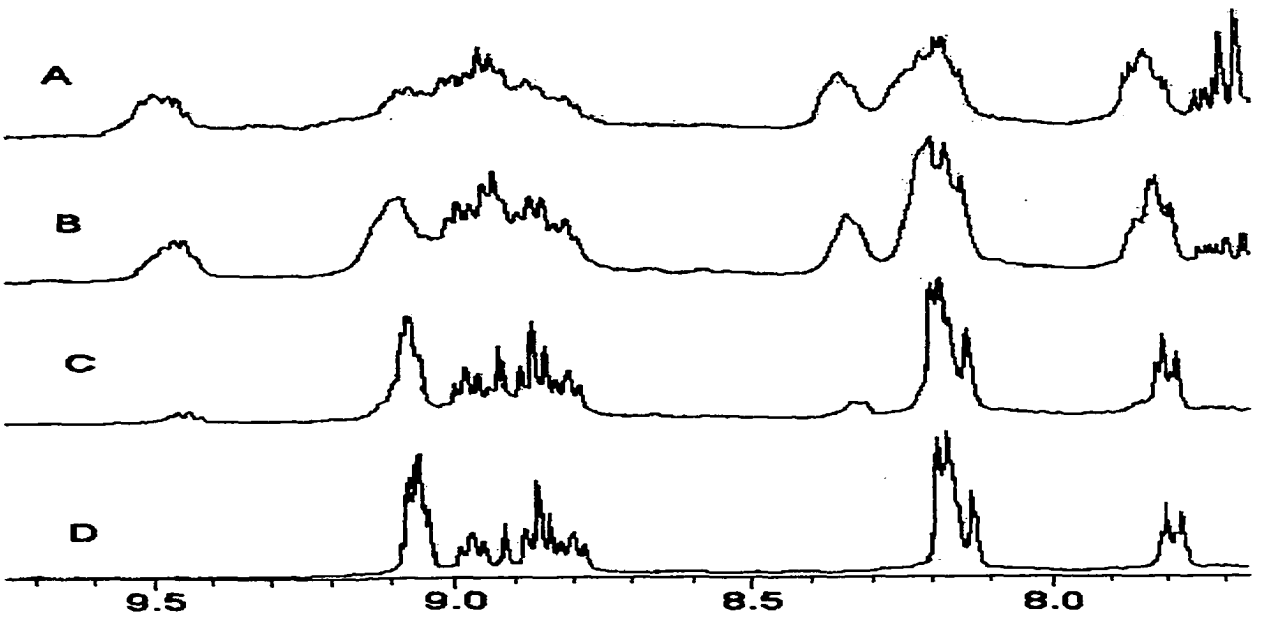

Figure 3.6 *^{1}H-NMR titration of the T,L,X-porphyrin mixture with trans $Pd(PhCN)_2Cl_2$*
A. 100% of the Pd compound added to form the nonameric array.
B. 50% of the Pd compound added.
C. 25% of the Pd compound added.
D. mixture of the porphyrins.

3.2.2.3. ESI-MS

Electrospray mass spectra of the **3a** (in $CHCl_3$ with 0.3% trifluoroacetic acid) shows the expected signals for molecular ions with charges of 3+ and 4+, consistent with the array. Figure 3.7 shows the tri- and tetra-protonated nonamer at m/z=2619 and 1965, respectively.

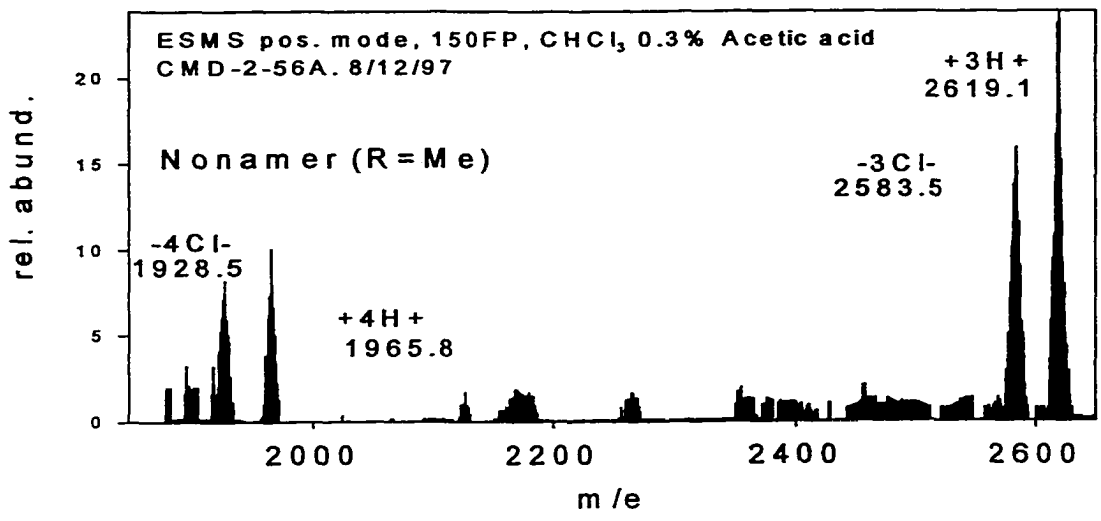

Figure 3.7. *Electrospray MS of **3a**, positive ion mode, 120 ionizer, direct injection, 0.1ml min^{-1}, carrier gas 1ml min^{-1}. Similar results are found for **4a**.*

The highly characteristic envelope due to the various isotopes, especially of Cl and Pd, greatly assist in the identification of the arrays. Additionally it shows the loss of three and four chloride ions at m/z=2583 and 1928 respectively.

3.2.2.4 Formation of Nanoparticles[3.15]

Light scattering results suggest that clusters with a radius of 5-7nm are present in solutions of the nanomer **4a** in toluene or chloroform. Depending on solution conditions, deposition of the aggregates of nonameric arrays on polished glass substrates allows characterization of the three-dimensional arrangement of these clusters of **4a** by contact mode atomic force microscopy (AFM). These studies suggest that there is weak interaction between the nanoparticles of **4a** and the glass. Non-contact mode AFM indicates that the nonameric arrays deposit as columnar structures on the glass surface, potentially as nanocrystals (fig. 3.8).

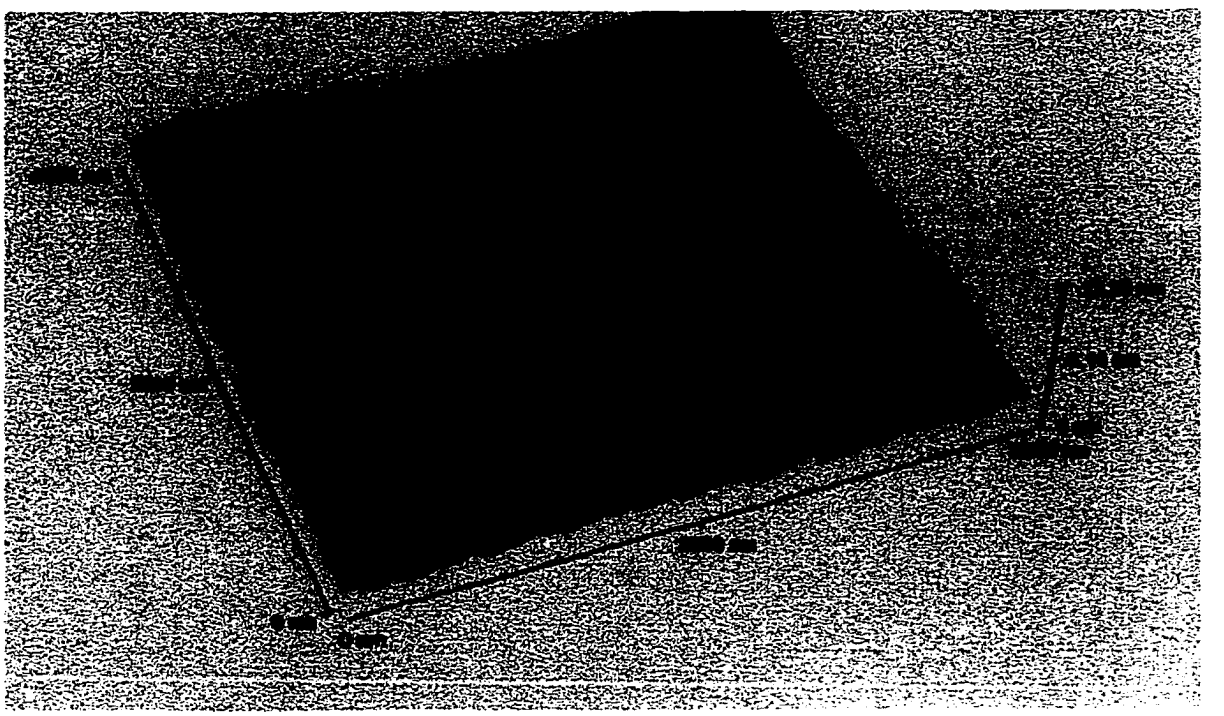

Figure 3.8 *Topography. Typical atomic force microscopy image of* ***4a*** *on a glass surface showing the sharp AFM probe tip structure produced from scanning the columnar stacks of nonameric arrays.*

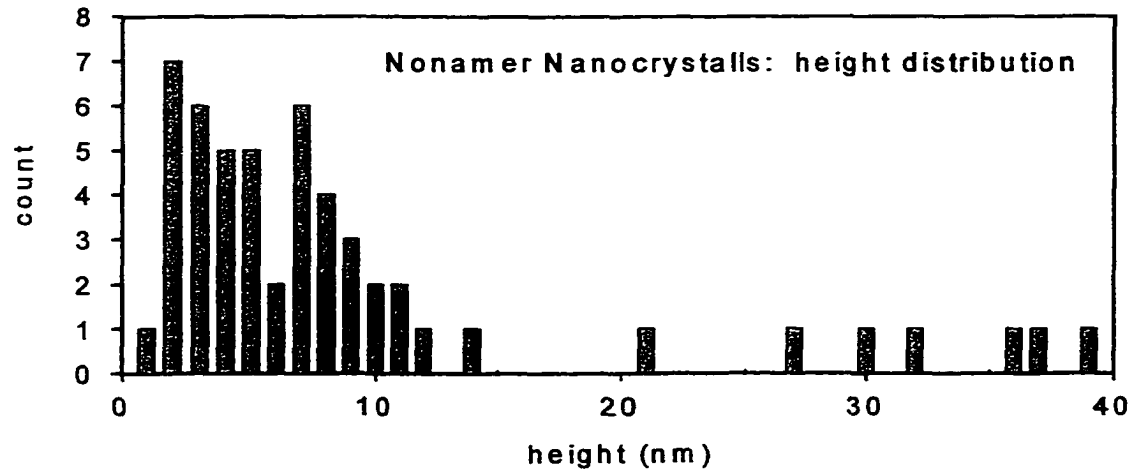

Figure 3.9 *Height distribution of nanocrystalline nonameric arrays of* ***4a*** *on glass as determined by non-contact scanning AFM.*

The clusters range in height from 1.3 to 39nm with over 75% between 4.5-6.5nm (fig. 3.9), which is consistent with the light-scattering data. Widths of 5nm for single nonameric arrays on the surface were not observed, because the images of the clusters so closely match that of the expected AFM tip profile. The nonamers likely stack as columns on the surface with widths less than that of the nominal radius of curvature of the AFM probe tip that is about 20nm. Therefore, such sharp, clear image of the tip structure, as those obtained in figure 3.8 strongly suggest that nonamers deposit as columnar stacks on the order of 5nm tall with a radius of less than 10nm. These arrangements are induced by a significant intermolecular pi-stacking energy of about 5kcal/mol per porphyrin face depending on solvent and concentration. These nanocrystalline materials or aggregates are expected to have interesting photo- and electro-chemical properties and are currently under further investigation.

For the deposition, the glass slides were thoroughly cleaned and dipped into a 0.5μM solution of **4a** in toluene (formed at 1μM and diluted) for 10 minutes. Plates, after the deposition, were rinsed with chloroform and dried under a vacuum for several days. Control experiments with individual porphyrins, mixture of them, or the Pd complex gave no discernable structures. Many different samples and tips yield the same results.

3.2.3 Metalation of the Arrays

The metalated linear tape **6b** and square **4b** have been obtained by metalation of the building blocks and by metalation of the multiporphyrin arrays. Treatment of the metalated subunits with the transition metal complex (fig. 3.11), $PdCl_2BN_2$, had significant solubility problems due to the well-known lower solubility of the metallo-porphyrins in most organic solvents. Metalation of the porphyrins results in increased bacisity of the pyridyl nirtogens, which in turns increases the strength of the pyridyl Pd bond in the macrocycle. This alone will shift the equilibrium of the self-assembly towards the nonamer **4b,** but requires additional time or heat to assure that thermodynamic equilibrium is reached. The reasons for this are essentially three-fold.

1. The stronger the intramolecular force(s), the greater the energy needed to "anneal" the system and achieve the thermodynamic product.
2. The open axial position on the zinc porphyrins affords additional sites for the pyridyl groups to coordinate, but this is a much weaker interaction than with Pd. Thus at minimum, the presence of the zinc porphyrins complicates the assembly mechamism by adding additional erroneous steps and therefore additional annealing steps.
3. An additional factor is the decreased solubility of the zinc porphyrins compared to their free base precursors, which either sets limits on experimental conditions or requires additional heat to reach the thermodynamic product.

Also, zinc-metallated Pd-containing arrays, *e.g.* **4b**, were formed in one step process by mixing the stochiometric amount of porphyrins, the Pd(II) complex, and a 10-fold excess

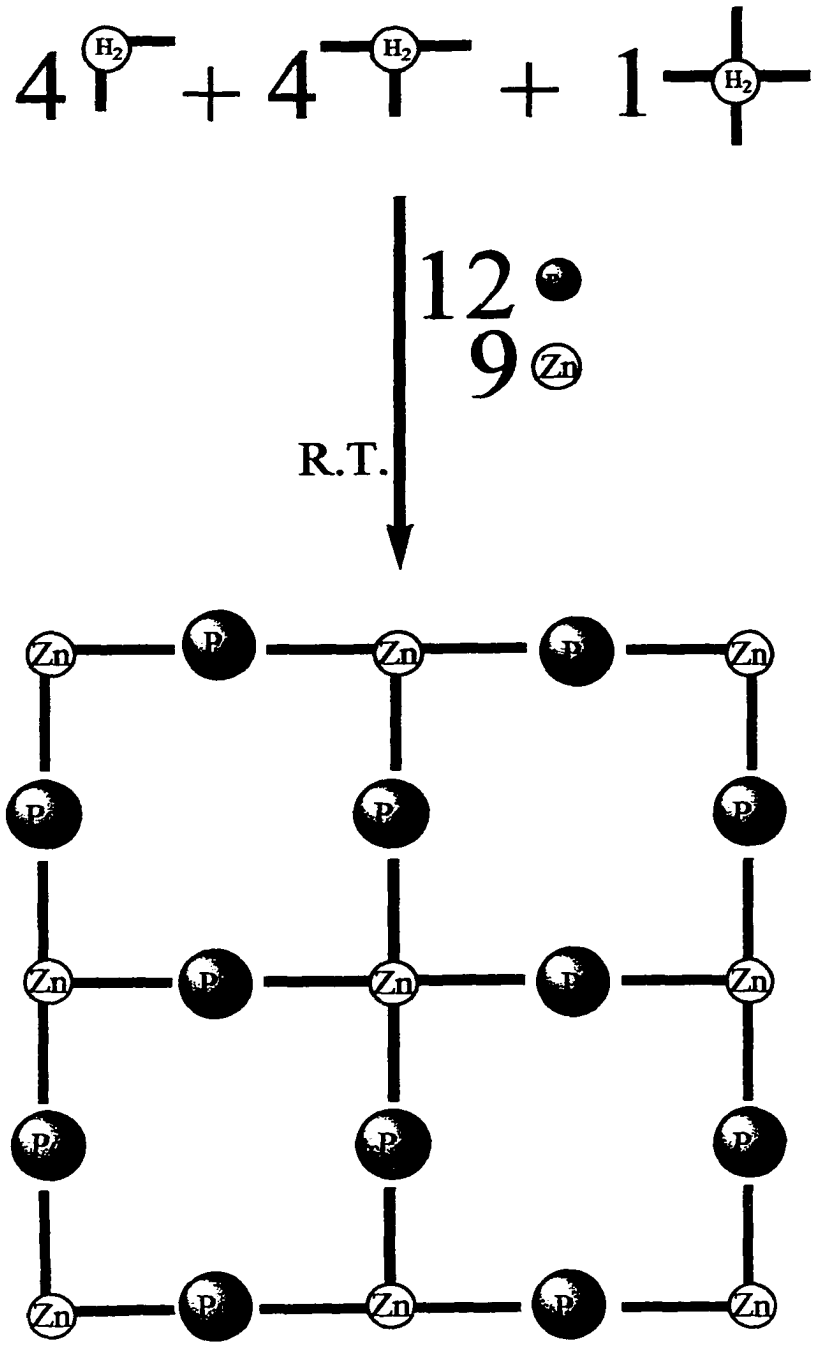

***Figure 3.10** Formation of the metallated nonamer **4b** in one step.*

of $Zn(AcO)_2$ (fig. 3.12). In this system we bring together 30 molecules, that represent 5 different types, to form a 5x5 array. The formation of the metallated array was confirmed by the absence of two out of the four Q-bands in the UV-Vis spectra of the resulting species (fig. 3.12). UV-Vis data show that the selectivity observed in this experiment is due to the different reactivity of the two metals and different strength of Zn-Py-N and Pd-Py-N bonds. Though porphyrins chelate Pd(II) stronger than Zn(II), there is a substatial activation energy because of the differences in ionic radii and solvation effects.

Figure 3.11 shows the UV-Vis spectra of the three metallo-porphyrin mixture, at the appropriate stochiometric amounts, before and one week after the addition of the Pd complex. The formation of the metallo array **4b** is responsible for the observed red shift while the reasons for the low yield (strong intramolecular forces, self-coordination, and decreased solubility for the metallo-species) have been discussed earlier.

Figure 3.12 shows the UV-Vis spectra of the three free base porphyrins, at the correct stochiometric ratios, before the addition of the Pd(II) and Zn(II) complexes, immediately after the addition, and one week later. The order that the metals were added does not seem to make any difference for the experiment, since UV-Vis spectra shows no change of the UV-Vis spectra of the mixture after the addition of the Zn(II) to the porphyrin mixture in the absence of the Pd(II) complex. The experimental data show that immediately after the addition of the two metals, the free-base nonamer is formed preferentially while its metalation takes place at a later and slower step. The metalation of the array is proved by the absence of the two out of the four Q-bands in the UV-Vis

spectra (fig. 3.12). The spectra of the resulting species one week after the addition of the two metals, Zn(II) and Pd(II) resembles to that of that formed from the metallo-subunits. Although the more red shifted spectra observed in figure 3.12 indicates the greater yield of the assembly by mixing the free-base subunits with the two metals. Zinc metalation of the assembly was faster than metalation of the individual species, without requiring external heat for the metallation. This is attributed to the increased basicity of the inner pyrrole nitrogens upon Pd binding to the pyridyl groups..

Therefore it seems feasible to assemble the metalated array *in situ* from the 30 constituent parts - 9porphyrins, 9 zinc, and 12 palladiums for the formation of a 5x5nm array.

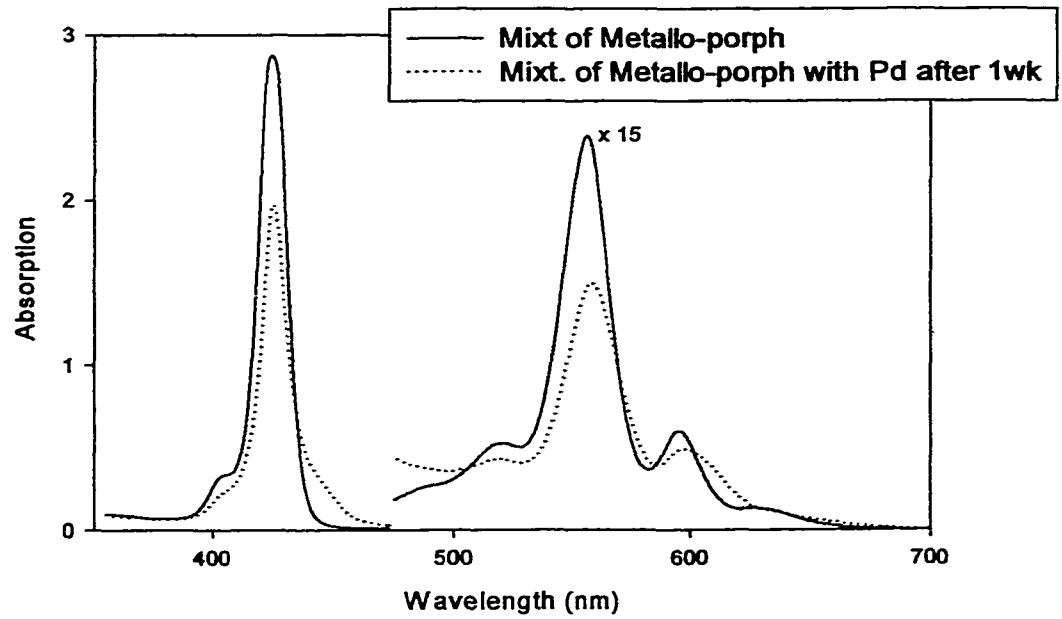

	Porphyrin Mixture	*Porphyrin Mixture with Zn(II) and Pd(II) after 1week*
Soret *(nm)*	425.0	425.5 (shoulder at ~440.0)
1st Q-band *(nm)*	555.5	557.5

Figure 3.11 *UV-Vis. spectra. Incomplete formation of* ***4b*** *by mixing Zn metallo-porphyrins with* $(PhCn)_2PdCl_2$ *in a 1x1cm cuvette. Total porphyrin concentration is 9μM.*

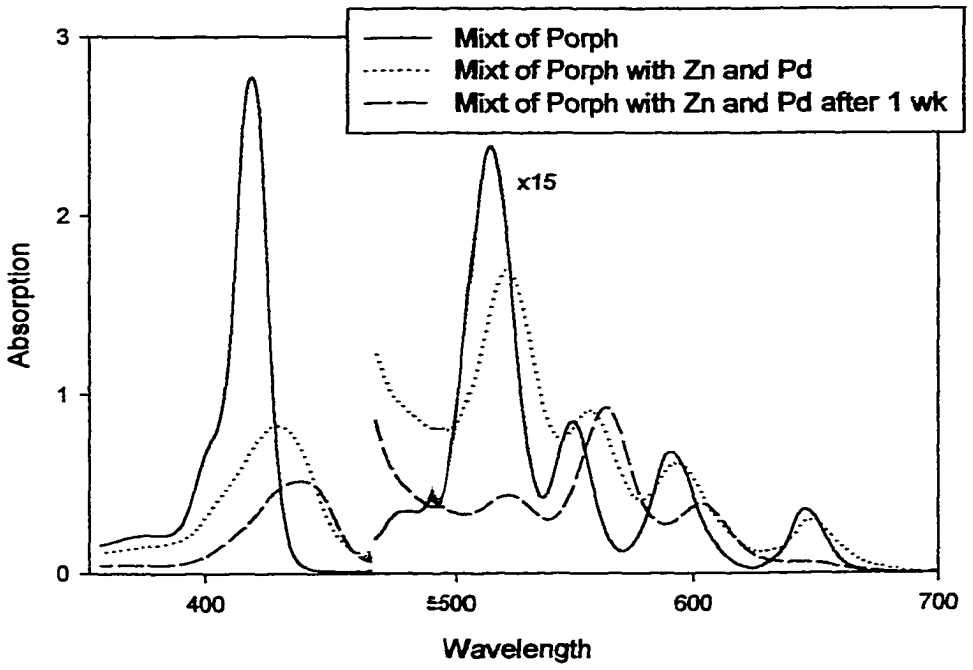

	Porphyrin Mixture	*Porphyrin Mixture with Zn(II) and Pd(II)*	*Porphyrin Mixture with Zn(II) and Pd(II) after 1 week*
Soret (nm)	419.5	430.5	440.0
1st Q-band (nm)	514.0	520.0	521.5 (next Q-band at 563.0)

Figure 3.12 UV-Vis. spectra. Nearly quantitative formation of ***4b*** *by mixing free-base porphyrins with the Zn(II), $(PhCN)_2PdCl_2$ and starting material in a 1x1cm cuvette. Total porphyrin concentration is 9μM.*

3.2.4 Attempts for the Formation of a 3-Dimensional Array

The three-dimensional array (fig. 3.13) can be formed upon titration of 4.5 equivalents of 4,4'-bipyridine (bpy) to a solution of Zn metalated array **4b** to give a "sandwich" of nine bpy molecules between two nonamer Zinc-porphyrin arrays. The 3-D array contains 18 porphyrins in one system. Figure C1.appendix shows the emission titration of the metallo-porphyrin mixture, in toluene, with the Pd complex for the formation of the metalated nonamer **4b**. The titration shows about 90% quenching, as expected.

The UV-Vis titration (fig. C2.appendix) shows that upon addition of the bpy in the

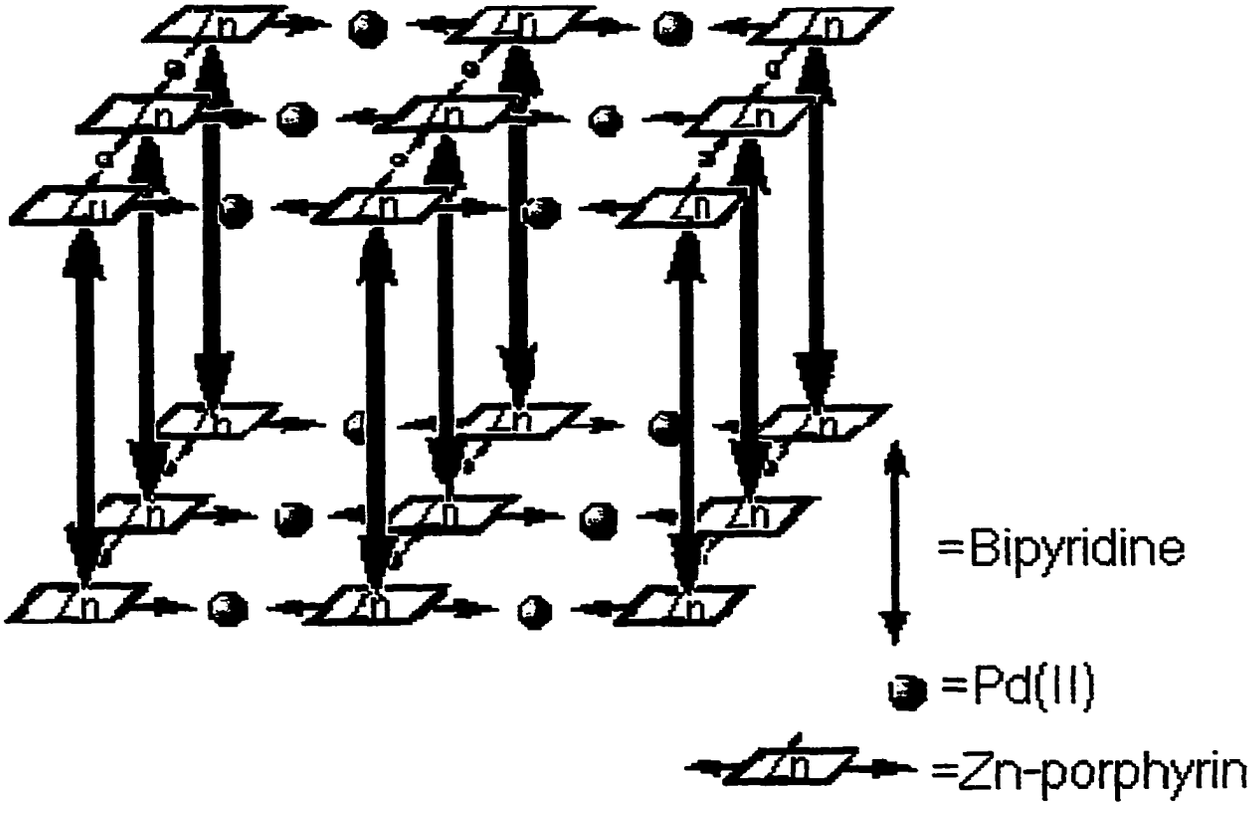

Figure 3.13 3-D Array.

metallo-array **4b**, in toluene, lower extinction coeffecient (ε) for the resulting species is observed. The same experiment indicates some precipitation after the addition of the bpy. That weakens the argument that the bpy may break up the nonamer or aggregates. If that were the case, the product(s) would be expected to have greater solubility in organic solvents, making the amount of porphyrin in solution, and concequently the area under the peak, greater. The small precipitation after the addition of the bpy indicates the formation of larger species but not polymers that could further reduce the solubility of the product(s) in the media. Although a further blue or red shift is not observed indicating that there is no additional electronic communication through space between the two parallel arrays, maybe a shorter ligand would give different results.

Figure C3 in appendix shows the emission titration of 4.5eq. of bpy in the toluene solution of **4b**. A small increase of the fluorescence emission is observed upon the addition of the bpy indicating that self-absorption becomes less important in the new solution but not significantly different. The time between each aliquot was 5 minutes while the bpy was added to the metallo-nonamer after the solution had been left at R.T. for 15 minutes.

The above work indicates possible formation of the desired product (fig. 3.13), but for complete characterization of the array additional experiments are required.

3.3 Hydrogen-Bonded Complexes

Hydrogen-bonding is a donor acceptor interaction involving hydrogen atoms. Very strong hydrogen bonds resemble covalent bonds, while very weak hydrogen bonds are close to Van der Waals forces. The majority of the hydrogen bonds are distributed between these two extremes. Hydrogen bond energies extend from about 15-40 Kcal/mol, for strong bonds, to 4-15 Kcal/mol for moderate bonds and 1-4 Kcal/mol for weak bonds.

Strong hydrogen bonds are formed by groups in which there is a deficiency of electron density in the donor group D, e.g., $RO^{+}H_2$, and/or an excess of electron density in the acceptor group A, e.g., F^{-}, RO^{-}. Moderate hydrogen bonds are formed generally by neutral donor and acceptor groups, i.e., -O-H, in which donor atoms are electronegative relative to hydrogen and the acceptor atoms have lone-pair electrons. Weak hydrogen-bonds are formed when the hydrogen atoms covalently bonded to a slightly more electronegative atom relative to hydrogen, as in C-H, or when the acceptor group has no lone-pairs but has π-electrons, such as C≡C or an aromatic ring.[3.19]

Electron density studies show accumulation of electron density between the atoms in the D-H covalent bond, with anelectron density deficiency at the proton position, leaving the proton partially deshielded. This gives rise to a strong dipole that makes the hydrogen bond unique. For no other atom there is an equivalent deshielding as of the proton on

formation of a polar covalent bond. The nearest is the Li-A bond where the deshielding can be as high as 20% of that observed with hydrogen.[3.20, 3.21]

In many biological systems, hydrogen bonding is a way of achieving supramolecular self-assembly. It has been used as a process for the formation of new materials. The principles of this intermolecular synthetic chemistry together with a significant number of characteristic examples have been included in several reviews.[3.22, 3.23, 3.24] The crucial parameter for the formation of useful materials by intermolecular interactions is that the equilibrium must be shifted to the formation of association complexes. Otherwise, a mixture of the interacting components with the hydrogen-bonded complex is obtained. Common practice for efficient interaction between the complementary components is the formation of a multiple hydrogen bonds coupled with cooperative interactions.

However, in order to achieve a supramolecular macrocycle based on H-bonding information, it is necessary first to design a suitable pattern of H-bond donor (D) / acceptor (A) sites. 5,10(AA)15,20(tbuPh)PH_2 (**12**) possessing DADA/ ADAD, can only form a fully interconnected array in a square arrangement (**17**), in figure 3.16. Figure 3.15 illustrates examples of 1-dimensional H-bonded motifs, where **15** represent homo-complimentary and **16** hetero-complementary one-dimensional examples. Similary, figure 3.16 illustrates examples of homo-complementary **17** and hetero-complimentary **18** two-dimentional H-bonded motifs. The challenge for the formation of the 2-dimensional motifs was to have sufficiently stable 1-dimensional species so their integrity maintains in the more flexible and complex 2-D system.

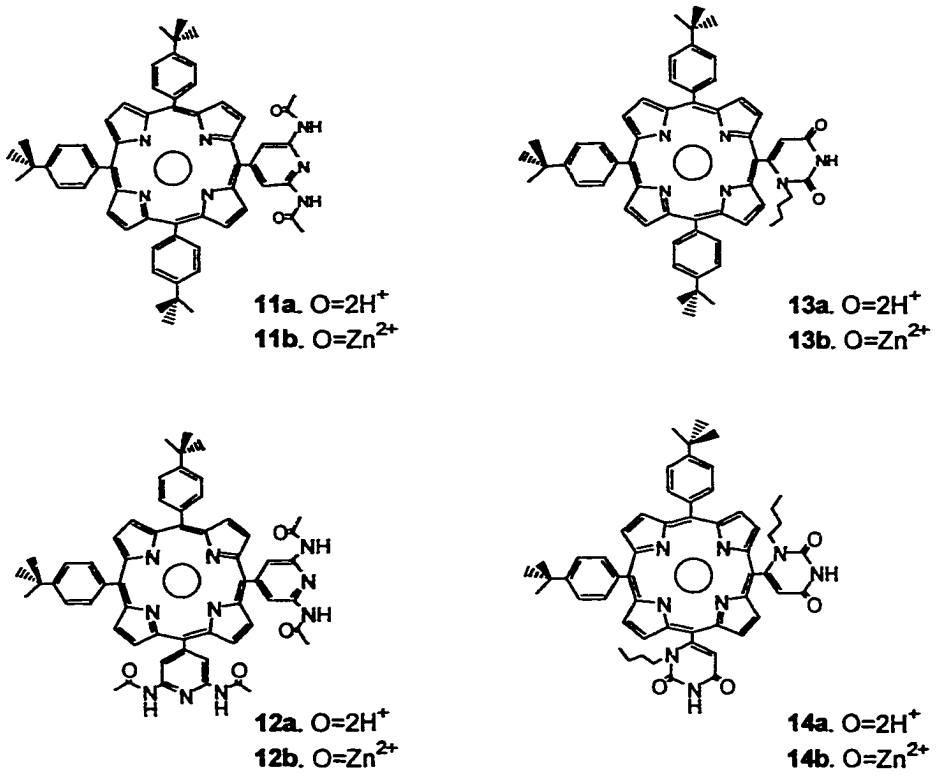

Figure 3.14 Mono and di acetoaminopyridyl- and uracyl- porphyrins.

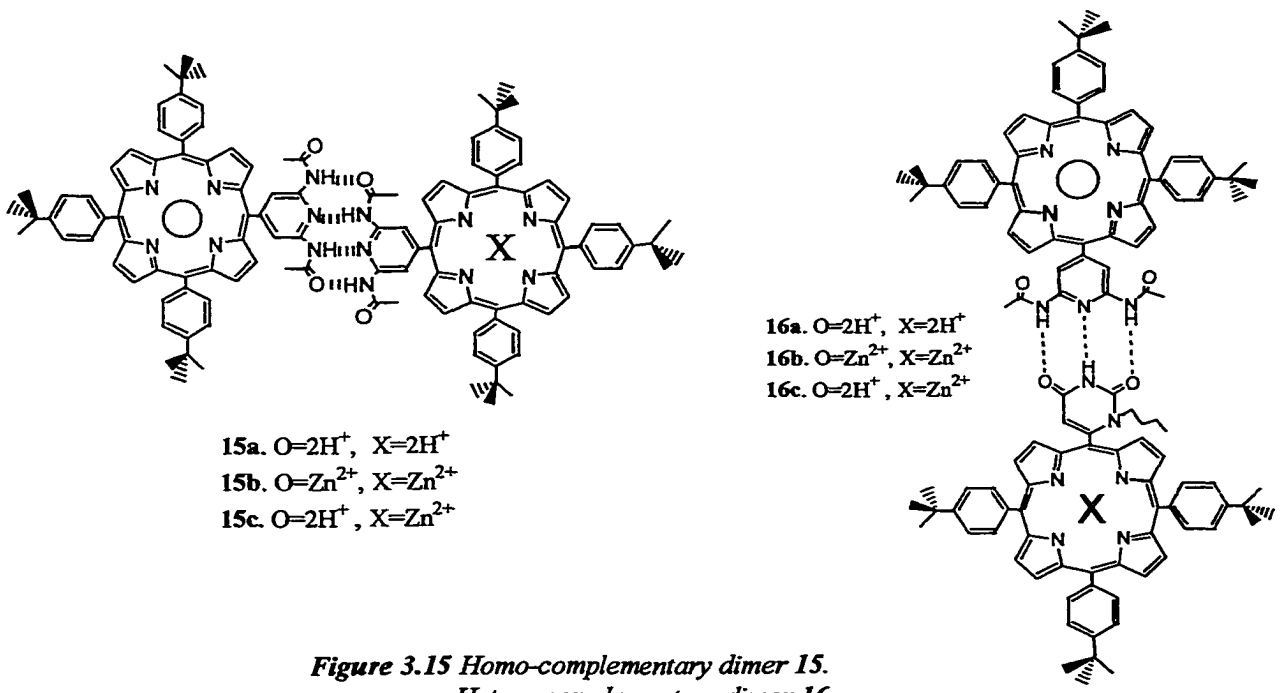

Figure 3.15 Homo-complementary dimer 15.
Hetero-complementary dimer 16.

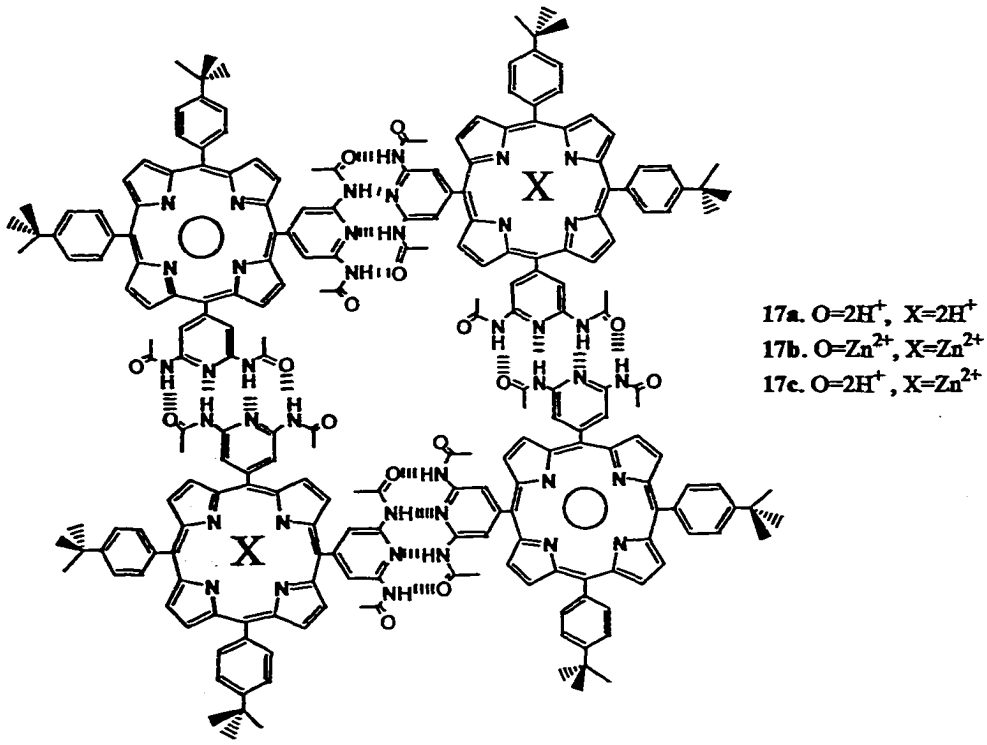

17a. O=$2H^+$, X=$2H^+$
17b. O=Zn^{2+}, X=Zn^{2+}
17c. O=$2H^+$, X=Zn^{2+}

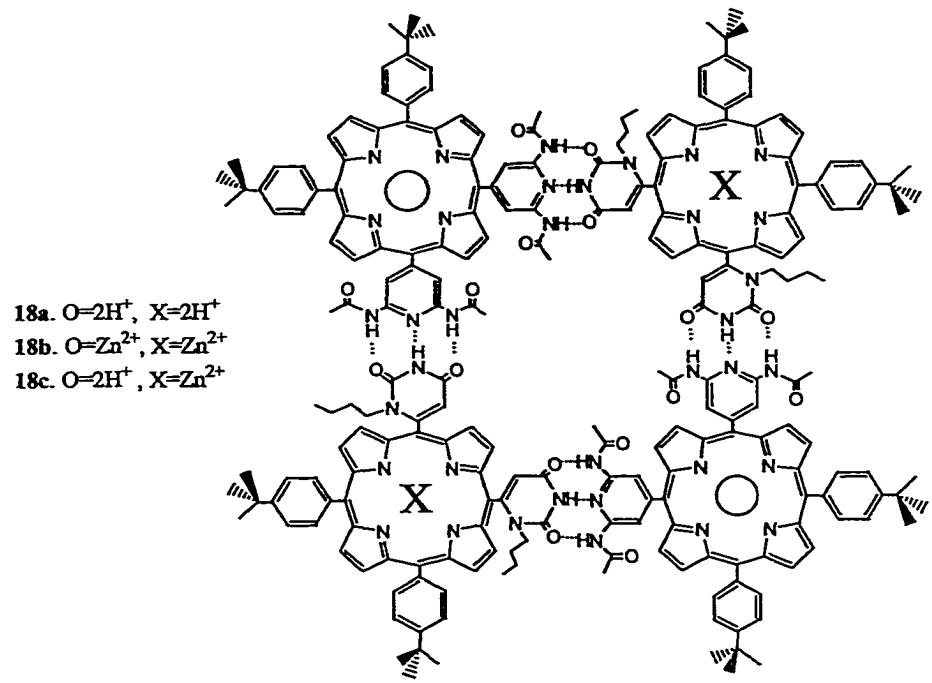

18a. O=$2H^+$, X=$2H^+$
18b. O=Zn^{2+}, X=Zn^{2+}
18c. O=$2H^+$, X=Zn^{2+}

Figure 3.16 Homo-complementary square tetramer 17.
Hetero-complementary square tetramer 18.

In addition to hydrogen bonding interactions, aromatic stacking, hydrophobic interactions, coordination bonds, ionic and/or secondary interactions are all factors that contribute to the hydrogen bond strength between the components of the complexes.

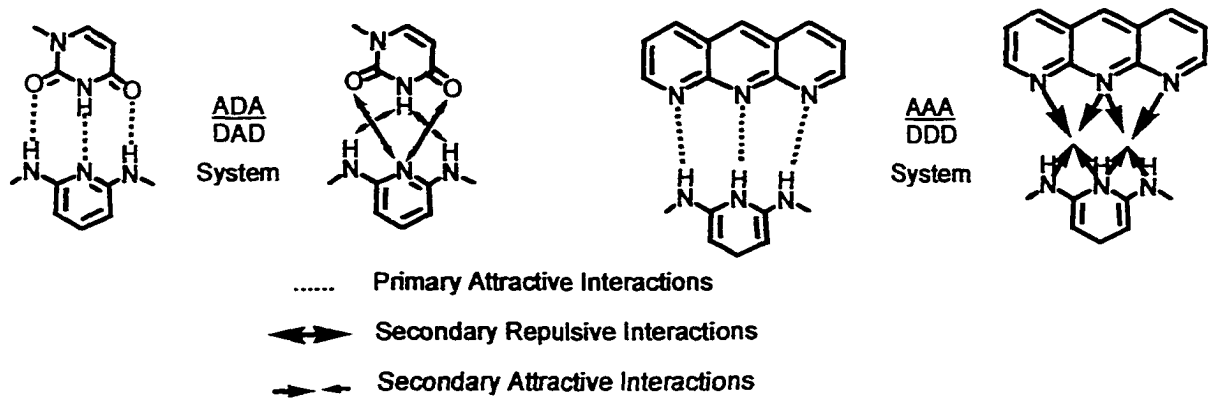

Figure 3.17 Triple hydrogen bonded donor/acceptor complexes of different pattern.[3.25]

It has been shown[3.25] that alternation of hydrogen bond donors (D) and acceptors (A) in the same functional group lowers the association constant and thus the overall binding free energy of a pair or molecules. For acceptor and donor groups involved in hydrogen bonds, a destabilizing effect of approximately 7KJmol^{-1} per secondary interaction is derived from calculations. If the groups responsible for the secondary interactions are not involved in hydrogen bond the destabilization is estimated to be approximately 11KJmol^{-1}. When a molecule consists of all donors and the corresponding partner of all acceptors, the secondary interactions are favorable, producing a stronger hydrogen bonded complex. The concept is shematically explained by secondary repulsive or attractive interactions in figure 3.17. The association constants of such triply h-bonded systems in chloroform vary between 10^2-10^3M^{-1} for DAD/ADA pairs and 10^5-10^6M^{-1} for DDD/AAA.

The strength of the hydrogen bond is also related to the acidity of the donor and the basicity of the acceptor. In our systems we are using diacetoamidopyridyl (AA) groups at the *meso* positions of the porphyrins. The acylation of the amino groups introduces two extra secondary repulsive interactions but also increases the acidity of the amino groups. It has been shown[3.25b] on similar systems, the the K_a, of the acylated species is 10-fold higher than that of the aminopyridyl groups under identical conditions.

The influence of solvent in hydrogen bonding has been studied by Lorenzi.[3.26] In these studies, it was shown that dimerization, of a small cyclic peptide, was not observed in chloroform while in a less competitive solvent like carbon tetrachloride a dimerization constant of 80 M^{-1} was calculated from the data. The solvation of the binding site is a critical factor on the strength of the binding at any kind of chemical interaction and more crucial in systems governed by the relatively weak character of hydrogen bonds. Compounds **15,16,17,18** have been formed in $CHCl_3$ as well as in toluene where the association contants are found to be higher.

Porphyrins **11, 12, 13,** and **14** were prepared by Xinxu Shi in the lab.[3.27] Formation of the dimers **15a**, **16a**, and square tetramers **17a** and **18a**, at relatively high concentrations, was confirmed by ^{1}H-NMR studies, in $CDCl_3$, and the results for the self-complementary **15a** and **17a** are reported in the literature.[3.28] the hetero-complementary assemblies are also characterized.[3.28b] Electron communication in the excited state and energy transfer has been studied and will be introduced in Chapter 5. ^{1}H-NMR experiments, done by X. Shi, are summarized for the characterization of **15a** and **17a**, as characteristic examples.

For all the hydrogen-bonded species, there is no a *priori* reason that all of the self-assembled structures in the chloroform solution are strictly the indicated products. The experimental results are likely indicative of a mixture of dimers, trimers, tetramers, etc. substantially weighted toward the structure resulting from the starting stoichiometries by ΔG.

3.3.1 ^{1}H-NMR Studies

If there are no dynamic processes occurring on the NMR time scale, both the number of species self-assembling into the final structure, n, and the association constants K_a can be determined by ^{1}H-NMR experiments that monitor the chemical shift of suitable protons versus the concentration of the self-complementary porphyrin.[3.29]

Formation of the hydrogen-bonded species at high concentration was confirmed by ^{1}H-NMR studies. Specifically, as illustrated in figure 3.19, analysis of the downfield shift for the amide (N-H) as the function of its increasing concentration in $CDCl_3$ provides support for the formation of the H-bonded assemblies. Curve fitting methods yield n=3.9 for the square, ~2.0 for the dimeric structure, and n=4.1 for a 2:2 ratio of the 5,15(AA)10,20(tbuPh)PH_2, **12a**, and 5(AA)10,15,20(tbuPh)PH_2, **11a**, the 4-membered tape, **19**, is shown in figure 3.18.

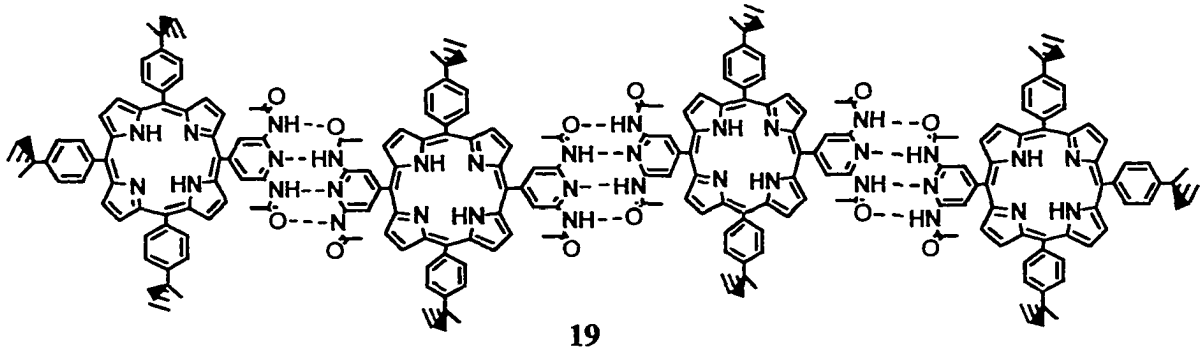

19

Figure 3.18 Homo-complementary tape (**19**).

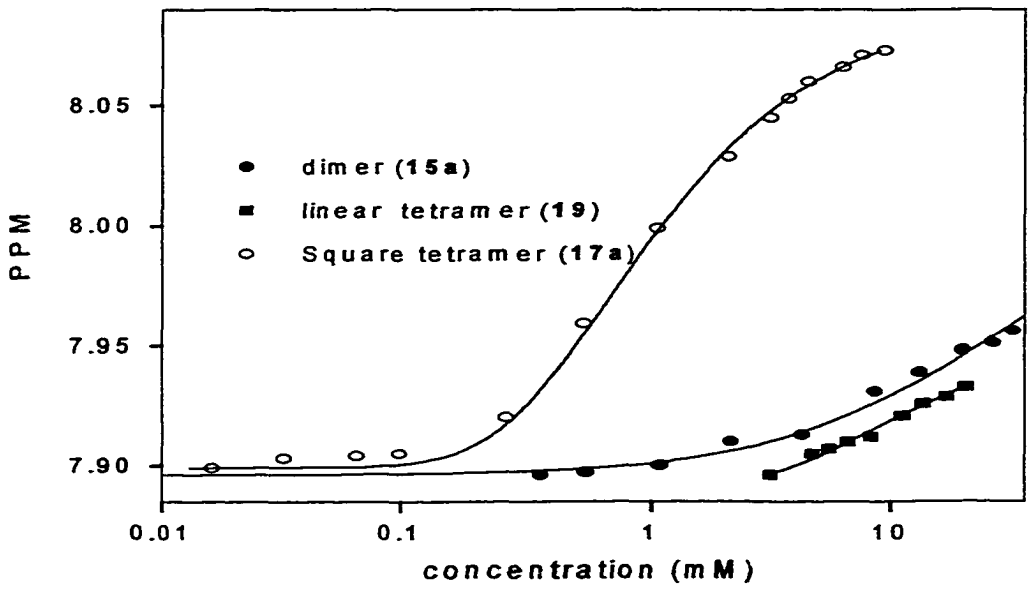

Figure 3.19 *Chemical shift vs. concentration plots for the self-complimentary porphyrins. At any concentration or temperature, only one amide proton is observed; thus supporting the quadruple and dynamic nature of the intermolecular interactions.*

Even if there are several products or dynamic processes, such as the breaking apart of one or more sets of hydrogen bonds occurring on the NMR time scale, these results will mostly affect K_α and to a much lesser extent n. Table 3.3 summarized the results of the fits of the ^{1}H-NMR including the number of particles, n, and association constants, K_α.

The chloroform solution of the hetero-complementary square **18a** is expected to consist of a mixture of the two homo-complementary square tetramers and the desired hetero-complementary species. Due to the weak hydrogen bond character of the uracyl self-complementary dimer (2-4 Kcal/mole), the amount of the self-complementary uracyl porphyrin oligomers in the reaction mixture is expected to be low. The same is true for the association constant of the acetoaminopyridyl in the homo-complementary square (~4

Kcal/mole). Consequently, for thermodynamic reasons, the system, consisting of 1:1 in **12a** and **14a**, is expected to favor the formation of the hetero-complementary assembly. Fluorescence experiments that prove energy transfer (see Chapter 4) between the two building units support the above theory. Also, the 180° or 90° geometry of the recognition groups on the porphyrin(s) plays the most important role in the structure of the assembly.

Array	*Number of Particles, n*	*Association Constant, K_a*	*Correlation Coefficient of the Fit, r^2*	*Conentration of Porphyrin at ½ Maximum, $C_{½}$*	*ΔG^a ($KJmol^{-1}$)*
Dimer (15a)	2±0.5	$160\pm80M^{-1}$	0.9943	125	-12.6
Linear Tape (19)	4.1±1.8	$70\pm40M^{-1}$	0.9925	111	-10.5
Square (17a)	3.9±1.1	$2400\pm220M^{-1}$	0.9977	1250	-19.3

a: calculated from $\Delta G=-RTln(K)$

***Table 3.3** Fits of the ^{1}H-NMR data at 298K in $CDCl_3$ for the self-complementary.*

In figure 3.19, the dramatic difference in the plots for the linear tetramer and closed square can be observed. The rapid increase in the chemical shift with the concentration for the linear tetramer, is indicative of the cooperative formation of a closed system with more favorable free energy.

Equilibrium constants, K_a, have been calculated by fluorescence titrations. The K_a values found by the ^{1}H-NMR data are about 4-fold weaker than those found by fluorescence quenching experiments, indicating that dynamic processes are occurring during NMR

acquisitions. Because of the different powers of the concentration units, it may be more informative and useful to compare the $C_{½}$ values, where this represents the concentration at the half maximum increase in the chemical shift. The $C_{½}$ value for the ^{1}H-NMR data of the homo-complementary square tetramer is 0.8 mM (figure 3.19) which makes it about 10 times smaller than the $C_{½}$ obtained for the homo-complementary linear dimer (8mM) and tetramer (9mM). The K_a values of the two tetramers, 2400 M^{-3} for the closed square versus that of the linear species 70 M^{-3}, illustrates the cooperativity in forming closed systems. It is worth noting that both linear systems have very similar $C_{½}$. The ^{1}H-NMR experiments is toluene-d_8, where hydrogen bonding is expected to be stronger in the less polar solvent, produce similar results although the $C_{½}$ values are about 4-fold lower for the linear assemblies and about 2-fold lower for the square.

CHAPTER 4

Photophysical Properties of Multiporphyrin Arrays

4.1 Introduction

The design of a fluorescent chemical sensor should involve:

1. recognition of the analyte and
2. signaling to the surrounding that recognition event has occurred .

Size, shape and functionality may be important for the recognition function. Molecular sensors respond to the macroscopic world by a variety of means – photo, ionic electrochemical, etc. thus a variety of instruments may be used. Fluorescence emission is widely used due to the high sensitivity and the simplicity of the method. Both the change in intensity (fig. 4.1a) or in the energy (fig. 4.1b,c) of the emitting light, due to the recognition process, can be used as a monitored property. Both examples in figure 4.1a, c. are based on electron transfer while the example in figure 4.1b is based on electron communication. If recognition significantly quenches the magnitude of the emitting light then fluorescent sensor can be used also as a switch where off and on states can be either after recognition or prior to recognition. An important requirement for a molecular switch is for the process to be reversible.[4.1]

Simply linking the subunits does not necessarily make a molecular sensor. Linkers that mediate neither energy nor electron transfer will provide a complex where the photophysical properties would be the linear combination of the starting materials. The components of the fluorescence sensor system should provide an efficient mechanism to significantly modify their emission properties after recognition. Two efficient and widely

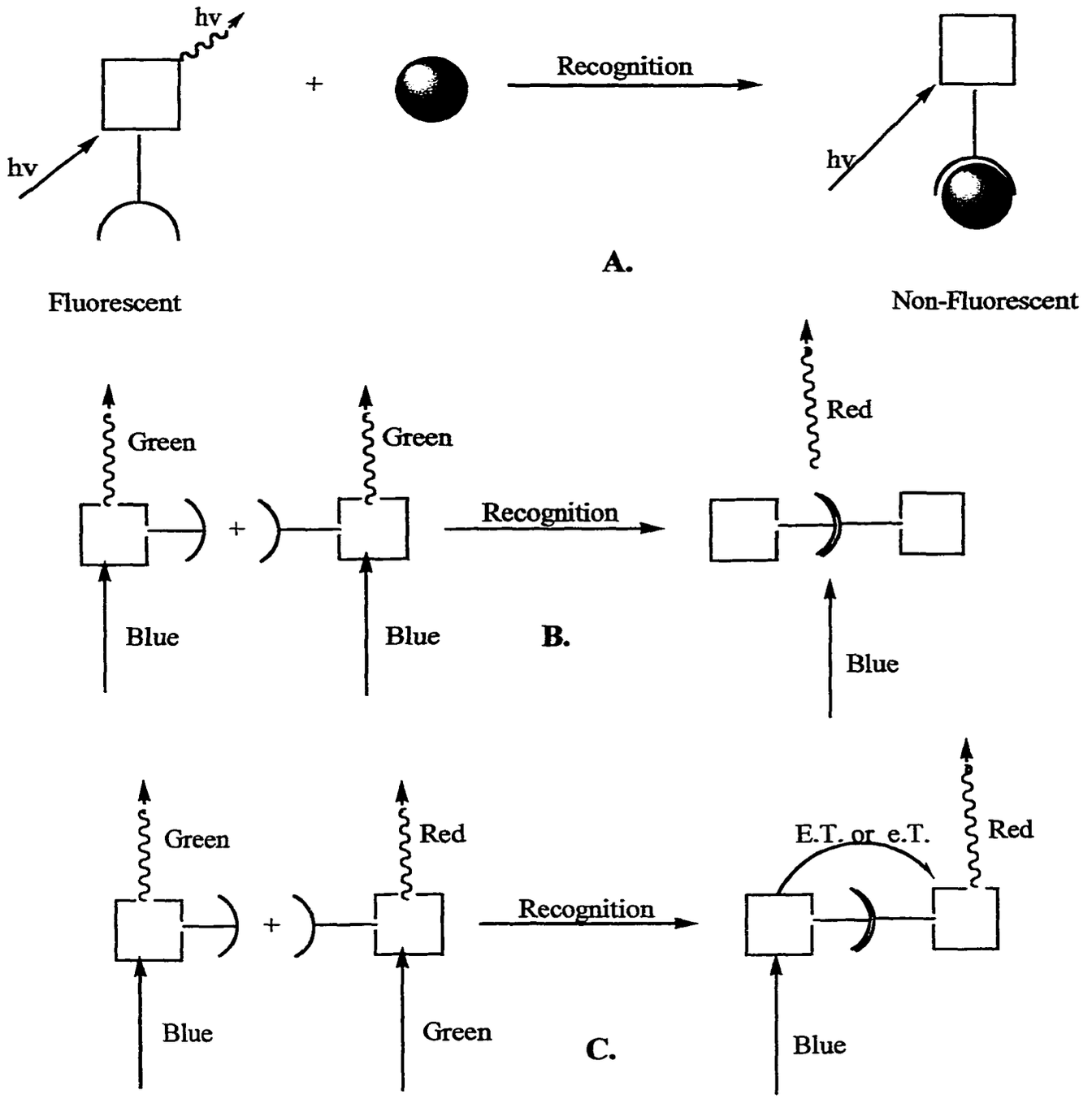

Figure 4.1 *Recognition can be used as communication link between nanoscopic and the macroscopic world by monitoring the fluorescence*

A. *Energy Transfer (ET) or electron Transfer (eT) to a non-luminescent species.*

B. *Energy Coupling in a supramolecular fluorophore.*

C. *Energy Transfer (ET) or electron Transfer (eT) to a luminescence species.*

used mechanisms available for influence the fluorphores is energy transfer (ET) and electron transfer (eT).

Also, photo-induced electron transfer plays an important role in photosynthesis, where sunlight is harnessed for the growth and nourishment of plants. The early events of photosynthesis involve light absorption by an antenna system followed by energy migration to a trap where a series of fast electron transfer events occur. The electron-transfer processes cause separation of positive and negative charges within the photosynthetic reaction centers, that are critical for the biochemical reactions.[4.2] By mimicking the light-harvesting ability of the plants, chemists have attempted to duplicate the events in photosynthesis with model porphyrin-like compounds.[3.1] These models have been used as artificial photosynthetic systems for harvesting solar energy.[4.3]

Due to the fundamental importance of photo-induced electron and energy transfer to systems like sensors, and natural light-harvesting, much effort has been expended to understand their principles. Here I will try to present a very brief mechanism of the above process, and demonstrate the existence of these processes in multi-porphyrin arrays.

Figure 4.2 illustrates the mechanism of the E.T.[4.4] from a photo-excited fluorophore P* to a metal center M. The metal M has some empty, or partially filled energy levels whose energy are between the π and π^* of the fluorophore. This requirement is easily met for aromatic fluorophores, as the energy of the π bond, that determines the π-π^* separation, is much greater than the energy of most metal-ligand interactions, that determines the

splitting of the d-orbitals. During energy transfer, exchange of two electrons takes place simultaneously: from the π^* orbital of the fluorophore to an empty d-orbital on M and from a filled orbital on the metal to the ground state π-orbital of the fluorophore. This double exchange brings the fluorophore back to the ground state P and produces an excited state metal M*. In most cases, (d-d) excited states return back to the ground state by non-radiactive pathways (vibrationally) and thus the fluorescence emission quenches. All metals with d^{1-9} electronic configuration that have at least one half-filled orbital below the energy of the π^* orbital of the fluorophore can undergo the above mechanism. In practice, it means that the d-d absorption of the metal has to be at longer wavelength than the emission of the fluorophore P. Instead of a metal, a second fluorophore can be used if the above criteria are met. For instance, energy transfer from a metalated to a non-metalated porphyrin is observed.

Figure 4.3 uses an orbital diagram[4.4] to illustrate an electron transfer (e.T.) from a fluorophore P to a metal M. The first step is determined by the redox properties of the metal (M) leading charged separated species. Back-electron transfer returns the subunits at the ground state.

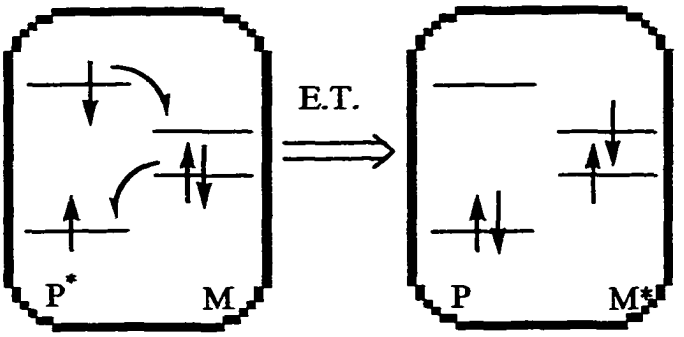

Figure 4.2 Orbital system of E.T. from a photo-excited fluorophore P to a metal center M.*[4.5]

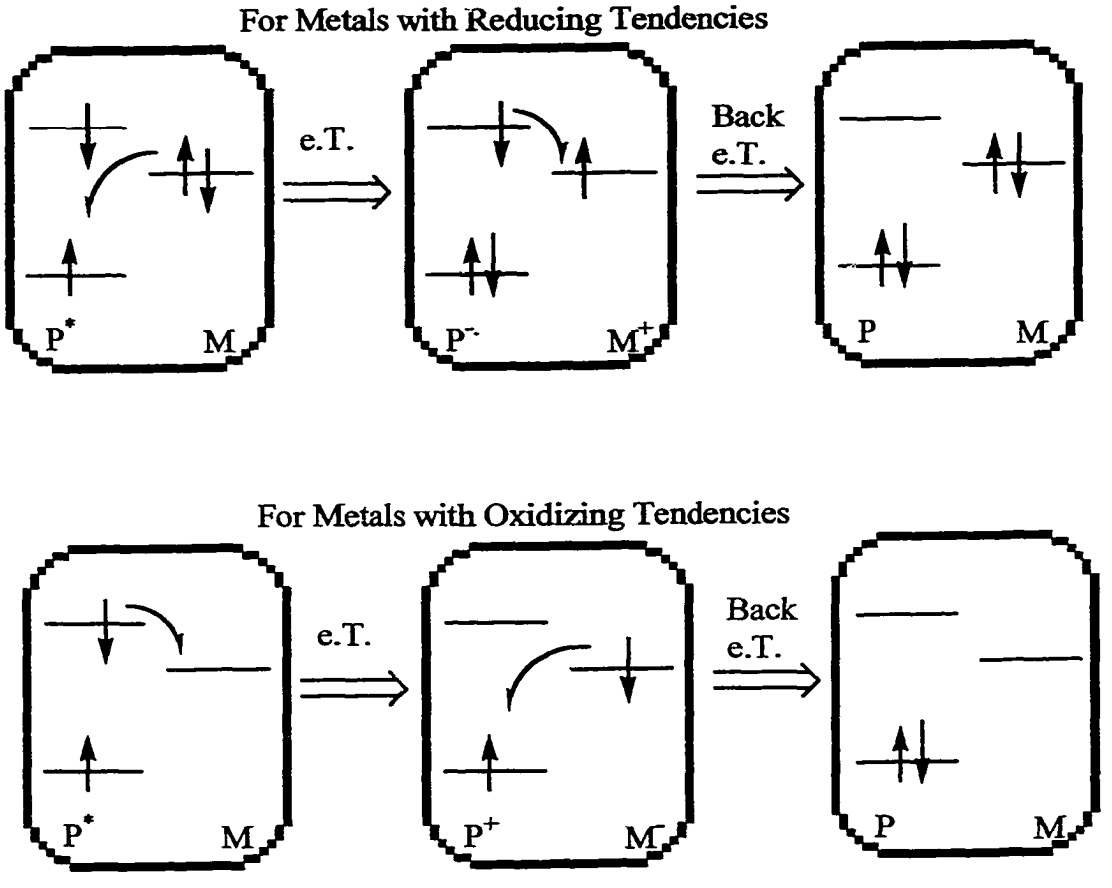

Figure 4.3 Orbital system of e.T. from a photo-excited fluorophore P to*
Upper *a metal M with reducing tendencies.*
Lower *a metal M with oxidizing tendencies.*[4.5]

4.2 Metal Mediated Arrays

4.2.1 Emission Titration

A steady decrease in the fluorescence emission spectra is observed during the titration of the Pd transition metal linker into the stochiometric porphyrin solution (fig. 4.4). An overall of 40-90% quenching in the emission of the porphyrins is observed upon formation of the supramolecular structures (table 4.1). The observed quenching is attributed to the heavy atom effect, electron communication, energy transfer between the

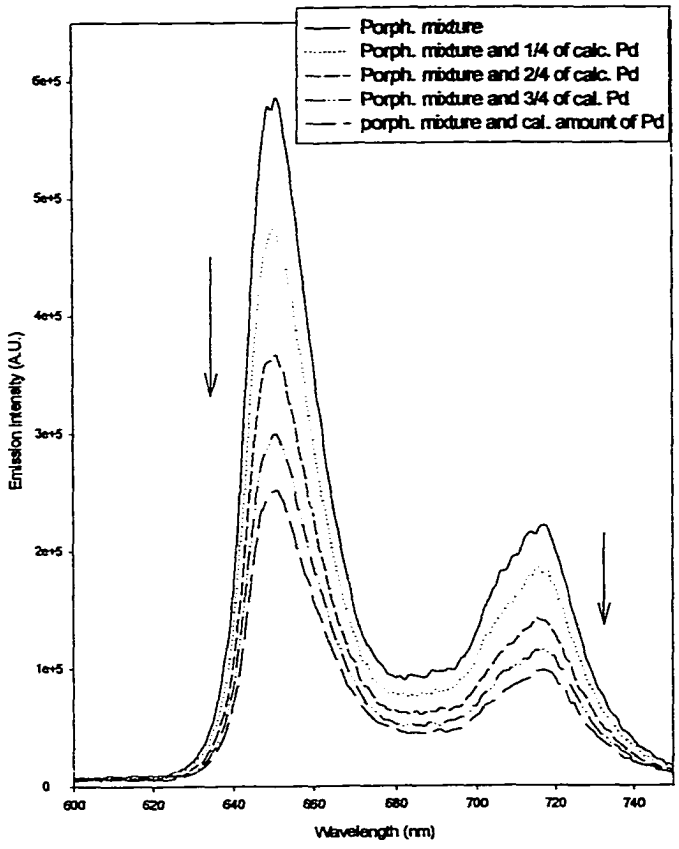

Figure 4.4 *Fluorescence titration of trans $PdCl_2$(benzonitrile)$_2$ into 1:4:4 stochiometric mixture of free base porphyrins (L,T,X-shape) in mineral oil to form the nonamer* ***4a.***

porphyrins, and π-stacking.

Titration of the Pd(II) metal complex into a stochiometric porphyrin mixture of the three porphyrins (L, T, and X-shaped) in toluene (total porphyrin concentration 9μM) indicates the solution of the porphyrin mixture must contain some aggregated species mediated by π-stacking, and/or by hydrogen bonding of the pyridyl nitrogen to the pyrrole N-H. Pyridyl coordination to the Pd complex alters the porphyrin molecular orbitals and makes the pyridyl moiety unavailable for hydrogen bonding. As a consequence, a ~15% increase of the emission intensity is observed upon the addition of the first aliquot of the metal complex. Further aliquots result in a decreased fluorescence emission as expected. The above observation indicates that the actual fluorescence quenching due to the Pd, upon formation of the multiporphyrin array, is higher than observed in toluene (table 4.1). The differences observed in toluene and mineral oil as the solvent may be due to the following:

1. equilibrium and rate of nonamer formation
2. the excited state properties, to a small extent
3. the extent and rate of nonamer aggregation.

The rate of formation and aggregation is faster in toluene because of the greater viscocity of mineral oil. The equilibrium is somewhat shifted to the nonamer in mineral oil, and the extent of nonamer aggregation is less. For these reasons the observed red shift of the UV-Vis spectra, and the fluorescence emission quenching is greater when mineral oil was chosen as the media.

Array	*Number of Heavy atoms*	*Number of Porphyrins*	*Exc. at (nm)**	*Soret λ_{max} Por. Mix. (nm)*	*Exper. % Quenching*
Pd Linear Tape In toluene C_{tape}=1μM	4-Pd	4	423.7	420.10	38
Pt Planar Tape In toluene C_{tape}=1μM	6-Pt	4	427.5	419.20	67.9
Nonamer In toluene $C_{nonamer}$=1μM	12-Pd	9	425.8	419.80	57.9
Nonamer in mineral oil $C_{nonamer}$=0.33μM	12-Pd	9	425.7	419.6	52.0
Nonamer in mineral oil $C_{nonamer}$=1μM	12-Pd	9	419.5	418.9	81.0

***Table 4.1** % Quenching for the three different species in the fluorescence emission experiments.*

**where the UVVis spectra of the starting mixture and self-assembled product overlap.*

4.2.2 **Energy Transfer** (Coupling of Dye Molecules)

For the energy transfer experiments the array **4c** was designed. The array was prepared by mixing 5,10Py15,20(tbuPh)PZn with 5,10,15Py20(tbuPh)PH_2 and $TPyPH_2$ at the right stochiometric amounts (4:4:1). The concentration for the collection of porphyrins was 9μM in distilled toluene. Figure 4.5 shows the UV-Vis. spectra of the Zn porphyrin and that of the mixture of the free base porphyrins. Figure 4.6 shows the emission spectra of the above porphyrins. The features correspond to transitions between the ground states and the lowest excited states of the Zn and free base porphyrins. The Zn porphyrin has a Soret band at B(0,0) 428.5nm and Q-bands at Q(1,0) 555.0nm and Q(0,0) 603.0nm. The mixture of the free base porphyrins has a Soret band at B(0,0) 419.0nm and Q-bands at Q_y(1,0) 513.4nm, Q_y(0,0) 547.5nm, Q_x(1,0) 589.4nm and Q_x(0,0) 646.0nm.

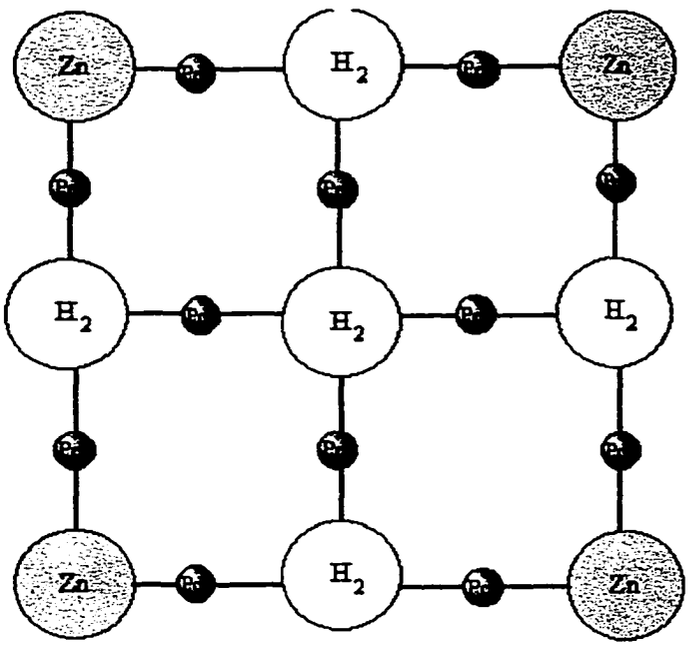

Compound 4c

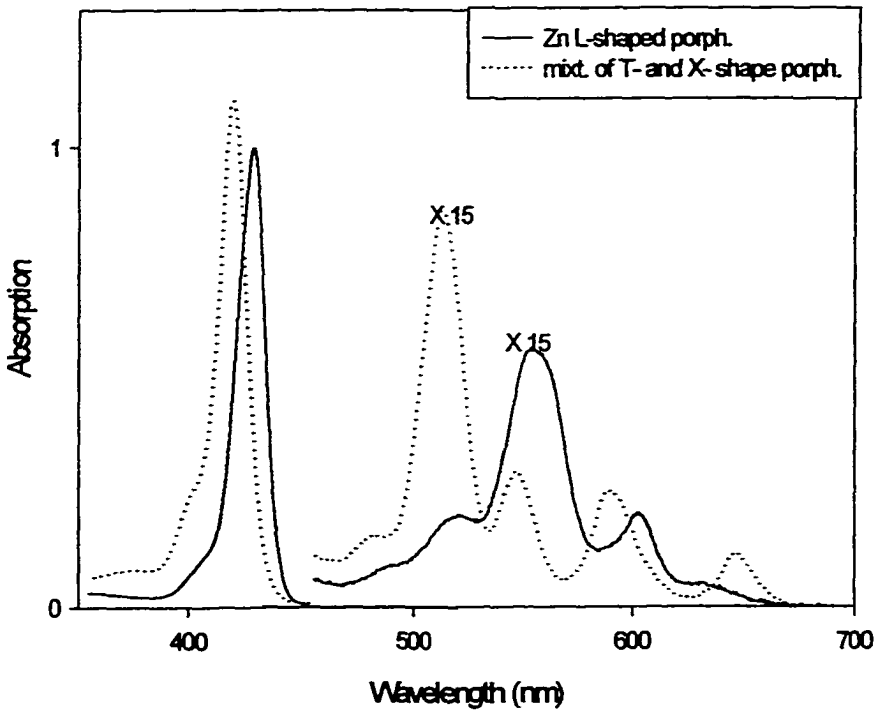

Figure 4.5 Absorption spectra of 5,10Py15,20(tbuPh)PZn 4μM (solid line) and the mixture of 5,10,15Py20(tbuPh)PH_2 4μM and TPyPH_2 1μM (dashed line) in toluene.

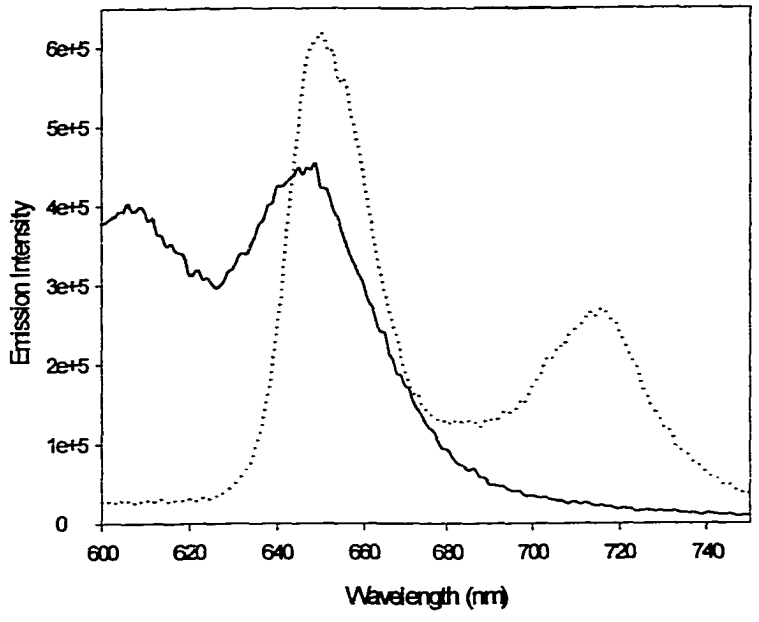

Figure 4.6 Fluorescence emission spectra of 5,10Py15,20(tbuPh)PZn 4μM (solid line) and the mixture of 5,10,15Py20(tbuPh)PH_2 4μM and TPyPH_2 1μM (dashed line) in toluene. Exc. at 433.0 nm.

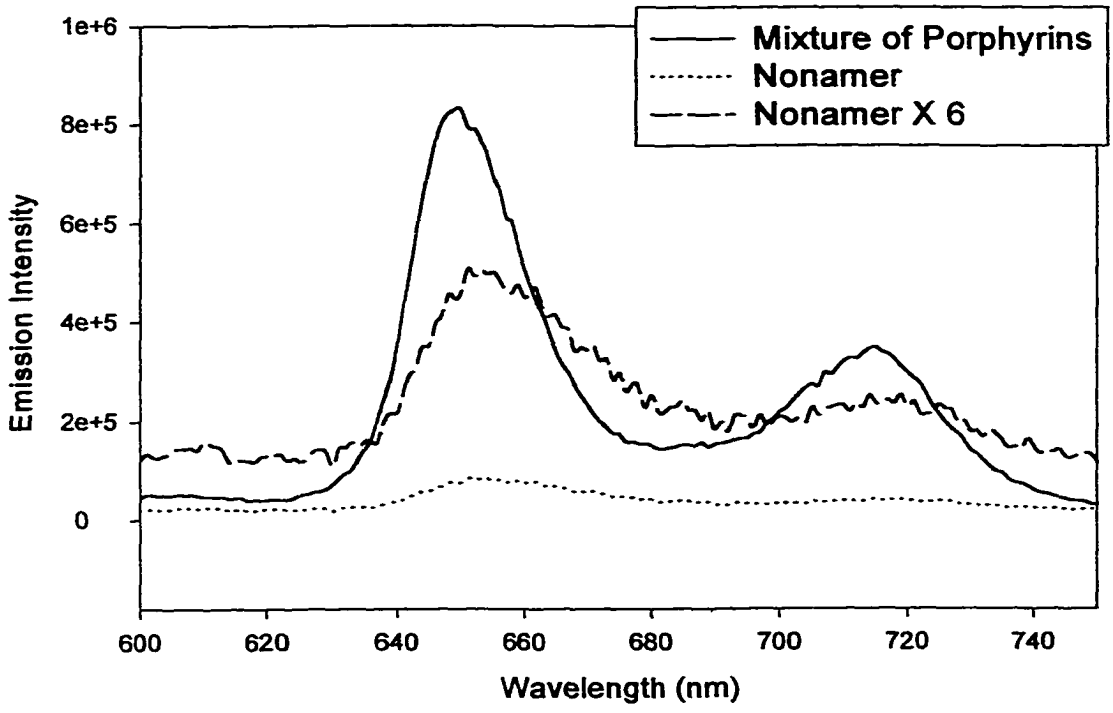

***Figure 4.7** Fluorescence emission (513.4nm, at the Q-band of the free base) of*
a. *mixture of L(Zn), T(Fb), and X(Fb) 9μM (____).*
b. *mixture of porphyrins after the addition of the 12 equivalents of trans-bisbenzonitrile)Pd(II)Cl_2 (.....).*
c. *spectra of porphyrins and Pd-complex multiplied by 6 (____).*

Fluorescence spectra of the Zn porphyrin exhibits Q(0,0) emission at 606.0nm and Q(0,1) band at 647.0nm. The mixture of the two free base porphyrins, the X-shaped and the T-shaped porphyrin, exhibit $Q_x(0,0)$ emission at 650.0nm and $Q_x(0,1)$ peak at 716.0nm (fig. 4.6).

In can be seen in figure 4.5 that photoexcitation at 513.4nm (Q-band of free base porphyrins) preferentially excites the free base porphyrins, while excitation at 551.8nm preferentially excites the Zn porphyrin. Figure 4.7 shows the emission spectra of the mixture of the three porphyrins before and after the addition of the 12 equivalents of the Pd(II) complex upon photo-excitation at 513.4nm (Q-band of the free base porphyrins).

The spectra after the addition is quenched, as was expected. The last spectrum has been multiplied by six in order to be compared in shape to that of the initial spectra. It can be seen that neither the mixture of the individual porphyrins nor the nonamer emits light at ~600nm, emission that corresponds to the metallo-porphyrins. Figure 4.7 indicates that there is no electron or energy transfer from the free base to the Zn porphyrin in the **4c** array.

Figure 4.8 shows the spectra of the mixture, consisting of the two free base porphyrins (T-, and X-shaped) and the metallo-(L-shaped) porphyrins, before and after addition of the Pd metal complex upon excitation at 551.8nm. From the absorption spectra (fig. 4.5) it can be seen that at 551.8nm mostly the zinc porphyrin absorbs with a ratio greater than 4:1, for the metallo-porphyrin versus the free base mixture. Significant quenching is observed upon the addition of the Pd-complex for reasons that have been stated earlier. The emission spectra of the resulting species has been multiplied by six for comparison of the relative ratios of the emission peaks before and after the addition. It can clearly be seen that emission spectra of the mixture of the metallo-porphyrin and the two free base porphyrins (fig. 4.8a) exhibits the characteristics of both the metallo- and the free base porphyrins. Since at the excitation wavelength both the free base and the metallo-porphyrins absorb to a different extent, one may estimate the expected ratio of the zinc to the free base bands at 610 and 719nm. Taking into acount that the optical density of the metallo over the free-base porphyrin, at 552nm, is 5/1, the number of metallo over the free-base porphyrin molecules, according to the concentration, is 4/5, and the emission of the metallo over the free-base porphyrin, from the lifetime data, is 3/12, the above ratio is

expected to be [(5/1)*(4/5)*(3/12)] about 1.5. What is observed is quite different, it is about 0.5.

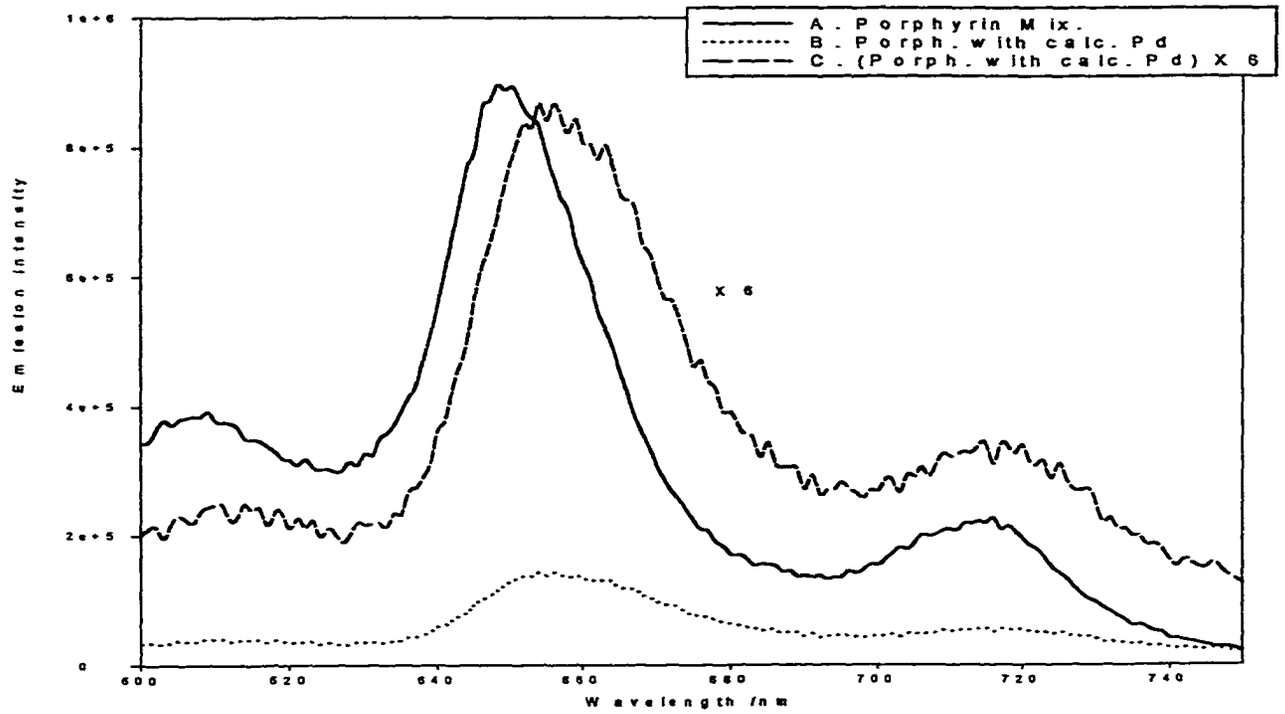

Figure 4.8 Fluorescence emission (excitation at 551.8nm (Q of Zn)) of
a. mixture of L(Zn), T(Fb), and X(Fb) 9μM (___).
b. mixture of porphyrins after the addition of the 12 equivalents of trans-bis(benzonitrile)Pd(II)Cl_2 (.....).
c. spectra of porphyrins and Pd-complex multiplied by 6 (-.-.-.-).

Both free-base and zinc porphyrins are observed in figure 4.8c, after the addition of the $PdCl_2BN_2$. A decreased intensity of the emission from both the metallo-porphyrin and the free base porphyrins is observed, due to the The heavy atom effect. But energy transfer from the metallo to the free base porphyrin also contributes to the emission spectral features as shown by the increase in the 720nm band relative to the 610nm band. The fact

that there is still emission out of the metallo-porphyrin indicates that the energy transfer is not quantitative, and/or may be due in part to unreacted starting material. If 10% of the Zn porphyrin remained unreacted, this would account for this part of the emission spectra.

Summarizing the above, fluorescence emission experiments indicate energy and/or electron transfer from the metallo-porphyrin to the free base but not the other way around. We expect that energy transfer to be in dynamic equilibrium between the free base porphyrins upon photo-excitation. The above observations are consistent with the electron coupling between the porphyrins and the relative energy levels of the free base and the zinc-porphyrin. These observations indicate energy transfer in the singlet state. However, since the vast majority of the porphyrins in the nonamer rapidly go to the triplet state, electronic communication in this manifold must also be considered.[4,5] the triplet manifold of these arrays will be the topic for future studies.

4.2.3 Heavy Atom Effect

4.2.3.1 Theoretical Background

An important factor for the decreased intensity of the fluorescence emission spectra observed in figure 4.4 is the heavy atom effect. The heavy atom effect presents a pathway for a "forbidden" electron transition from a singlet (n) excited state to a triplet (n) excited state (fig. 4.9). "Allowed" and "forbidden" are quantum mechanical descriptions. A "forbidden" is improbable and proceeds more slowly than an "allowed" transition. A forbidden transition may take place because of perturbation between states. For example, a "forbidden" transition involving a spin flip can be observable because of the coupling between the spin and orbital motion of an electron. This perturbation is known as spin orbital coupling and may be the only mechanism available for intersystem crossing (isc). Since, in any isolated system, the total momentum must be conserved, a change in an electron's spin angular momentum (which takes place during a spin flip) must be accompanied by a corresponding change in orbital momentum. This spin-orbital coupling may be accelerated by the presence of "heavy-atom" substituents (atoms of high atomic numbers) in the excited state or in the solvent, and the phenomenon is known as the "heavy-atom" effect.[4.6]

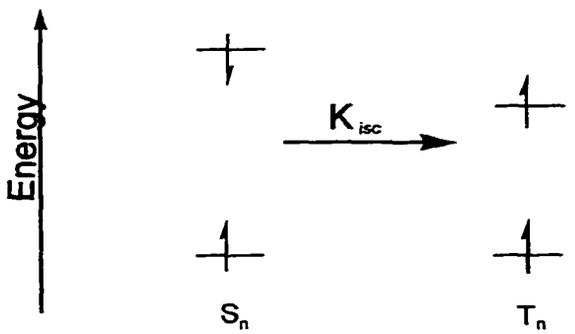

Figure 4.9 *Schematic presentation of the Heavy Atom Effect.*

The heavy atom has orbitals of appropriate energies to couple to the spin. In general the heavy atoms can arise from four situations:

1. chelation of the metal ion inside the porphyrin (to form a metallo-porphyrin)
2. covalently attached to the macrocycle or substituents, *e.g.* halogenation of pyrrole β-position or *meso* substituent
3. coordination of a metal ion by an exocyclic substituent ligand on the macrocycle, *e.g.* a pyridyl moiety
4. external solvent heavy atoms –if in a concentration sufficient to allow collision with the fluorophore.

Here we report the results of the external and of the exocyclic internal heavy atom effect, introduced by a mono-dentate Pt metal complex to pyridyl porphyrins.

4.2.3.2 External Heavy Atom Effect

The external heavy atom effect was studied on $TPyPH_2$, 1μM in toluene, in the presence of MeI. The heavy iodine atom facilitates the intersystem crossing, making the fluorescence emission decrease. Figure 4.10 shows the small effect that the MeI has on the emission of the porphyrin at concentrations up to 90mM, while table 4.2 contains the experimental data. Even at high concentrations, of 90mM in MeI, the porphyrin emits about 75% making external heavy atom effect negligible at concentration up to 5mM of the heavy atom.

Conc. of MeI (mM)	*% Emission*
0.00	100.00
10.70	96.97
21.41	91.67
32.12	88.73
42.83	85.60
53.54	81.98
64.25	80.30
74.96	76.90
85.67	75.12

Table 4.2 *Fluorescence of 1μM $TPyPH_2$ at the presence of MeI in toluene.*

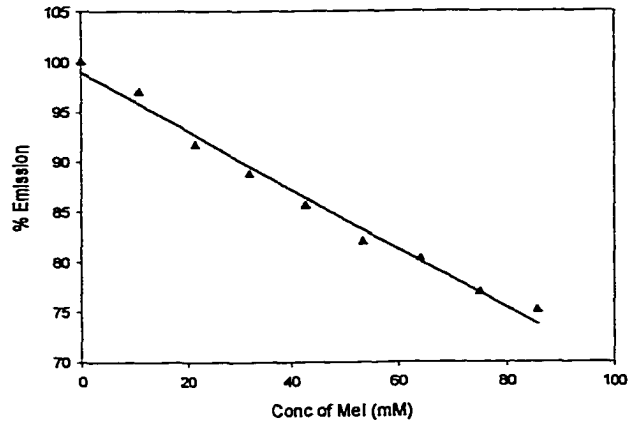

Figure 4.10 *External Heavy Atom effect in toluene at R.T.*

4.2.3.3 Exocyclic Internal Heavy Atom Effect

The need for a mono-dentate metal complex led up to the di-μ-chloro dichloro bis(triphenylphosphine)diplatinum(II) (**20**). The complex (**20**) was prepared according to the literature.[4.7] (see appendix.D) The heavy atom effect has been estimated for each one of the six *tert*-butylphenyl pyridyl porphyrins in toluene. A four-fold excess of the Pt-complex (**20**) was added to 1μM of porphyrin solution in toluene. Solution was stirred at

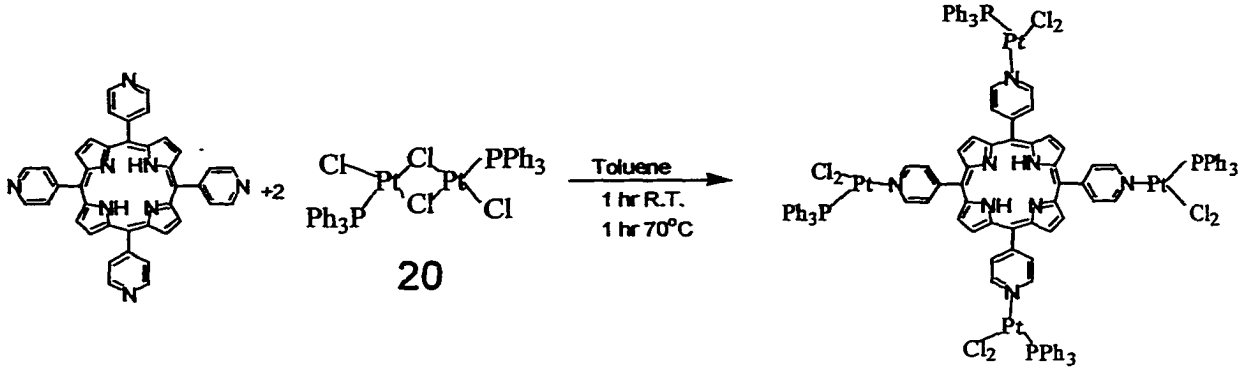

Figure 4.11 Reaction of Chloro-bridged Pt complex with $TPyPH_2$.

R.T. for 1 hour and then was placed in water bath at 70°C for another 1 hour (fig. 4.11). The reaction of the Pt complex with the $TPyPH_2$ goes to completion at R.T. while heating at 70°C does not introduce any difference in the UV-Vis or the fluorescence emission spectra. For the mono-pyridyl porphyrin heating at 70°C for 1 hour is necessary for the reaction to reach completion. UV-Vis spectra of the resulting species indicates, that at the above conditions, endocyclic Pt-metalation of the macrocyclic does not take place as the spectra of the reaction mixture keeps the characteristics of a free base –four Q-bands. The differences in the rates of exocyclic coordination are attributed to the cooperativity of the Pt-binding, via the mixing of the d-orbitals of the metal with the π cloud of the porphyrin

Porphyrin	After addition of Pt-complex (4-fold xs.)		
	Red Shift (nm)	% Decrease for (ε)	% Emission for Steady State
5,10,15,20(tbuPh)PH₂	0.0	0.0	100
5Py10,15,20(tbuPh)PH₂	2.3	6.2	49.8 ±4.0%
5,10Py15,20(tbuPh)PH₂	2.0	6.5	41.9 ±1.5%
5,15Py10,20(tbuPh)PH₂	3.7	2.0	50.8 ±0.5%
5,10,15Py20(tbuPh)PH₂	5.0	4.0	36.4 ±0.5%
TPyPH₂	6.0	0.0	28.0 ±1.0%

Table 4.3 *UV-Vis and emission data on heavy atom effect. 1μM porphyrin in toluene. 4-fold excess of Chloro-bridged Pt (20) was added. Temp. 70C for 1 hour. Excitation took place at a wavelength that the starting material and the resulting species absorbed equally.*

Porphyrin	BEFORE addition of Pt-complex (4-fold xs.)	AFTER addition of Pt-complex (4-fold xs.)	Calculated % Emission[a']
	Lifetime (ns)	Lifetime (ns)	
	(Exc. 417, em.650)	(Exc. 420, em.652)	
TPPH₂	12.2	12.2	100 ±0.5%
5,10,15,20(tbuPh)PH₂	12.05	12.05	100 ±0.5%
5Py10,15,20(tbuPh)PH₂	10.8	5.5	50.9 ±2.0%
5,10Py15,20(tbuPh)PH₂	12.3	4.02	32.7 ±3.5%
5,15Py10,20(tbuPh)PH₂	11.8	3.3	27.0 ±2.5%
5,10,15Py20(tbuPh)PH₂	13.6	2.79	22.1 ±4.5%
TPyPH₂	11.4	2.35	20.6 ±2.5%

a': calculated as $100-\{(\tau_b-\tau_a)/\tau_b\}$

Table 4.4 *Lifetime data on heavy atom effect. 1μM porphyrin in degassed toluene. 4-fold excess of Chloro-bridged Pt (20) was added. Temp. 70C for 1 hour.*

Porphyrin	*without Pt complex*			*with Pt Complex*		
	λ_{max} (nm)	$\varepsilon x\ 10^3$ ($cm^{-1}M^{-1}$)	*fwhm* (nm)	λ_{max} (nm)	$\varepsilon x\ 10^3$ ($cm^{-1}M^{-1}$)	*fwhm* (nm)
T(tbuPh)PH$_2$	420.6	394.594	12.5	420.6	394.594	12.5
5Py10,15,20(tbuPh)PH$_2$	420.4	396.632	13.0	422.5	369.125	14.5
5,10Py15,20(tbuPh)PH$_2$	419.9	405.954	13.6	423.9	386.265	15.8
5,15Py10,20(tbuPh)PH$_2$	419.7	394.211	13.3	423.4	386.658	15.4
5,10,15Py20(tbuPh)PH$_2$	419.1	396.319	13.8	424.1	386.211	16.7
TPyPH$_2$	418.1	340.501	14.5	424.1	334.751	17.4

Table 4.5 *UV-Vis. data of Soret band on heavy atom effect. 1 μM porphyrin in toluene. 4-fold excess of Chloro-bridged Pt (20) was added. Temp. 70C for 1 hour.*

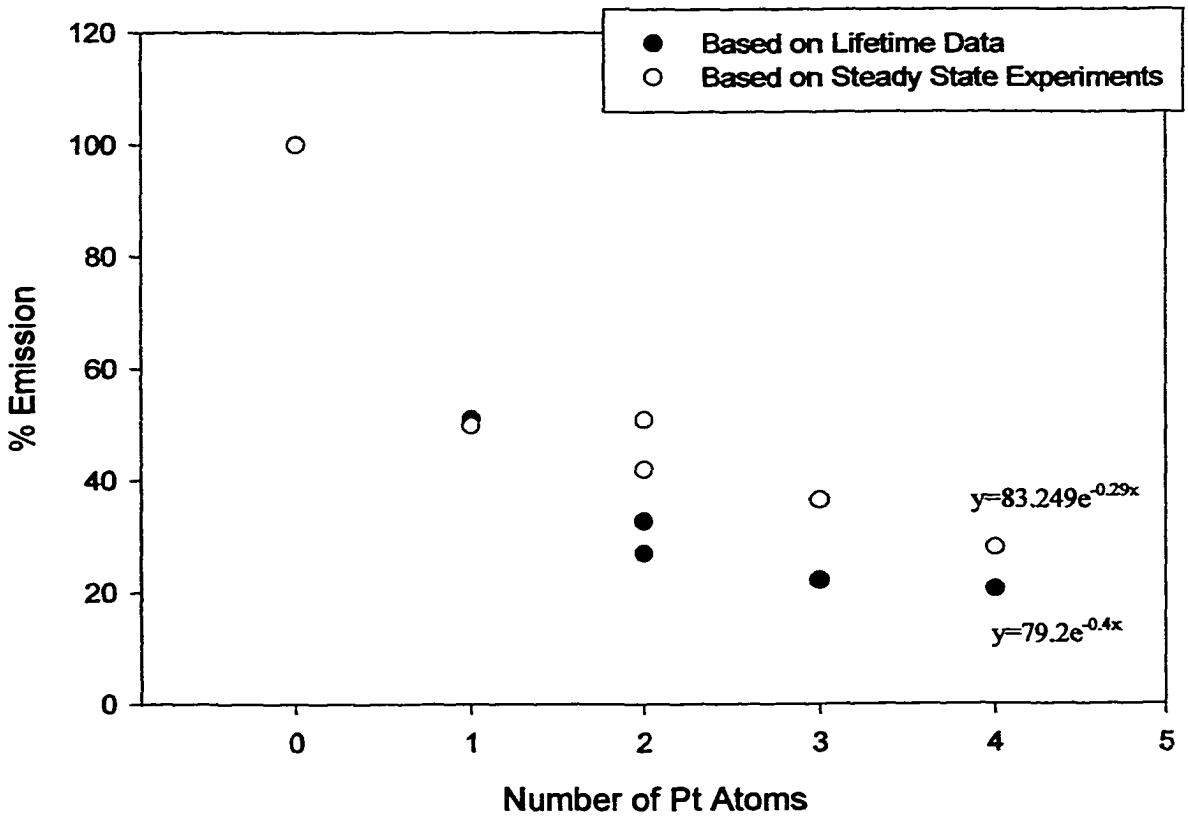

***Figure 4.12** Plot of the heavy atom effect data.*

that makes the other pyridyl nitrogens more basic. Additionally, back bonding of the Pt atom d-orbitals into the pyridyl anti-bonding orbitals adds electron density to the porphyrin macrocycle via both resonance and inductive effects. This, in turn, increases the electron density on the other pyridyl groups, making them more basic and better ligands. The increased rate is due to other reasons too. Though the concentration of the porphyrin was kept constant (1μM) for all the experiments, the number of pyridines increases, making its concentration up to 4μM, with a similar increase in the Pt complex concentration. Also, it is know from the literature[2,9] that the pyridyl groups on the $TPyPH_2$ are slightly more basic than those on a mono-pyridyl compound.

The heavy atom effect from the relative emission intensity of the exocyclic metalated porphyrins to that of the initial porphyrin has been estimated (table 4.3). The changes observed in the UV-Vis. spectra, upon exocyclic metalation of the porphyrins, are summarized in the same table. Neither the UV-Vis. nor the emission spectra of the 5,10,15,20(tbuPh)PH_2 is effected by the addition of the bridged Pt-complex (**20**) under any conditions. A red shift is observed for the pyridyl porphyrins upon the addition of the Pt-complex (**20**) that is accompanied by a decreased extinction coefficient (ε) for the complex. The extent of the red shift depends on the number of Pt atoms attached to the porphyrin. It indicates orbital mixing between the d-orbitals and the π-system of the porphyrin. It ranges for 2.3nm for the mono-pyridyl up to 6nm for the $TPyPH_2$. The decrease of the extinction coefficient (ε) also depends on the symmetry of the metalation. The greater decrease in ε is observed for the species with the lower symmetry, the mono-pyridyl and the *cis*-dipyridyl porphyrins. While exocyclic metalation of the $TPyPH_2$ has no effect on the extinction coefficient, there are indications that exocyclic metalation increases the number of vibrational levels making the absorption peak broader, and reflects the extinction coefficient of a new complex. In the case of a symmetric exocyclic metalation the are fewer vibrational modes. This hypothesis will be the subject of future studies.

The heavy atom effect has also been estimated from the lifetimes of the starting material and those of the exocyclic metalated species. The results are summarized in table 4.4. Both the data of the steady state experiments and those of the lifetime are plotted in figure 4.12. The above figure shows an exponential relationship between % emission and

Array	*Calculated*			*Experimental*	
	Calc.	*% Emission*	*% Quenching*	*% Emission*	*% Quenching*
Pd-Nonamer	{4*36.4 + 4*41.9 +1*28.0}/9	37.9	62.1	52.0	48.0
Pd-tape	{2*50.8+2*49.8}/4	50.3	49.7	38.0	62.0
Pt-tape	{2*28+2*41.9}/4	34.95	65.05	67.9	32.1

Table 4.6 *Calculated and experimental fluorescence quenching due to the heavy atom effect, in toluene.*

the number of Pt-atoms attached to the exocyclic positions of the porphyrin. Assuming that the heavy atom effect is an additional property of a system, we have calculated the percent emission expected from the multi-porphyrin arrays, assuming the heavy atom effect was the only factor on the emission quenching. The experimental percent emission is also summarized in the same table (table 4.6) measured after the coordination of the heavy metal (Pd or Pt) at the exocyclic positions of the porphyrins. The quenching, due to the heavy atom effect, is expected to be between 50 and 75% on the emission from the array. It is as low as 35%, in the case of the Pt-planar tape. Since there are other pathways that are expected to further quench the emission of the multi-porphyrin systems (like electronic communication and energy or electron transfer between the porphyrins) the measured emission, from the array, is expected to be lower than calculated from the heavy atom effect. The greater experimental quenching is only observed in the case of the Pt-planar tape. The greater quencing for the Pt arrays is somewhat due to the fact that the Pt is a heavier atom.[4.6b] The increased Pt-pyridyl bond strength may also contribute to

this. The greater than expected fluorescence emission from the Pd nonamer may be due to a variety of factors.

1. Incomplete reaction, so the remaining uncomplexed porphyrins substantially add to the emission spectra intensity.
2. The formation of the nonamer results in a new supramolecular species with substantially different photophysical properties than the constituent parts.

Although not completely resolved, several observations indicate both may contribute to the observed emission intensity, depending on the experiment.

1. UV-Vis titration shows isosbestic points, so little free porphyrin remains when toluene is the solvent at μM concentrations
2. The ^{1}N-NMR shows that at 70mM concentration, the formation of the nonamer is incomplete in chloroform.
3. Since there is a red shift in the UV-Vis spectra, including the lowest in energy Q-band, of ~4nm and the is little or no red shift in the emission spectra, one may conclude it is the unreacted starting material in the mineral oil experiment and toluene.

4.3 Hydrogen-Bonded Arrays

4.3.1 Energy Transfer

UV-Vis spectra of the Hydrogen-bonded porphyrin systems in chloroform, toluene, 2-methyl THF and ethanol, at various concentrations ranging from 2μM to about 500μM for the collection of the porphyrins, show no change for the Q-bands and about a 1-2nm red shift for the Soret band (fig. 4.13). This indicates very little electronic communication between the macrocycles in the H-bonded assemblies in the ground state.

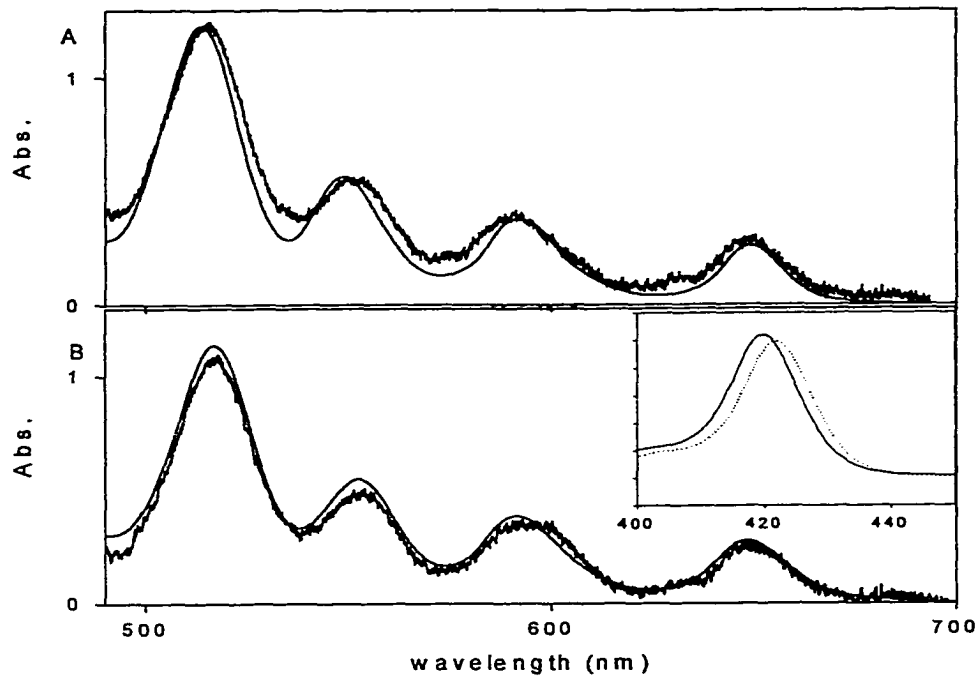

Figure 4.13 *The UV-Visible spectra of 5,10(AA)15,20(tbuPh)PH_2 (17a) in ethanol (A) and chloroform (B). The smooth lines are at ~250 μM, and the jagged lines are at 2 μM multiplied by a factor of 110.*
Inset: *the Soret band in chloroform (—) is ~ 3nm to the red of that in ethanol (___).*

The 5- and 5,10- diacoteamidopyridyl porphyrins, **11a** and **12a**, were used for the construction of the self-complementary linear dimer (**15a**) and square tetramer (**17a**), and exhibit a typical fluorescence at 652.7 and 716.6nm upon excitation at 585.0nm in dry $CHCl_3$. The solutions were placed in H_2O bath at 50°C for a couple of minutes for equilibrium to be established before any measurement. The fluorescence emission at 652.7nm, upon photoexcitation at 585.0nm, for the mono- and the di-diacedopyridyl compounds and that of the $TPPH_2$ are reported (figure 4.14).

Figure 4.14 plots the emission versus concentration of $TPPH_2$. The plot indicates pi-stacking of the porphyrins at high concentrations, that causes quenching of the emission intensity, internal shading, and self-absorption. The very weak interaction that forms the dimer (**15a**) is illustrated in the same graph (the OD at 585 is in a 3x3mm cell). The 5–acetoamidopyridyl porphyrin exhibits the same trends as those of the $TPPH_2$ for concentrations up to ~120μM in dry chloroform, where the predominant effect is pi-stacking. At concentrations higher than ~120μM, of **15a**, greater emission quenching is observed than that of the standard, $TPPH_2$. The phenomenon is attributed to the self-association of the porphyrin that results the formation of the dimer and energy transfer between the porphyrins. The small observed quenching is due to the weak quadruple H-bond. The rotational motion of a *meso* aromatic substituent on TPP is about ±30°C. the weak H-bond linkers further allows the porphyrins in the dimer to be non-planar. These factors weaken the electronic communication between the porphyrins and consequently reducing electron and energy transfer. The greater emission quenching observed for the

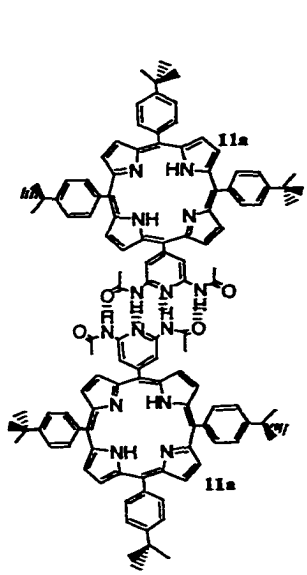

Dimer (15a)

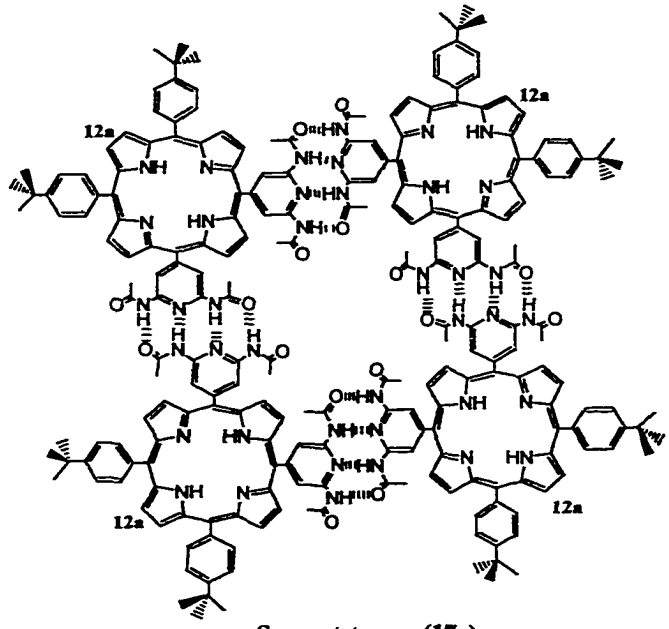

Square tetramer (17a)

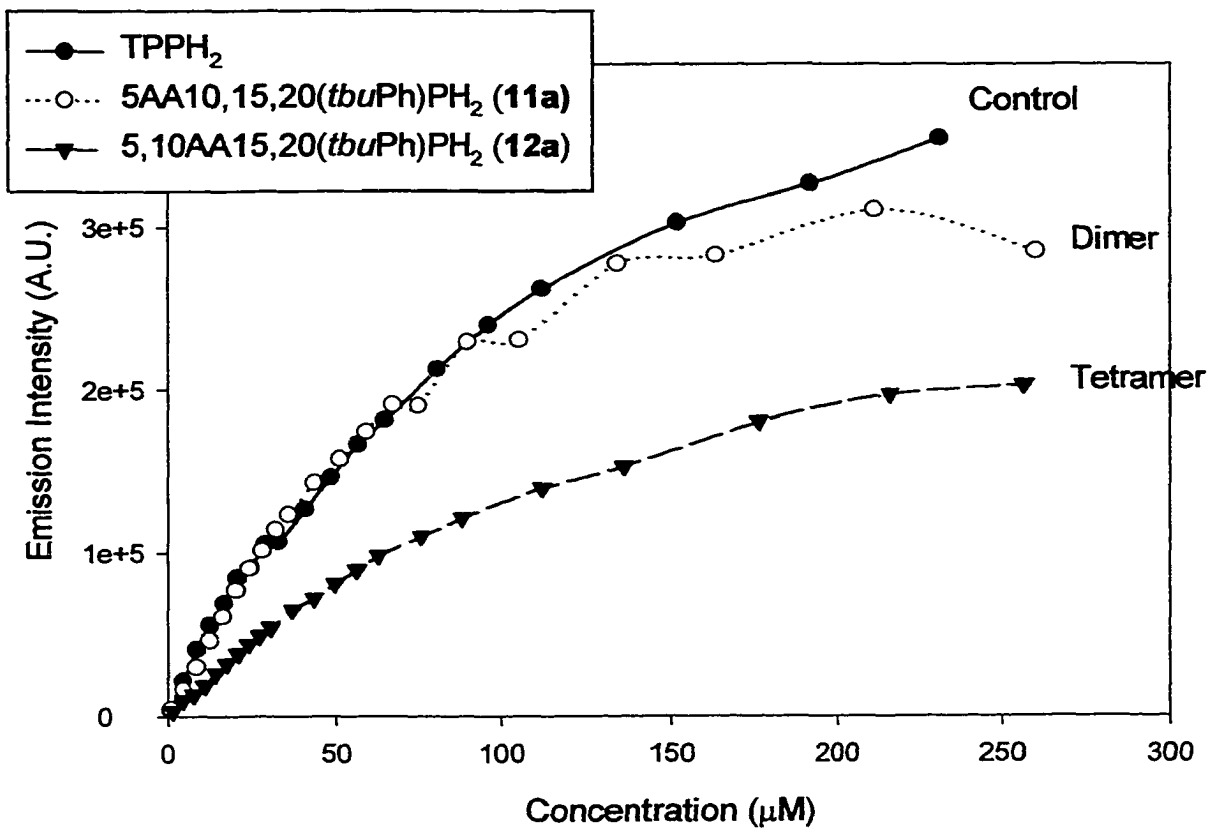

Figure 4.14 *Relative intensity of the fluorescence emission (right angle) at 652.7nm (λ_{exc}=585.0nm) of the free-base porphyrin*
___ $TPPH_2$
..... 5AA10,15,20(tbuPh)PH_2 (11a)
___ 5,10AA15,20(tbuPh)PH_2 (12a)
plotted vs concentration in dry $CHCl_3$ in a 3x3mm cell.
The solutions were placed in H_2O bath for 50°C for a couple of minutes for equilibrium to be established.

5,10bis(acetoamido)pyridyl porphyrin, which forms the square tetramer (**17a**), is due to the relative position of the porphyrins in the assembly and the stronger association constant due to cooperativity. The porphyrins in **17a** are essentially coplanar because two sets of H-bond linkers would have to be attached or broken for a porphyrin to bend or twist out of the plane of the tetramer. The coplanar orientation of the porphyrins, in the square tetramer favors excited state electron communication and energy transfer between the porphyrins. Its reflection on the emission is indicated by the greater quenching compared to the dimer.

Figure 4.15 shows the emission spectra of equimolar (250μM) amounts of (**11a**) and (**13b**) in absolute EtOH and in dry 2Me-THF. The mole ratio and the pattern of the H-bonding recognition groups of the porphyrins are appropriate for the formation of the hetero-complementary dimer **16c**. In the dry 2-Me-THF the assembly (**16c**)is expected to be formed while in EtOH the individual subunits are observed due to the strong solvation of the hydrogen bonding sites. The above solutions were photoexcited at 553.0nm (fig. 4.15), where the metallo porphyrin (**13b**) absorbs ~2 times more than the free base (**11a**). UV-Vis. spectra of the two solutions (fig. 4.15 lower, EtOH (solid), 2Me-THF (dashed)) indicate that the concentration of the porphyrins in solution is kept the same as we are changing the solvent system and no electronic communication in the ground state. Also, DLS and RLS experiments indicate that pi-stacking aggregation is identical in both systems. Fluorescence emission spectra (fig. 4.15 upper, EtOH (solid), 2Me-THF (dashed)) show decreased emission out of the metallo-porphyrin, and increased emission out of the free base porphyrin as we are going from the solution in EtOH, individual

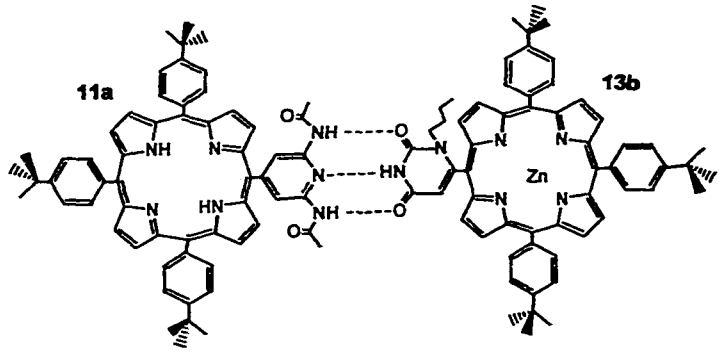

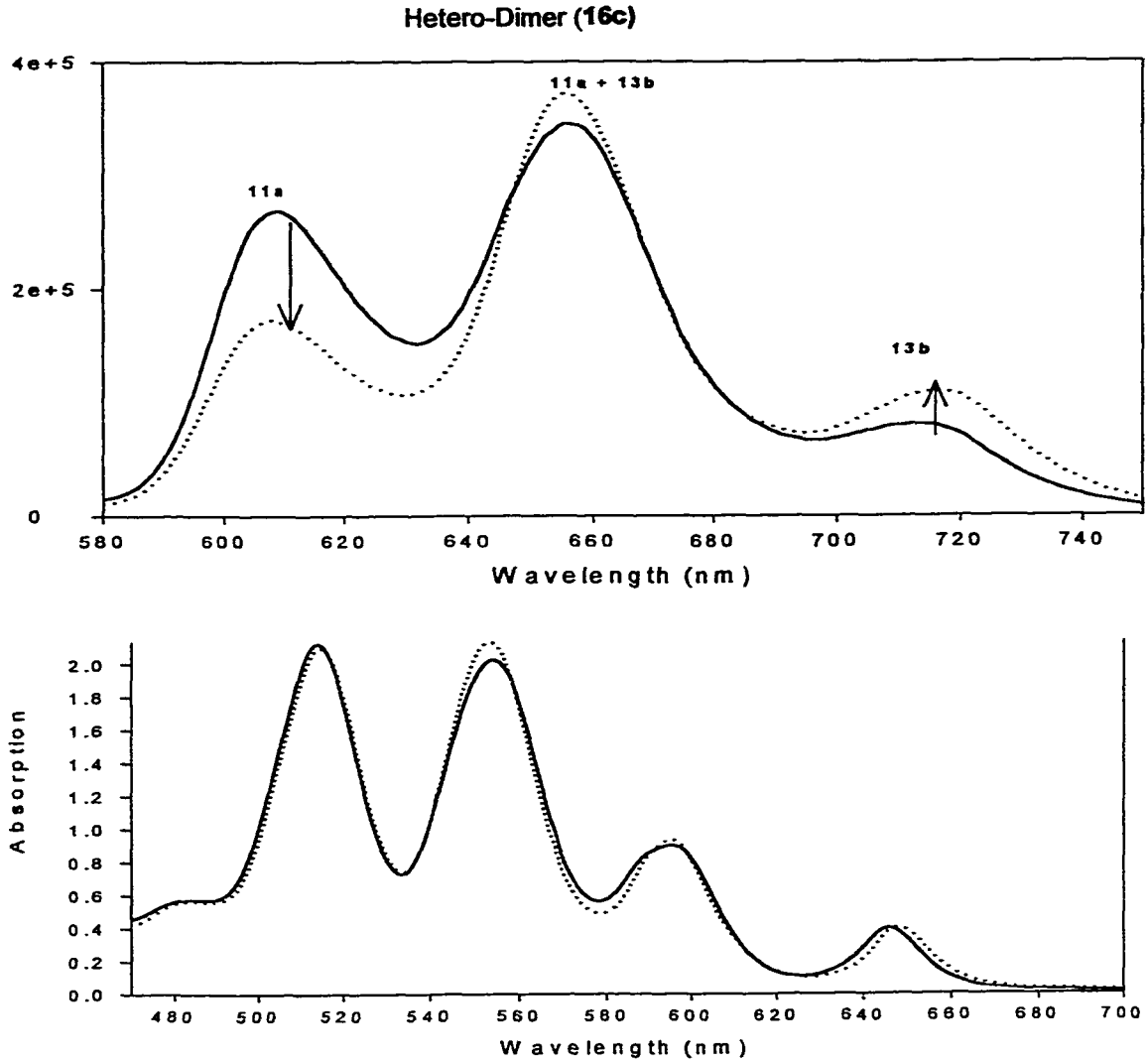

Figure 4.15 *Mixture of 5AA10,15,20(tbuPh)PH_2 and 5U10,15,20(tbuPh)PZn, 250μM in each*
___EtOH.
.....dry 2Me-THF.
solutions were placed in H_2O bath at 50℃ for a couple of minutes for equilibrium to be established. (0.3cm pathlength)
Upper: *Fluorescence emission spectra. (right angle)*
λ_{exc}=553nm.
Lower: *UV-Vis spectra of mixture.*

porphyrins, to that in 2Me-THF, dimer. The above observation is attributed to energy transfer from the metallo to the free-base porphyrin. Identical experiments, where photoexcitation is at a wavelength where mostly the free base porphyrin absorbs, show no difference for the emission from the free base nor metallo-porphyrin, indicating no energy transfer from the free base to the metallo-porphyrin.

In a similar way energy transfer has been shown in the hetero-complementary square tetramer (**18**) where **18c** was designed for the experiments. Figure 4.17 shows the UV-Vis spectra of the mixture of 5,10AA15,20(*tbu*Ph)PH_2 and 5,10U15,20(*tbu*Ph)PZn, 300μM in each, in EtOH and in dry 2Me-THF. The UV-Vis spectra indicate that the total concentration of the porphyrin in the two solvents is the same, and no major spectral shifts. The fluorescence emission spectra follow the same trends as those observed for the dimer. Decreased emission from the zinc porphyrin is observed upon change of the solvent from EtOH, monomers, to dry 2Me-THF, square tetramer. This is accompanied by an increase of the emission from the free base porphyrin. The above observation also indicates energy transfer from the metallo to the free-base porphyrin. The experiment was done using front face geometry. In both cases, hetero-dimer (fig.4.15) and of the square tetramer (fig. 4.16), it can be seen that the decrease of the metallo-porphyrin is greater than the increased emission from the free base. This may be attributed to increased self-absorption in the 2Me-THF solution, to increased non-radiative relaxation of the assembled species,an to the 2:1 ratio of the absorption spectra at the excitation wavelength. The latter means that these are fewer PZn excepted and more PH_2.

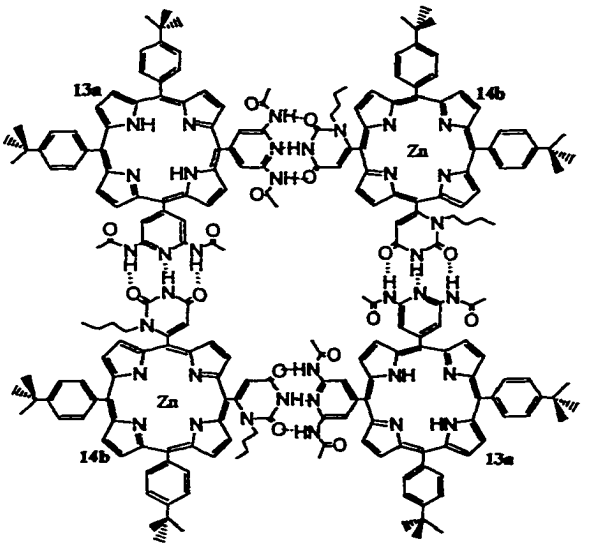

Hetero-square tetramer (18c)

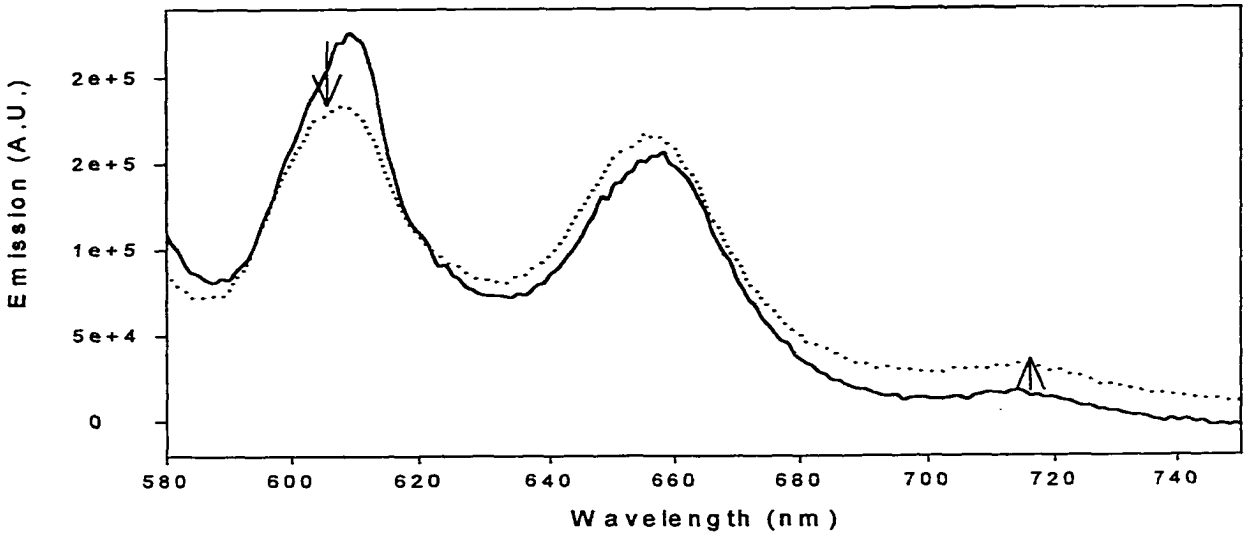

Figure 4.16 *Fluorescence emission spectra, of a 5,10(AA)15,20(tbuPh)PH_2 and 5,10U15,20(tbuPh)PZn mixture, 300μM each, in (___)EtOH, and (.....)dry 2Me-THF. $\lambda_{exc.}$=564nm. Solution was placed in H_2O bath at 50°C, for a couple of minutes, for equilibrium to be established. (Front-face, 0.1mm pathlength cuvette).*

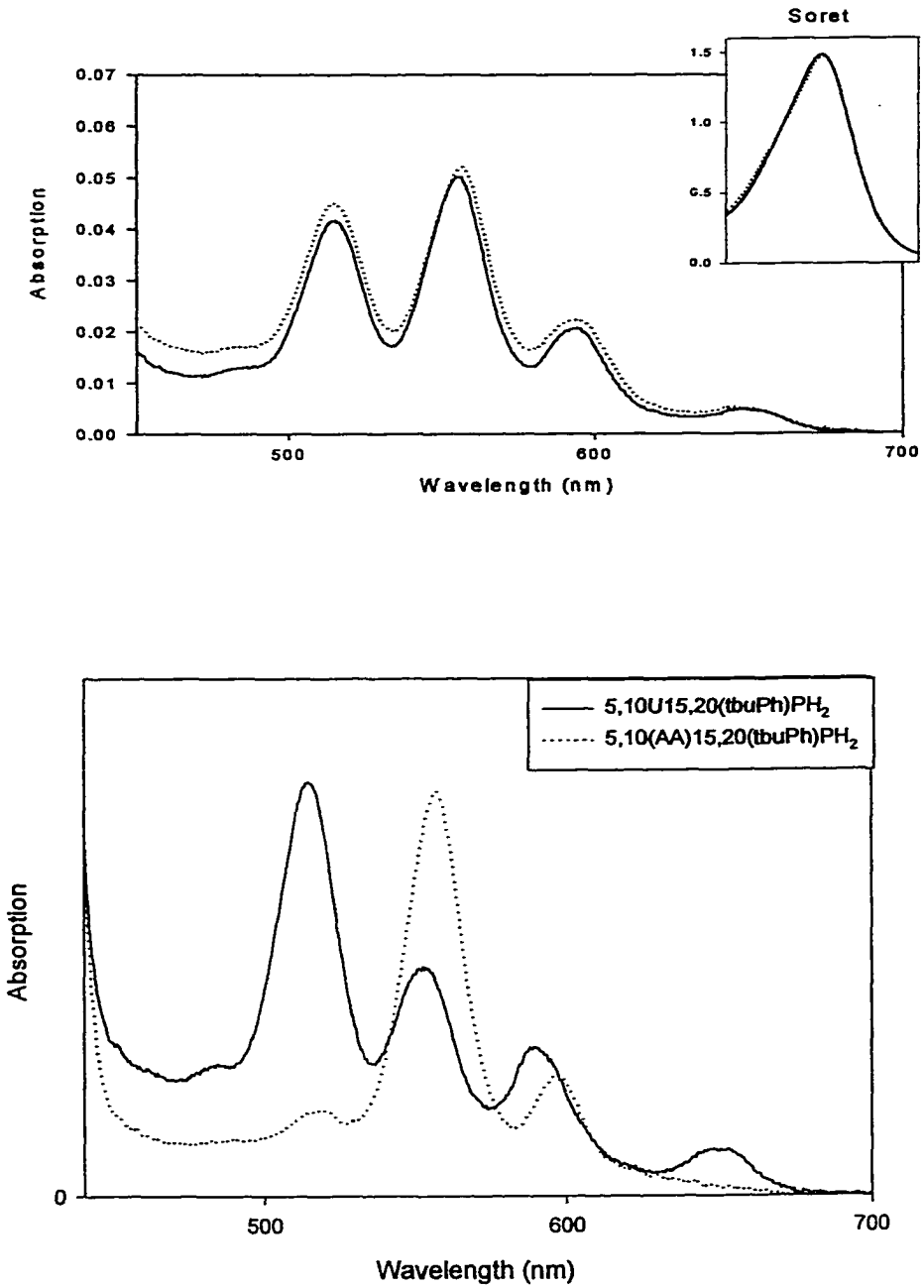

Figure 4.17 *5,10(AA)15,20(tbuPh)PH_2 and 5,10U15,20(tbuPh)PZn, 300μM each*
All solutions were placed in H_2O bath at 50 °C for a couple of minutes for equilibrium to be established (0.1mm pathlength).
Upper: *UV-Vis. spectra of mixture. (___)EtOH, (.....)dry 2Me-THF.*
Lower: *UV-Vis spectra of 5,10U15,20(tbuPh)PZn(solid line) and 5,10(AA)15,20(tbuPh)PH_2(dashed line) in dry 2Me-THF.*

APPENDIX

A. Four Orbital Model

B. ^{1}H- and ^{13}C-NMR of (pyridyl) (t-buPh) Porhyrins

C. Additional data for 3D-Compound

D. Formation of μ-bridged compound

A. Four Orbital Model

The electronic heart of a regular metallo-porphyrin is an inner 16-membered ring with 18 electrons. According to the cyclic wire model, orbitals with m_l=0, ±1, ±2, ±3, ±4 are occupied in the ground state that have energies:

$$\frac{\hbar^2 m_l^2}{2mR^2}$$

where ħ: Planck's constant
m: electron mass
R: radius of the ring

The lowest energy excited state is ±5 and the total angular momentum of the transition is L_z=±1, ±9. Each transition has one singlet state, S=0, and three triplet states, S=1. The energy of the transition is $\hbar^2(5^2-4^2)/2mR^2$. Then if R=4Å, the transition requires light of 580nm.

According to Hund's rule, the higher the multiplicity of a state the lower the energy of the state, and for states with the same multiplicity, the higher the angular momentum (L_z) the lower the energy of the state. The above rule defines the porphyrin's energy levels in figure A.1. Since the ground state is a closed shell with L_z=0, according to the selection rule ΔL_z= ±1, just the highest in energy singlet excited state, shown in figure A1, is allowed while the triplet and the lowest in energy singlet transition are forbidden. The UV-Vis spectra of a porphyrin consists of an intense absorption between 400nm and 500nm, that is called Soret or B-band, and two, for metallo-porphyrins, or four, for free-base-porphyrins, other bands between 500 and 700nm that are called Q-bands. The allowed transition is identified with the Soret-band while the lower in energy singlet transition with the Q-bands.

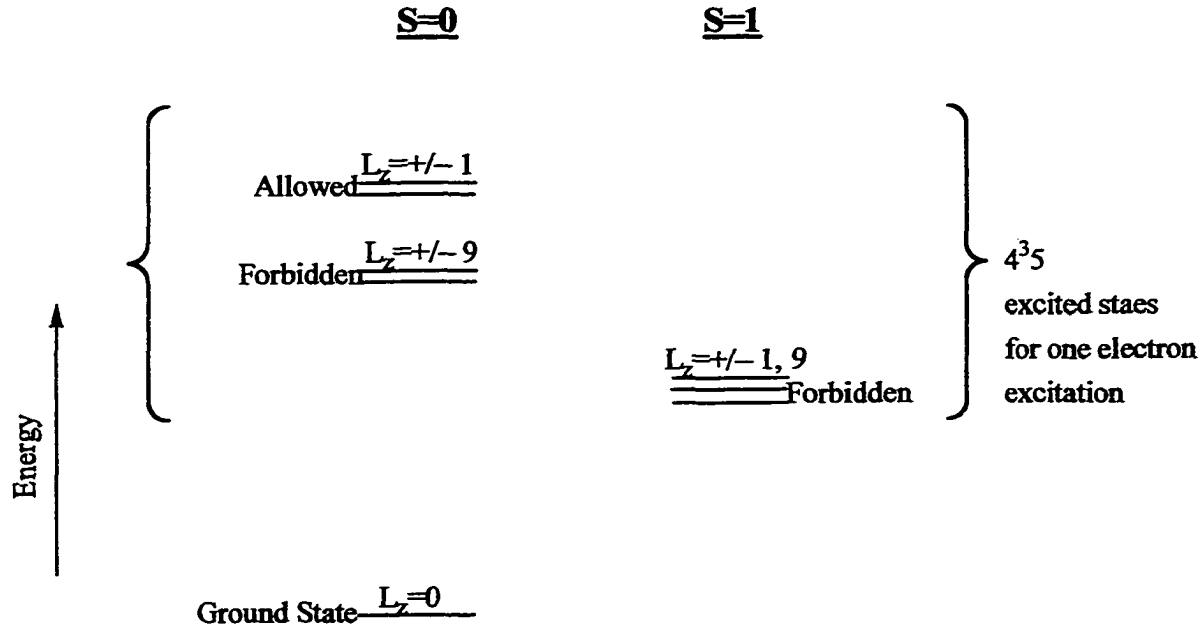

***Figure A.1** Porphyrin energy levels for circular box model.*[A.1]

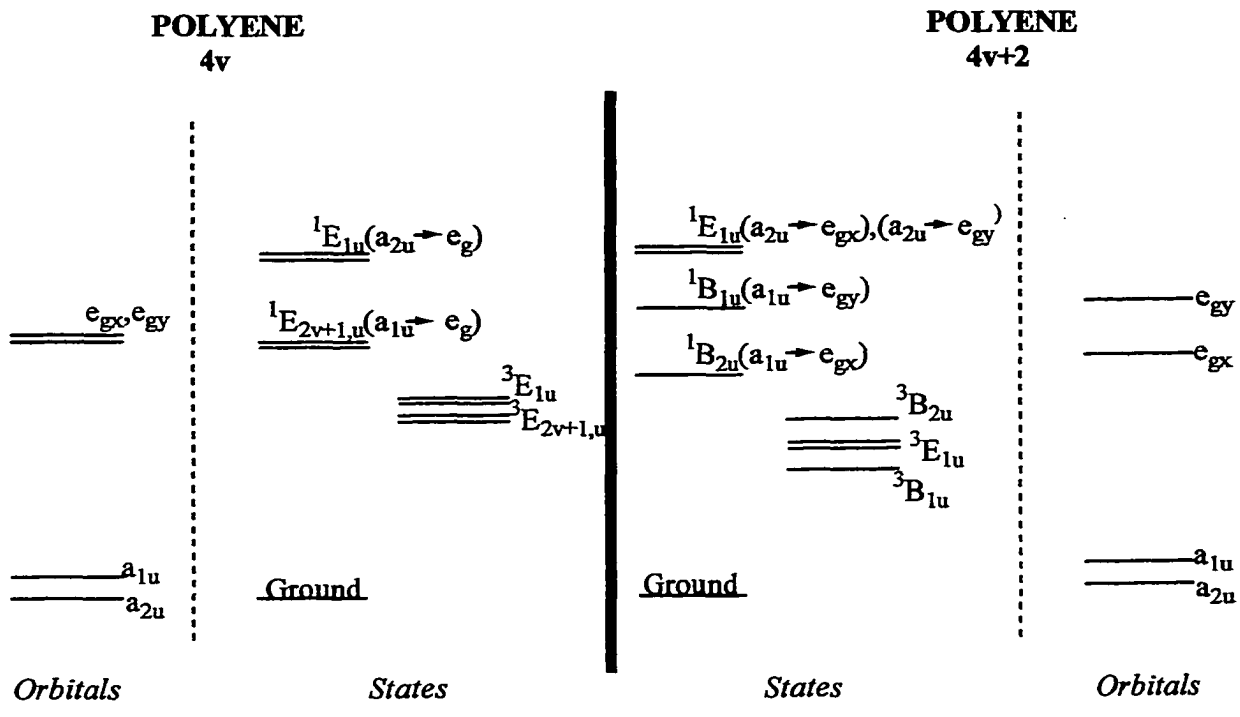

***Figure A.2** Orbitals and states of a cyclic polyene, modified for a free base porphyrins and a metallo porphyrin.*[A.3]

Adapting the cyclic polyene model, the change from the metallo-porphyrin to a free base porphyrin can be seen as a change from a 16- to an 18-membered polyene, where in both cases there are 18 electrons. A metallo-porphyrin can be represented by a 4v polyene system were both systems have $D_{4v,h}$ symmetry. A free-base and a 4v+2 polyene system have $D_{4v+2,h}$ symmetry. In the cyclic polyene system, the orbitals that participate to the $\pi \rightarrow \pi^*$ transition have symmetry e_v and e_{v+1} with v and v+1 nodes, respectively. In 4v systems (or metallo-porphyrins) the e_v orbitals are half-filled and the transition $e_v \rightarrow e_{v+1}$ give rise to the E_{1u} and $E_{2v+1,u}$ singlet states which are two pairs of degenerate states. The $e_v \rightarrow e_{v+1}$ transition in a 4v+2 (or free-base porphyrin) system give rise to the E_{1u}, B_{1u}, and B_{2u} singlet states. In the case of the cyclic polyene 4v+2 system the B_{1u} and B_{2u} states are not degenerate any more. The E_{1u} is the allowed transition while the E_{2v-1}, B_{1u}, and B_{2u} transitions are forbidden.

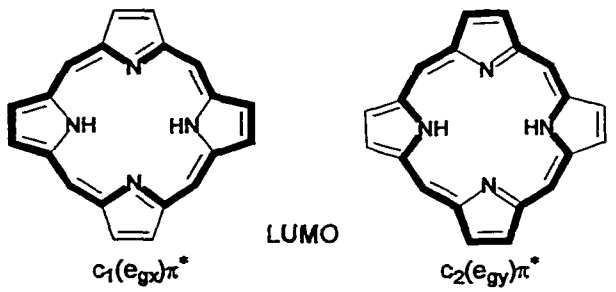

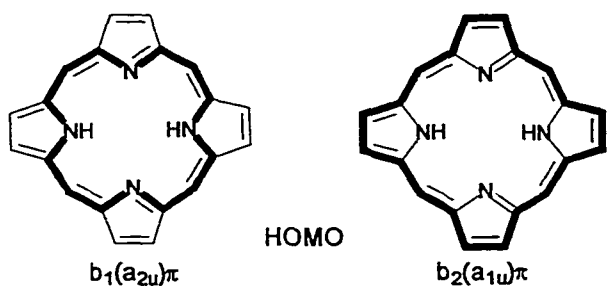

Figure A.3 Porphin MO's.[A.3]

M.O. calculations (fig. A.3) show that the top filled orbitals of porphin have symmetry a_{2u} and a_{1u} and we refer to them as b_1 and b_2 respectively. According to the same calculations, the lowest empty orbitals have symmetry e_g and are labeled

c_1 and c_2. The b_1 and b_2 have 4 nodes each, while the c_1 and c_2 have 5 nodes each, including the non-symmetry nodes. The above orbitals, resemble the e_4 and e_5 of a 16- or 18-membered cyclic polyene. The c_1 and c_2 are rigorously degenerate porphyrin ring LUMO orbitals, while the b_1 and b_2 are nearly degenerate porphyrin ring HOMO's, where the degree of degeneracy depends on the porphyrin substituents.

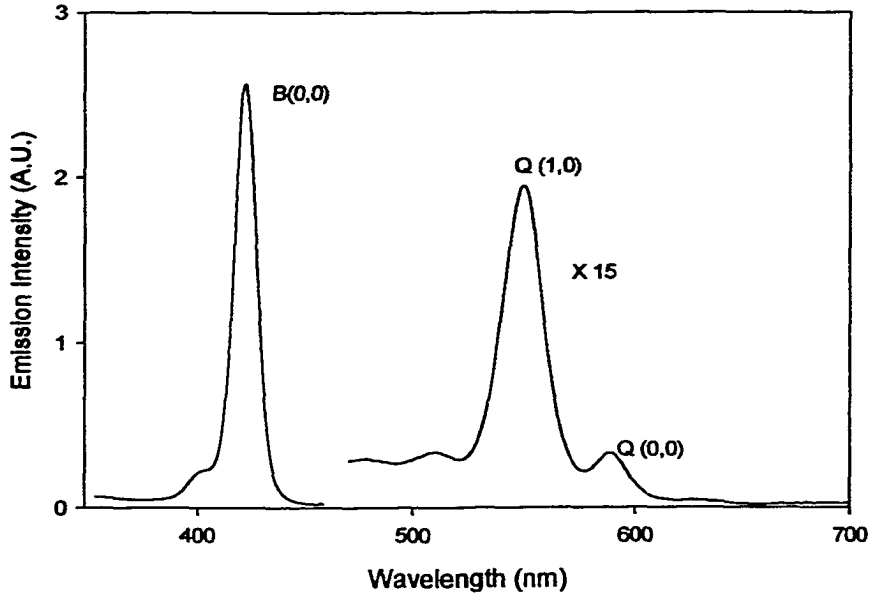

Figure A.4 UV-Vis spectra of TPPZn.

Figure A4 shows the UV-Vis spectra of a metallo-porphyrin were B(0,0) is the allowed $^1E_{1u}(a_{2u}\rightarrow e_g)$, double degenerate, and Q(0,0) the forbidden $^1E_{2v+1,u}$, double degenerate. The characteristic absorption ~1500cm^{-1} to the blue of the Q(0,0) electron origin band observed in regular porphyrins is the Q(1,0) band. This band arises from the coupling of the Q electronic state to the strongly-allowed B-state by a quantum of vibration

possessing the proper symmetry, a process usually referred to as Herzberg-Teller vibronic coupling. The intensity of the Q(1,0) band is thus described as having been vibrationally borrowed from the much more intense B-band. In D_{4h} metallo-porphyrins, these vibrational modes are in-plane non-totally-symmetric vibrations (1000-1700 cm^{-1}). These modes account for the highly consistent ~1500cm^{-1} separation observed between the Q(0,0) and Q(1,0) electronic absorption band, and also the relatively constant extinction coefficient ($\varepsilon \sim 1.5x10^4$ $M^{-1}cm^{-1}$) of the Q((1,0) band in a large number of porphyrins with only minor viriation with macrocycle substituents.[A.1] The Q(1,0) band can be used to normalize the UV-Vis spectra of a porphyrin.[A.2]

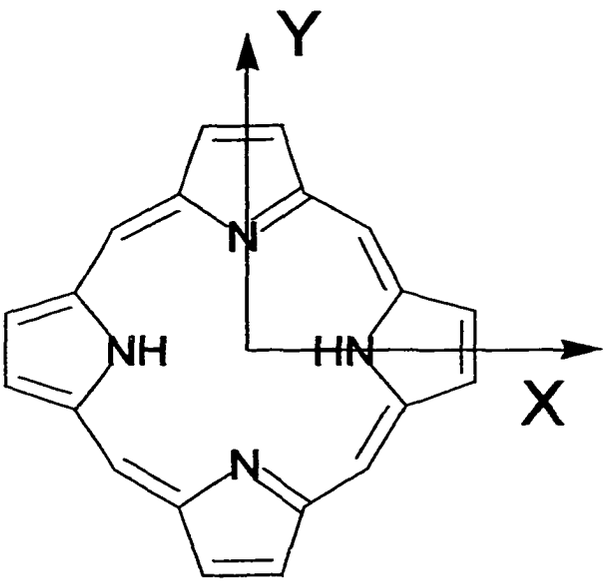

Figure A.5 Free base porphyrin skeleton.[A.3]

Porphin (fig. A.5) has two polarization axis the x and y. For a metallo-porphyrin the two axis are equivalent making the c_1 (e_{gx}) and c_2 (e_{gy}) degenerate. In the case of free base porphyrins the two axis are not equivalent. X is the axis that contains the two hydrogens, that stabilize the e_{gx}, and they remove the degeneracy from the e_{gx} and e_{gy} orbitals. The forbidden states $^1B_{1u}(a_{1u}\rightarrow e_{gy})$ and $^1B_{2u}(a_{1u}\rightarrow e_{gx})$ are the peaks $Q_x(0,0)$ and $Q_y(0,0)$ labeled in the UV-Vis. spectra (fig. A.6). The Soret band is expected to split too since the transitions $^1(a_{2u}\rightarrow e_{gy})$ and $^1(a_{2u}\rightarrow e_{gx})$ are not degenerate any more. Experiments at room temperature do not show the expected splitting due to the

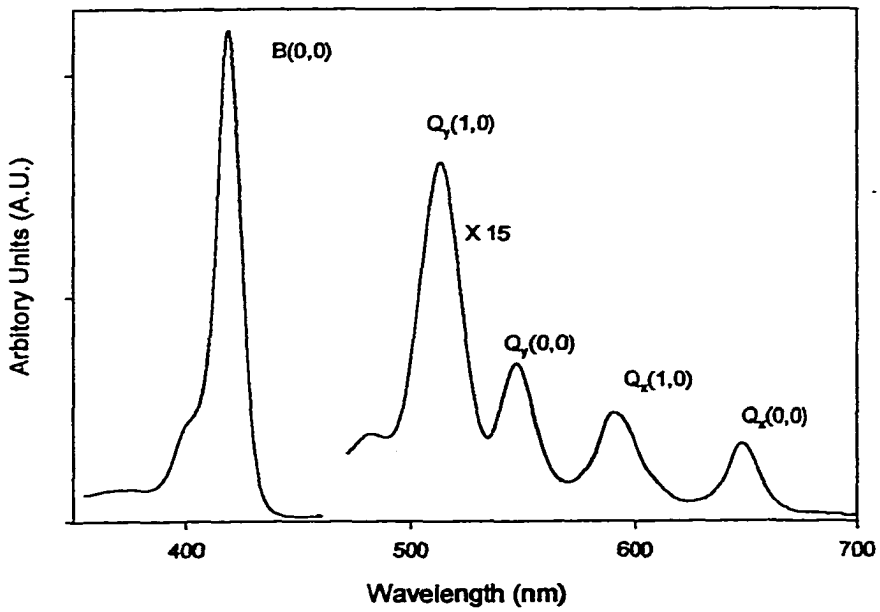

***Figure A.6** UV-Vis spectra of $TPPH_2$.*[A.3]

fast vibronic coupling between the two states, $B_x(0,0)$ and $B_y(0,0)$. Splitting of the Soret band has been observed at low temperatures.[A.1] Also the $Q_x(0,0)$ and $Q_y(0,0)$ give rise to the $Q_x(1,0)$ and $Q_y(1,0)$ respectively after vibrational coupling with the Soret band.

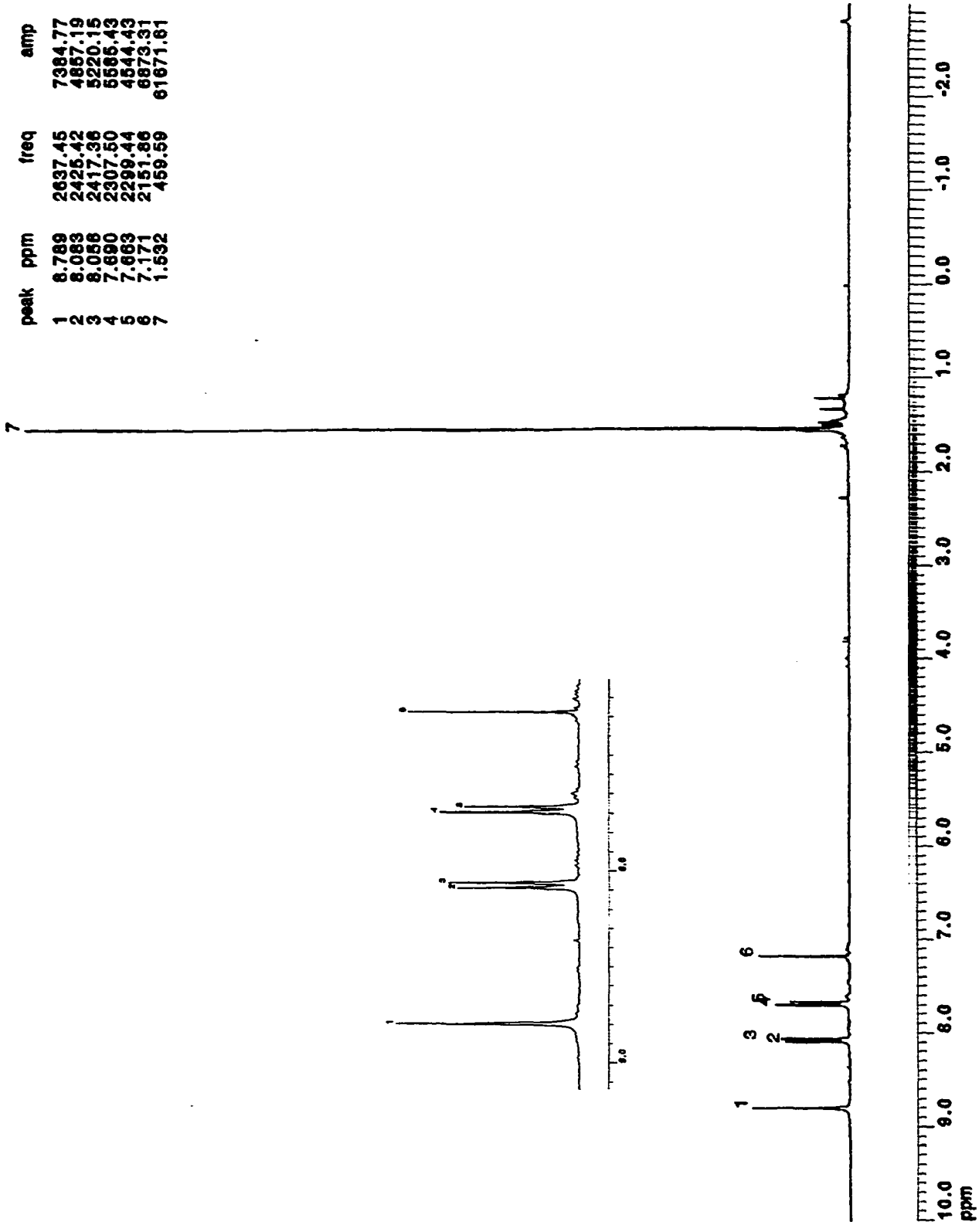

Figure B.1 ^{1}H-NMR spectra of 5,10,15,20(4-tert-butylphenyl)porphyrin.

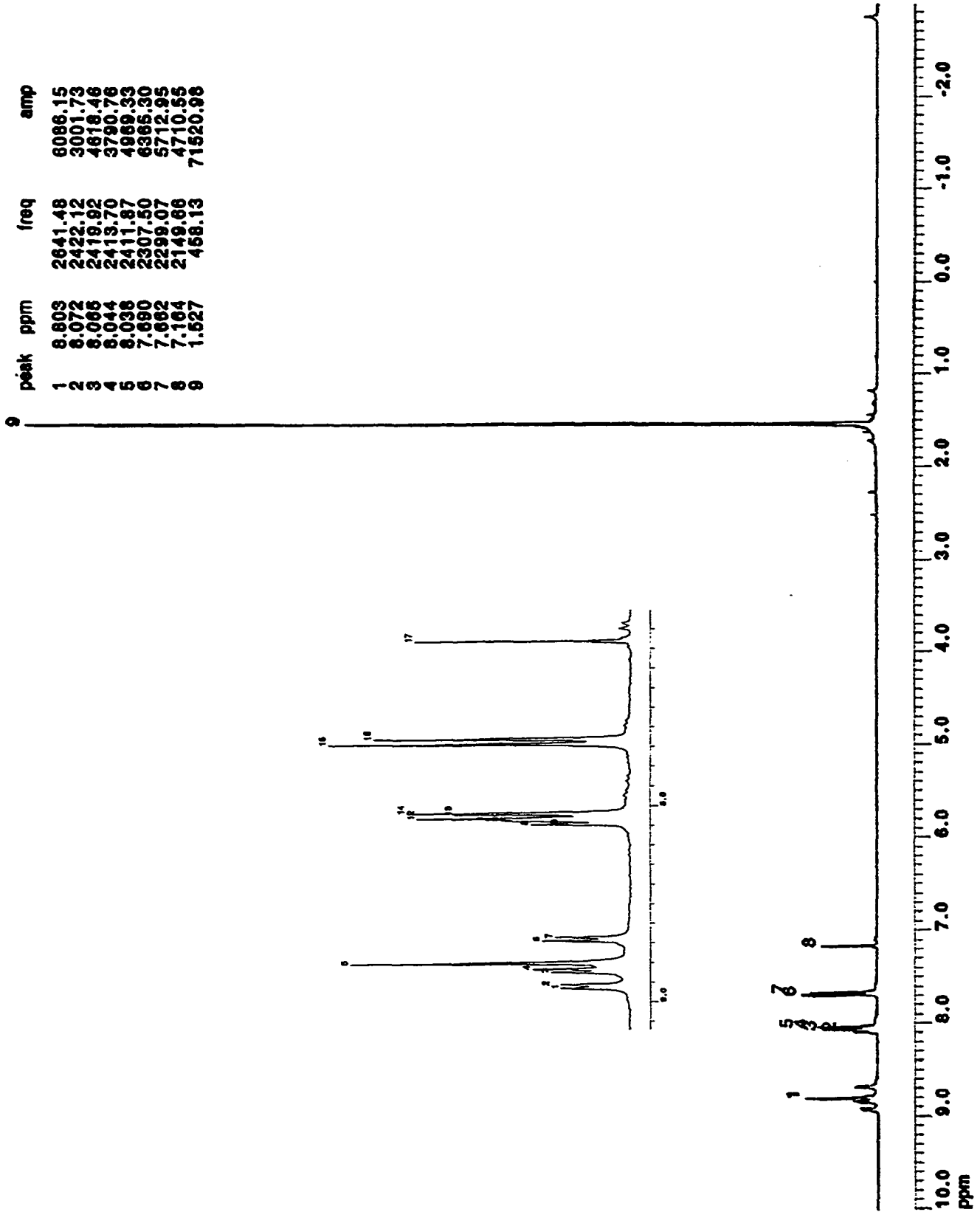

Figure B.2 ^{1}H-NMR spectra of 5Py10,15,20(4-tert-butylphenyl)porphyrin.

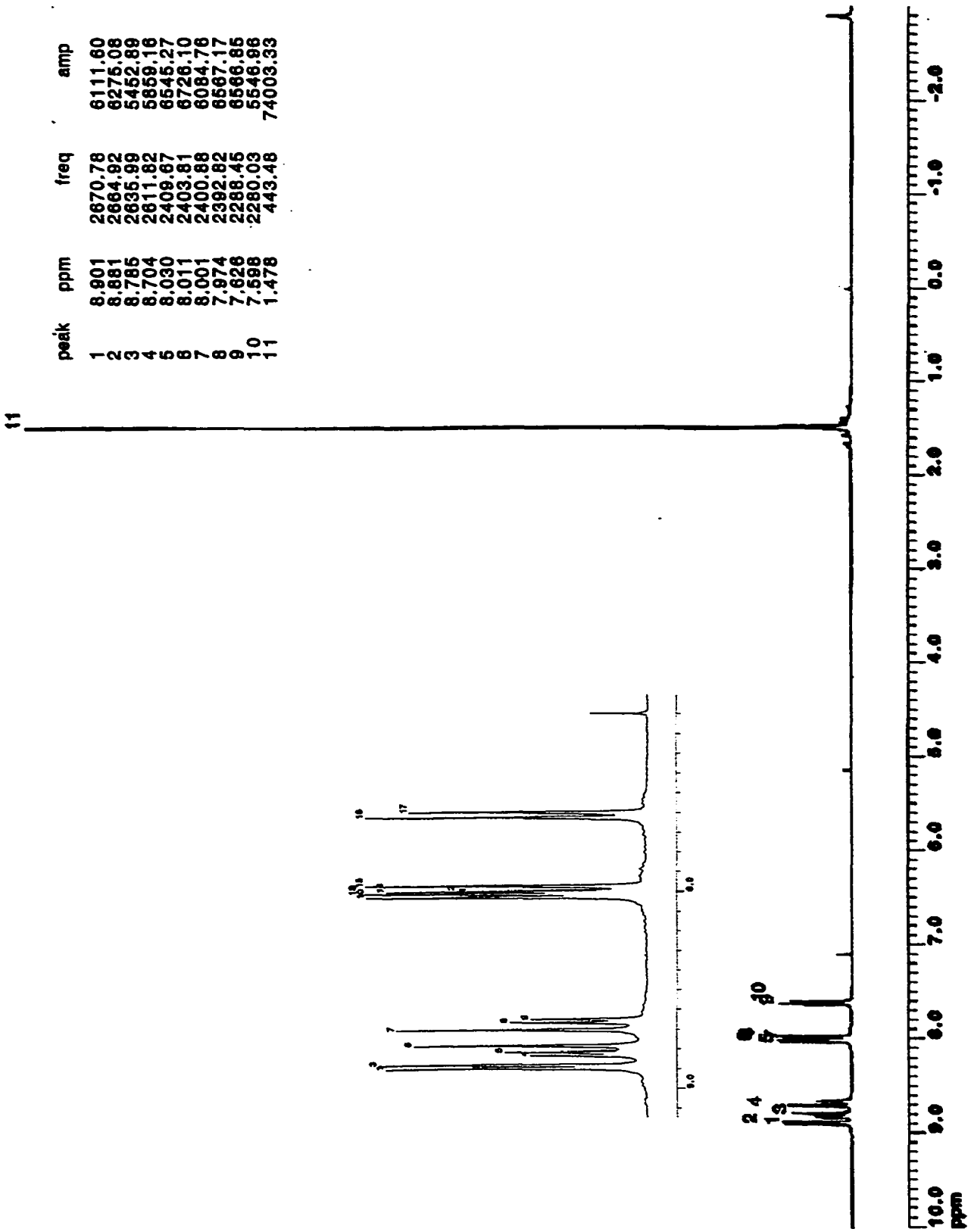

Figure B.3 ^{1}H-NMR spectra of 5,10Py15,20(4-tert-butylphenyl)porphyrin.

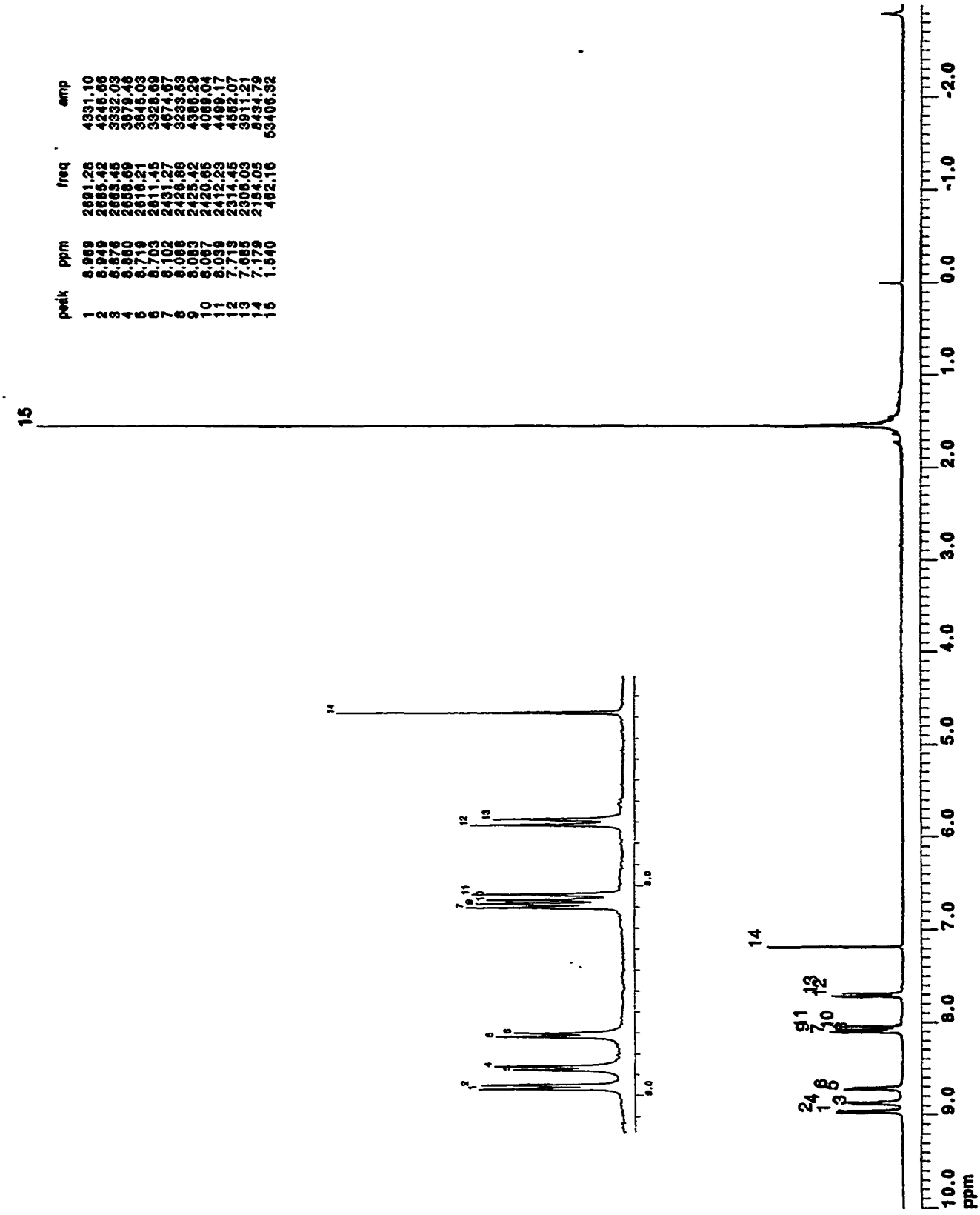

Figure B.4 ^{1}H-NMR spectra of 5,15Py10,20(4-tert-butylphenyl)porphyrin.

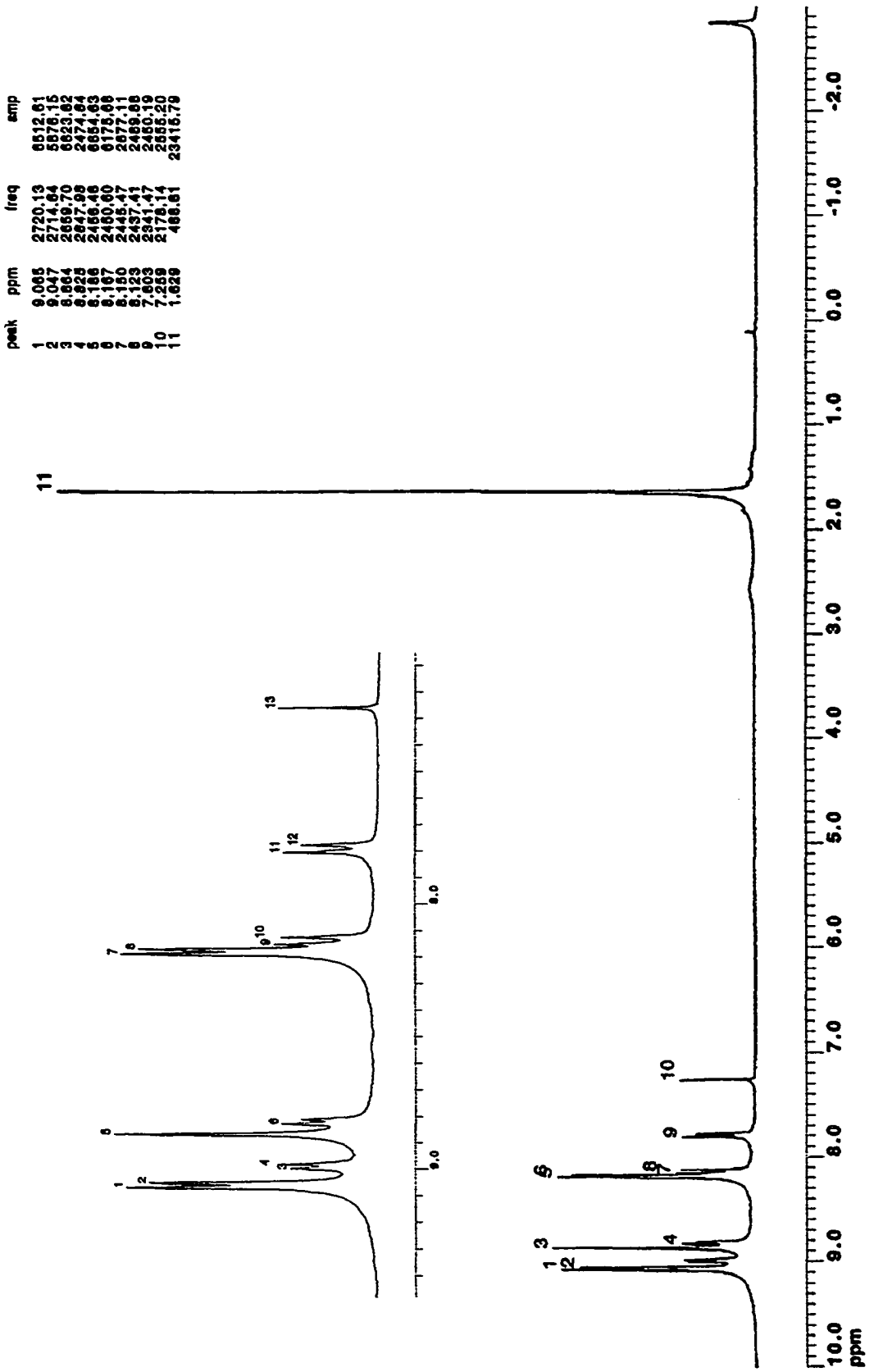

Figure B.5 ^{1}H-NMR spectra of 5,10,15Py20(4-tert-butylphenyl)porphyrin.

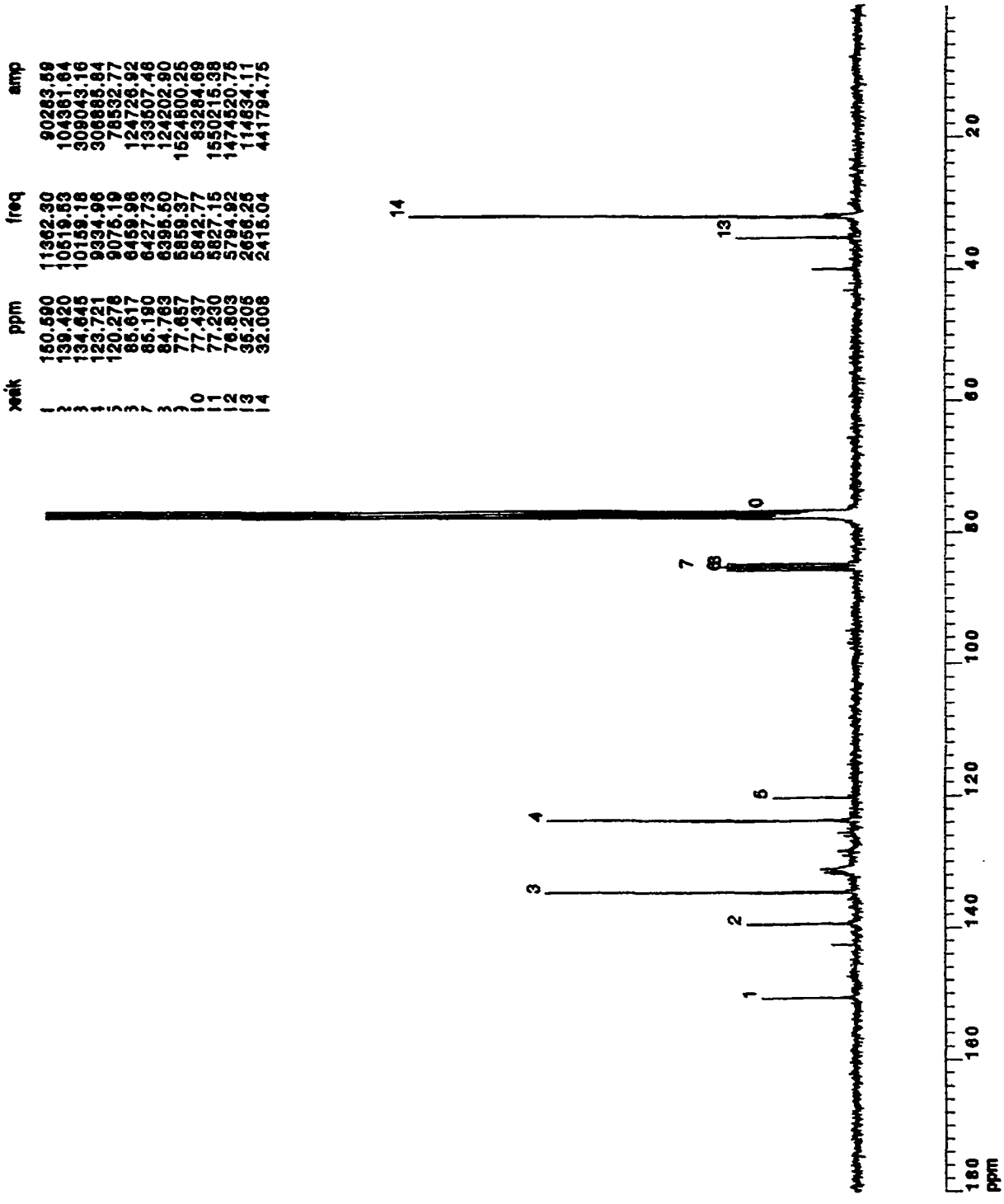

Figure B.11 ^{13}C-NMR spectra of 5,10,15,20(4-tert-butylphenyl)porphyrin.

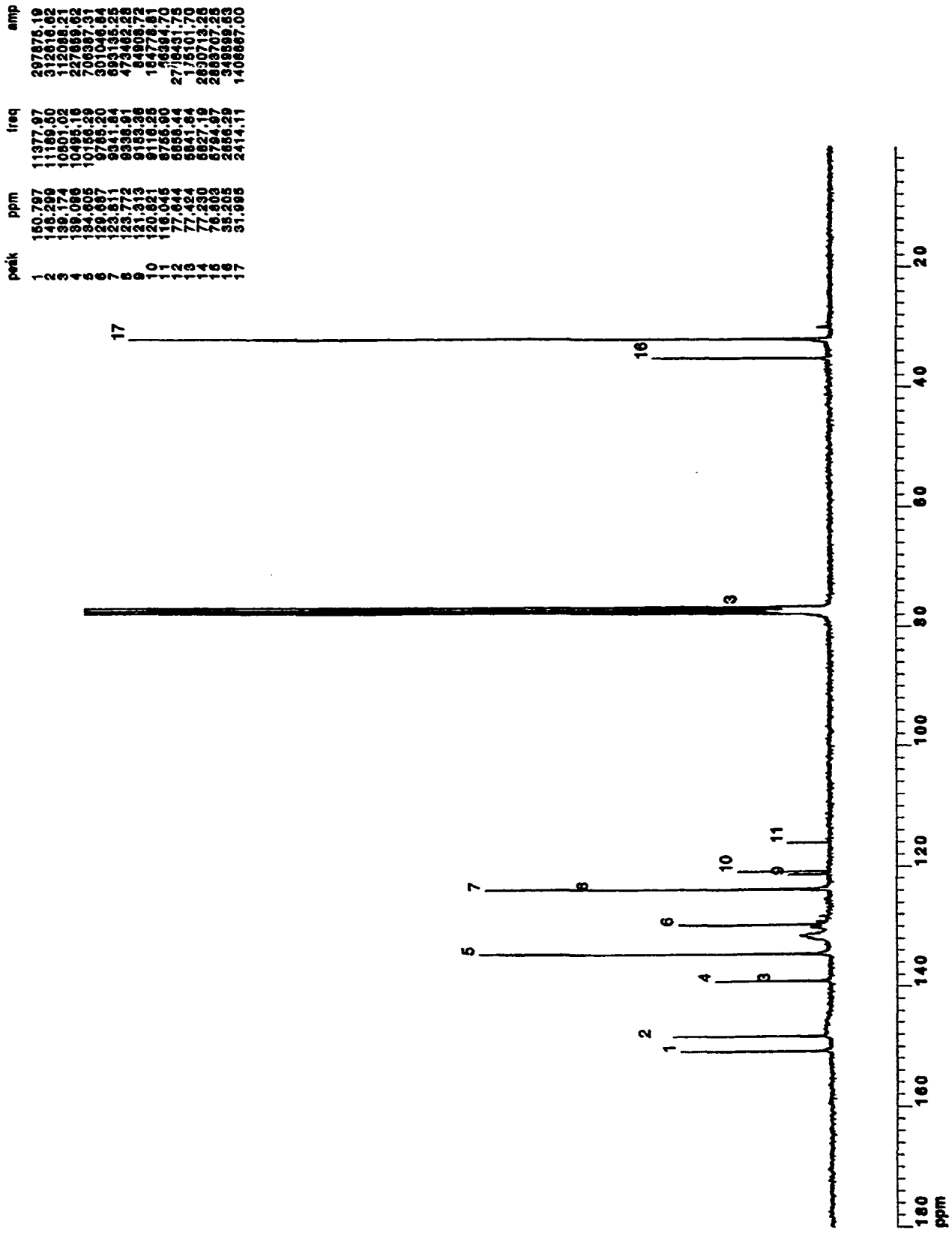

Figure B.12 ^{13}C-NMR spectra of 5Py10,15,20(4-tert-butylphenyl)porphyrin.

peak	ppm	freq	amp
1	150.965	11390.67	241226.16
2	150.421	11348.65	270149.00
3	148.415	11198.29	835183.19
4	138.863	10477.58	272394.28
5	134.592	10155.32	742913.56
6	129.571	9776.41	761334.88
7	123.837	9343.79	775640.81
8	121.805	9190.47	238706.81
9	116.602	8797.90	244768.72
10	77.657	5859.42	913846.62
11	77.230	5827.19	936761.06
12	76.803	5794.97	874346.94
13	35.205	2656.29	319378.28
14	31.956	2411.18	1205039.25

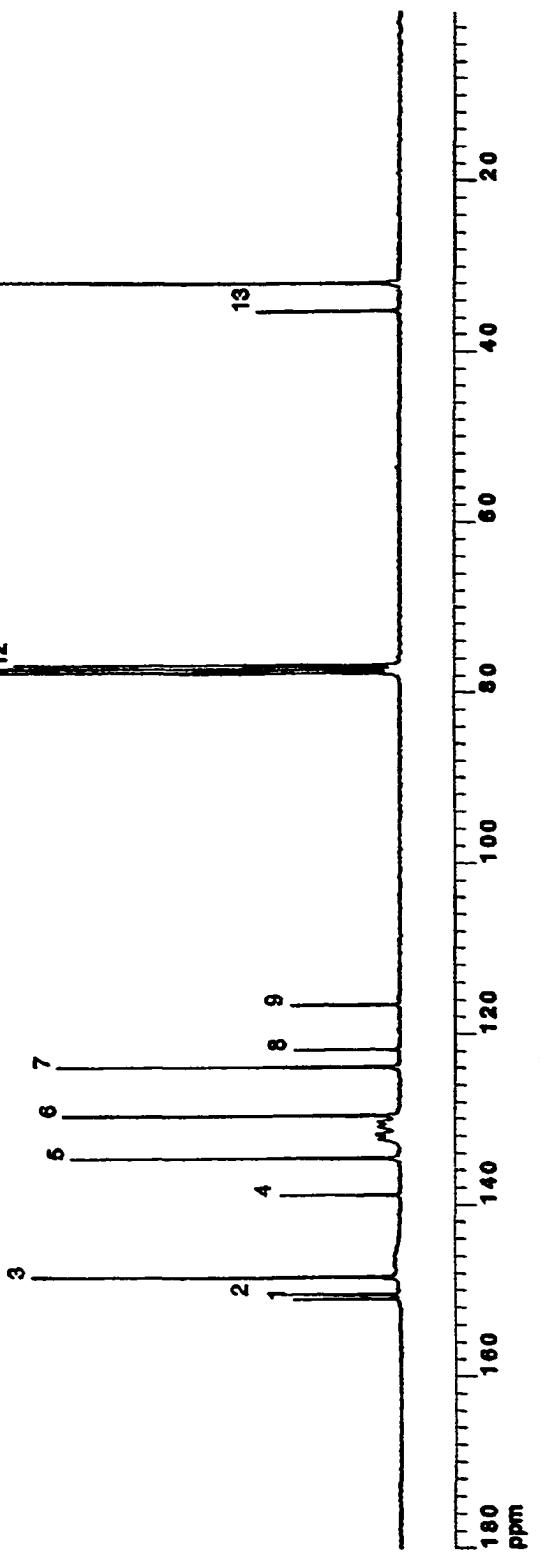

Figure B.13 ^{13}C-NMR spectra of 5,10Py15,20(4-tert-butylphenyl)porphyrin.

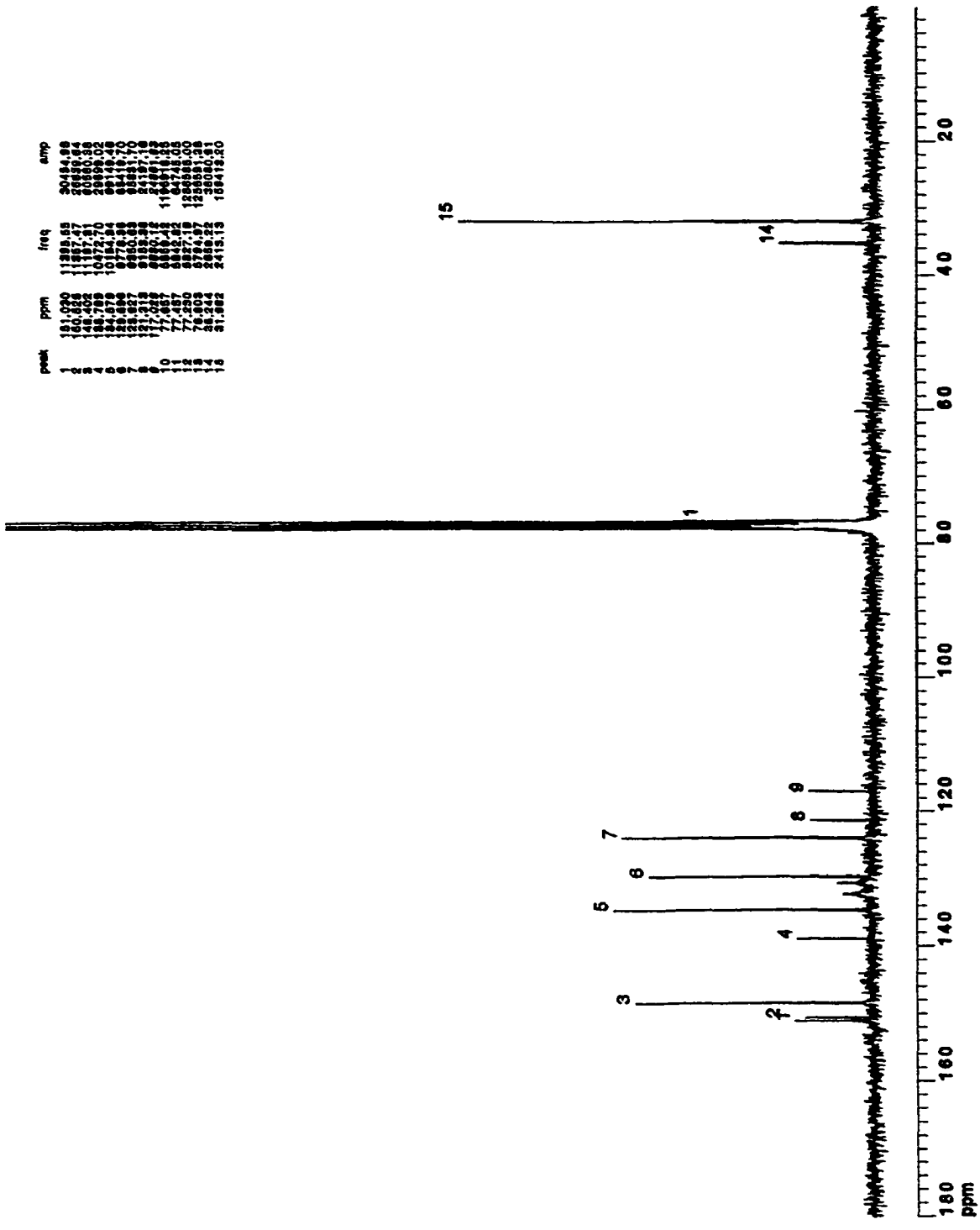

Figure B.14 ^{13}C-NMR spectra of 5,15Py10,20(4-tert-butylphenyl)porphyrin.

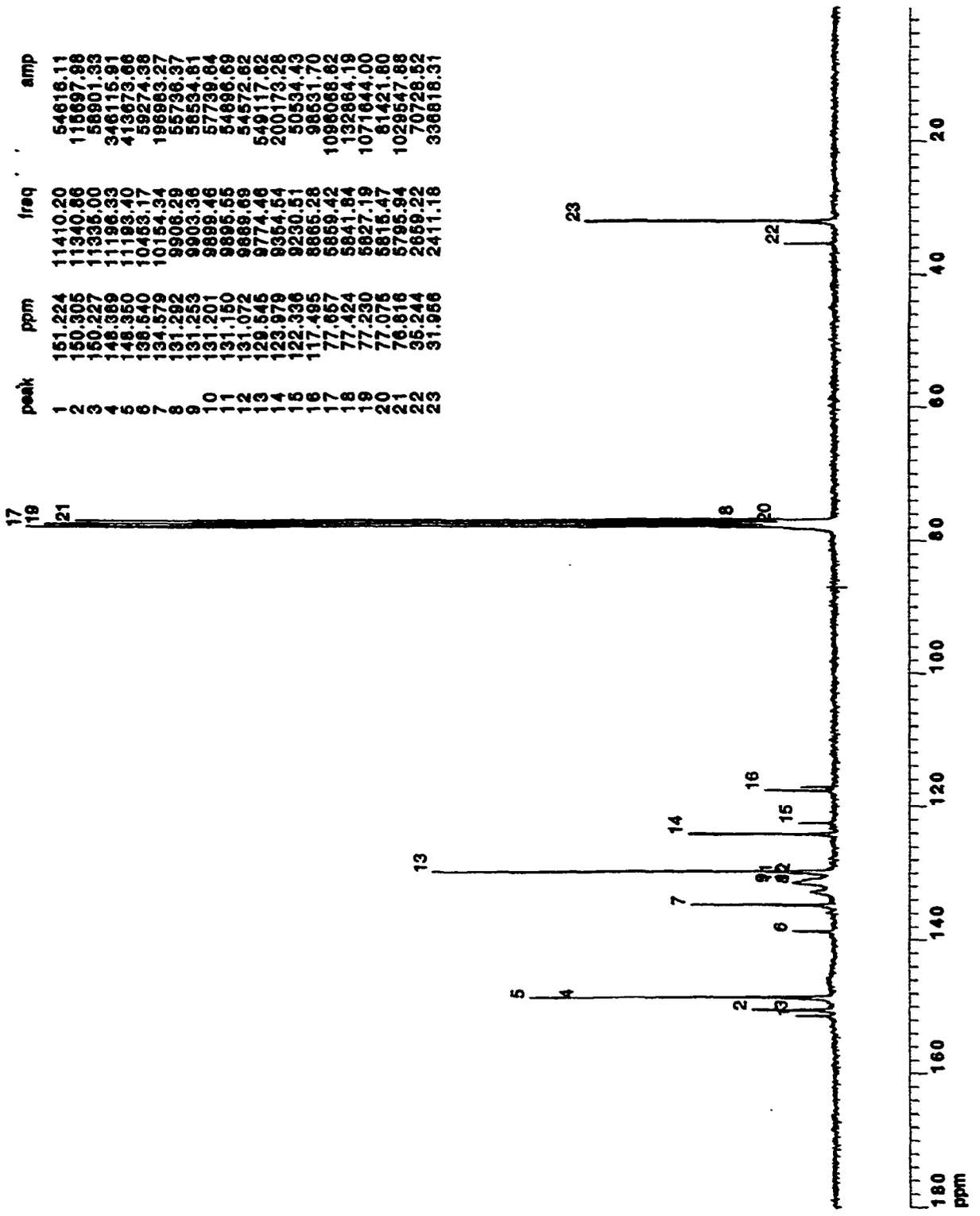

Figure B.15 ^{13}C-NMR spectra of 5,10,15Py20(4-tert-butylphenyl)porphyrin.

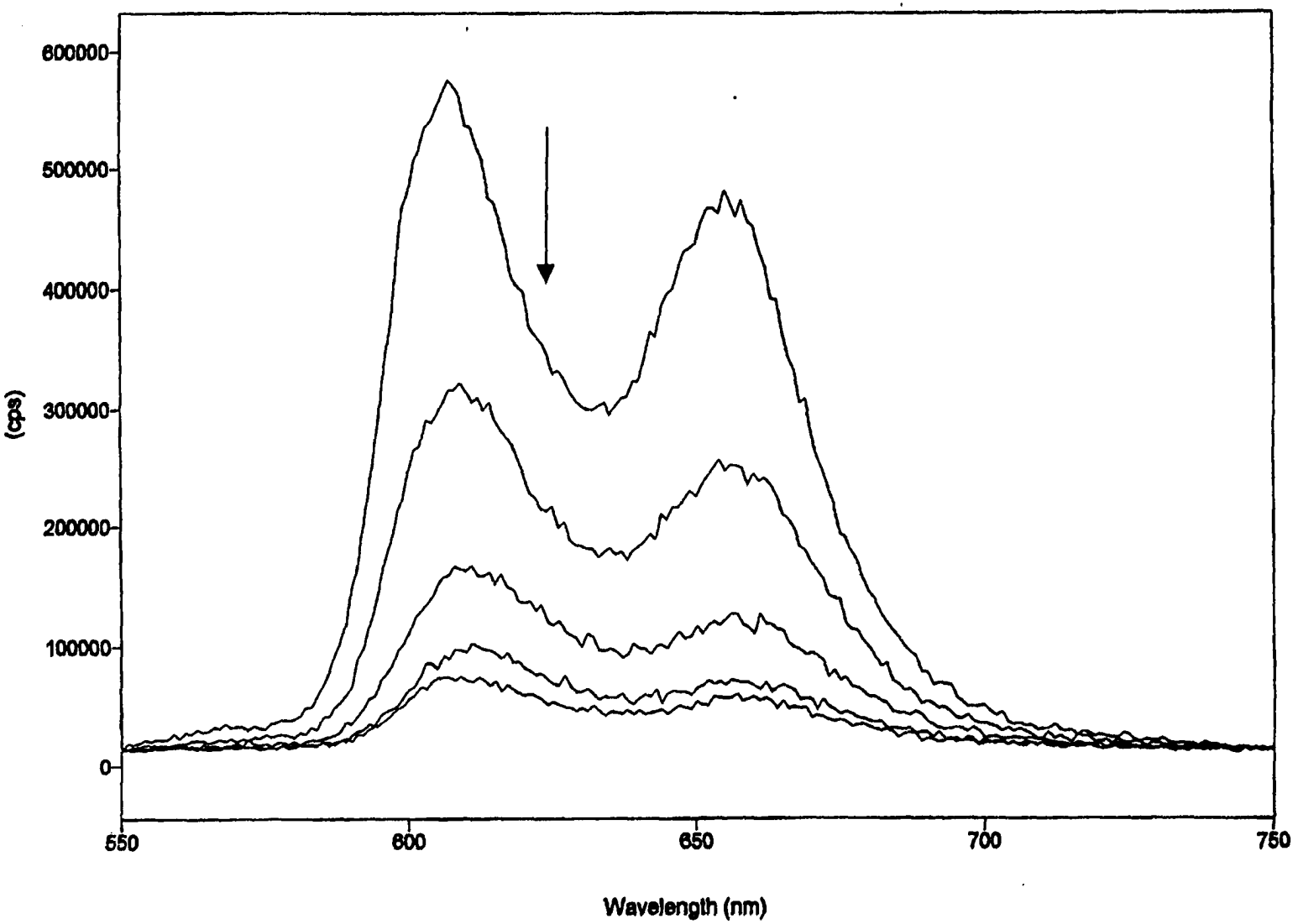

Figure C.1 Fluorescence emission titration of mixture of metallo-porphyrins (4L, 4T, 1X) with 12 eq. Pd-complex for the formation of **4b.**

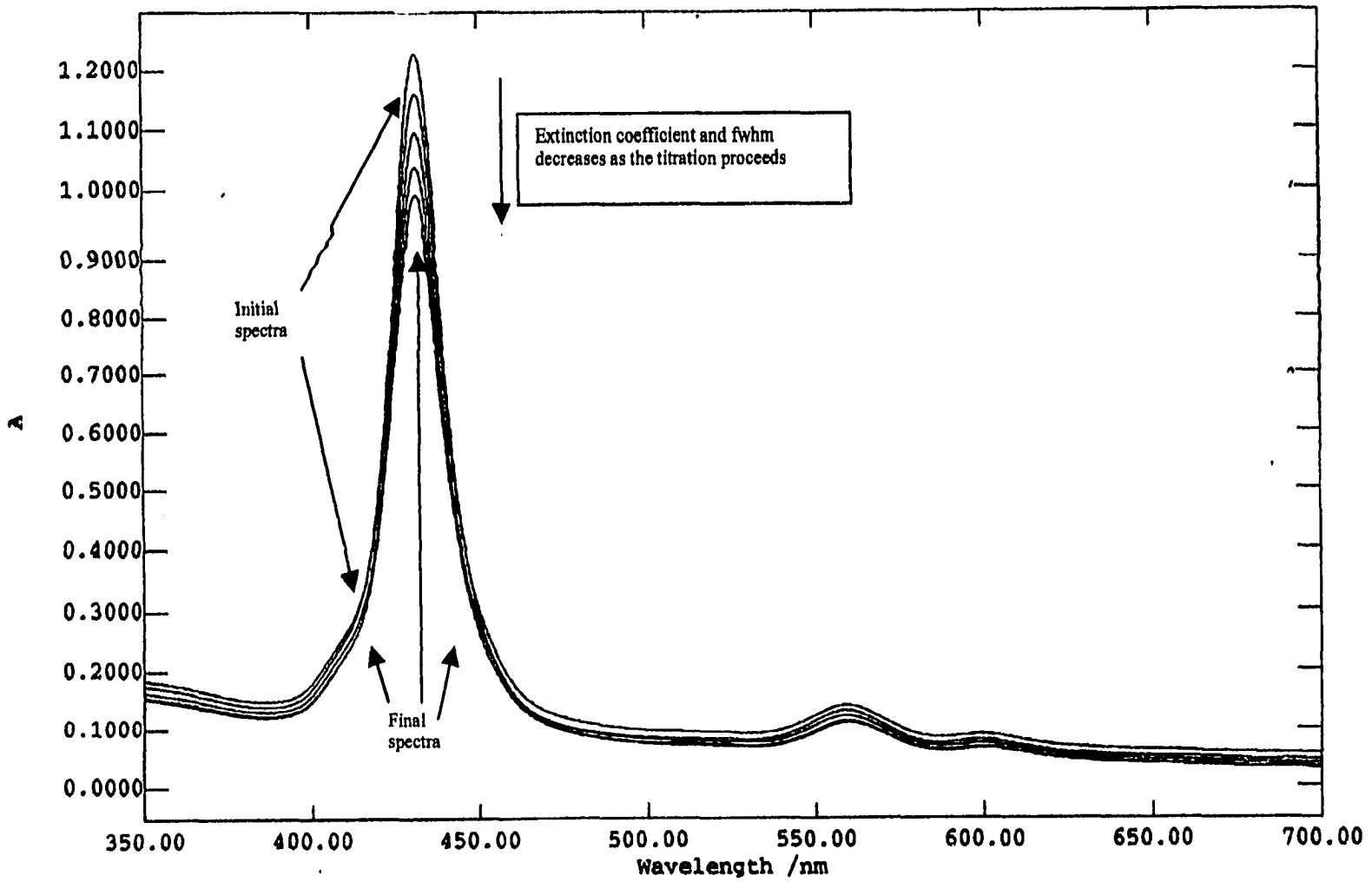

*Figure C.2 UV-Vis titration of the metallo-nonamer (**4b**) with 4.5 eq. Bpy.*

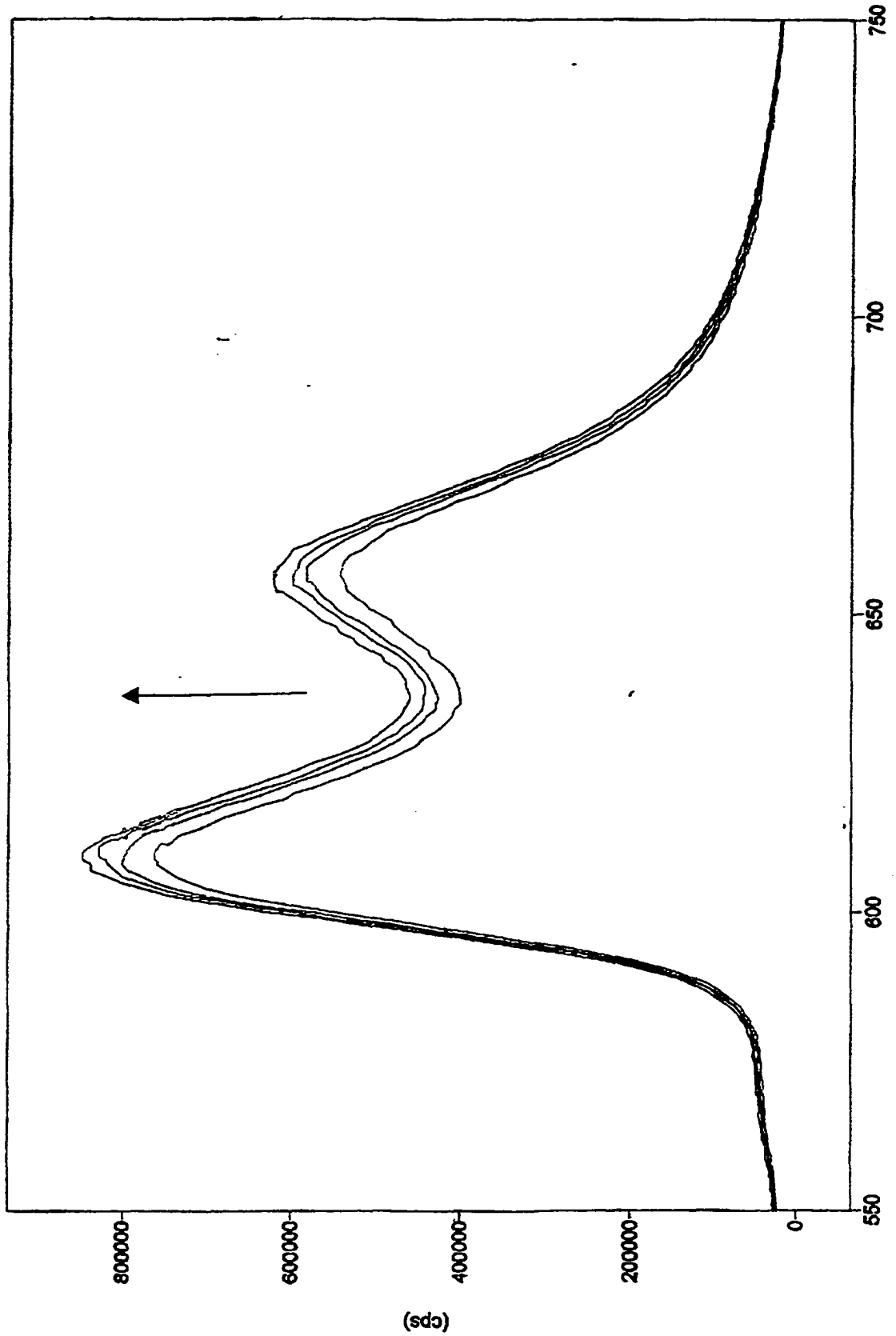

*Figure C.3 Fluorescence emission titration of **4b** in toluene with 4.5 eq. Bpy.*

D. Formation of the μ-bridged compound (20)

The chloro-bridged-Pt compound (**20**) was formed by mixing equimolar amounts of (0.0039g; 14.7μmol) $PtCl_2$ and (0.0119g; 15.0μmol) *cis*-$(Ph_3P)_2PtCl_2$ in naphthalene (0.2g) (fig. D.1).

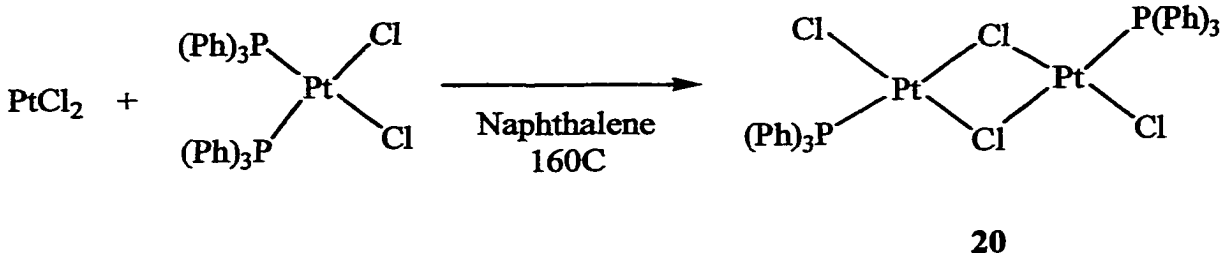

20

Figure D.1 Formation of Di-μ-chloro dichloro bis(triphenylphosphine)diplatinum(II).

The reaction mixture was heated and stirred at 160-170°C for 4 hours. Naphthalene sublimes very easily, so cautions must be taken so solvent is not lost. (Attempts to use mineral oil as the media were fruitless since no product was observed even after 12 hours of heating). The reaction mixture was treated with ligroin where the product precipitated out of solution, which dissolved in CH_2Cl_2. Further purification of the product in CH_2Cl_2 was achieved by flash chromatography over silica gel. Toluene was used to remove remaining naphthalene while 10% EtOH in toluene elutes the yellow-orange product (**20**). The orientation of the phosphine groups on the platinum is *trans* according to the literature.[D.1]

^{1}H-NMR of the product (**20**) was taken in CD_3CN (fig. D2), to show the phenyl protons as two multiplets, due to the phosphorous hydrogen coupling, between 7.5 and 7.8ppm. The spectrum shows that the solvent coordinates to the Pt, possible by breaking up the bridged compound, making the compound soluble in the solvent. The H-NMR spectrum has a multiplet peak at 1.94ppm for the free solvent and a singlet peak at 1.95ppm for the bound solvent.

Excess of pyridine was added to a CH_3CN solution of the bridged-Pt compound. ^{1}H-NMR (fig. D.3) and ^{31}P-NMR (fig. D.4) of the residue was taken in CD_3CN. The characteristic reaction[D.2] of pyridine with the halogen bridged binuclear complex $[Pt(PPh_3)Cl_2]_2$ to symmetrically cleave the halogen bridge is confirmed by the NMR experiments. Figure D.3 and D.4 indicate that the cleavage of the μ-bridged compound takes place simultaneously in a *trans* mechanism to give 100% compound **21t**, as indicated in figure D.9. We were of interest to examine the isomerization of *trans* to *cis* complex. ^{31}P-NMR spectroscopy was used to follow the process. The reaction product was left overnight in 5%EtOH in CH_3CN (^{1}H-NMR fig. D.5; ^{31}P-NMR fig. D.6) and in 20% EtOH in CH_3CN (^{1}H-NMR fig. D.7; ^{31}P-NMR fig. D.8). Solvent was evaporated to dryness and the residue was dissolved in CD_3CN for the ^{1}H-and ^{31}P-NMR. As it can be seen from the NMR spectra in the presence of EtOH the *trans* complex isomerizes to *cis*. There is co-existence of the two species in both solvent systems, while as we increase the concentration of the EtOH from 5% to 20% the percent of the *cis* species significantly increases.

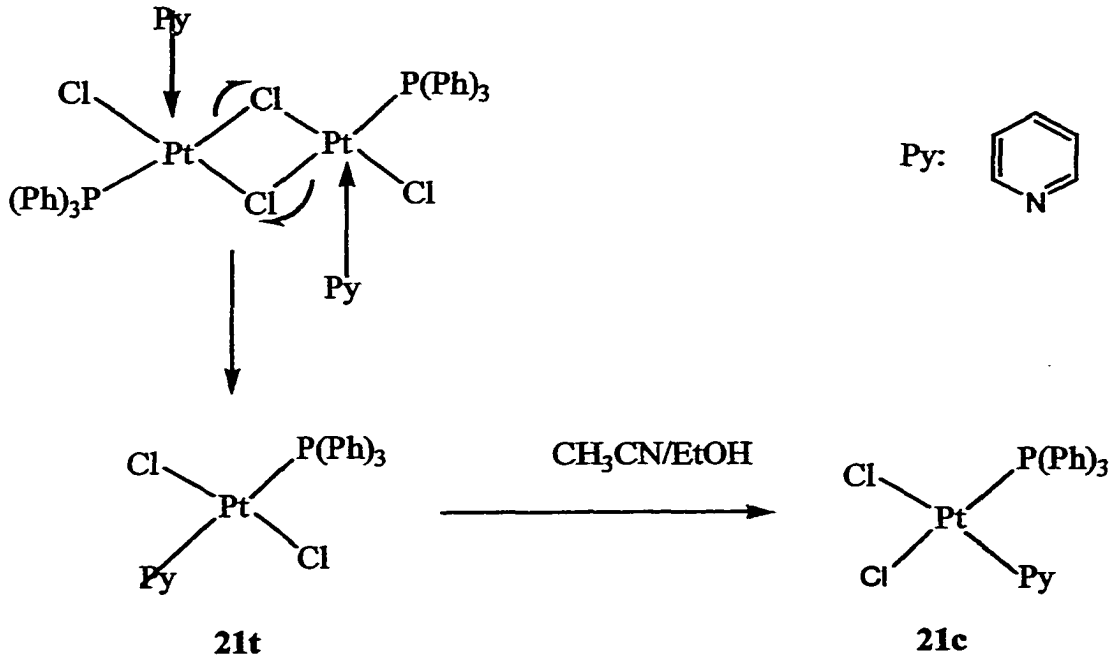

***Figure D.9** Cleavage mechanism of compound (20) with pyridine. Isomerization in EtOH.*

The *cis* (**21c**) and *trans* (**21t**) geometry for the platinum compounds was defined by the magnitude of the coupling constants, J(Pt-P). Clark et al.[D.2] prepared [(P-n-Pr_3)(CO)$PtCl_2$] by the bridge cleavage reaction of [(P-n-Pr_3)ClPd(μ-Cl)$_2$PtCl(P-n-Pr_3)] with carbon monoxide, and assigned a *cis* geometry to this product. The observed coupling constant, P-Pt, was of 2778Hz. The same group prepared[D.2] [(P-n-Pr_3)(Py)$PtCl_2$] (**22**) by the bridged cleavage reaction of the same hetero-nuclear compound with pyridine. The observed coupling constant, Pt-P, was of 3335Hz, and they assigned a *trans* geometry to the complex. In a similar manner compound [(P-n-Bu)(Py)$PtCl_2$] (**23**) has been formed[D.3] having J(Pt-P)=3360Hz and was assigned the *trans* geometry. The greater J(Pt-P) value for the **21c** than that of **22** and **23** is attributed to an increase in covalency of the Pt-P bond. The multiplet peak at 8.92ppm for the *ortho*-H of the pyridine in the ^{1}H-

NMR spectra of the *cis* compound **(21c)** indicates P-H coupling through space. This is not observed for the *trans* complex **21t** since the through space P-H interaction is not possible.

The greater downfield shift of the phosphorous signal of the *trans* complex indicates that the pyridine communicates with the phosphine through bond rather than through space, showing electronic communication between the *trans* positions of the square planar Pt complex.

	^{1}H-NMR (ppm)	^{31}P-NMR (ppm)
Trans-compound (21t)	8.35(d,1H)	
	7.57(m,2H)	7.8582(t, J(Pt-P)=3902Hz)
	7.22(m,2H)	
Cis-compound (21c)	8.92(m,1H)	
	7.73(m,2H)	3.2123(t, J(Pt-P)=3582Hz)
	7.34(m,2H)	

***Table D.1** ^{1}H- and ^{31}P-NMR data for cis (21c) and trans (21t) compounds.*

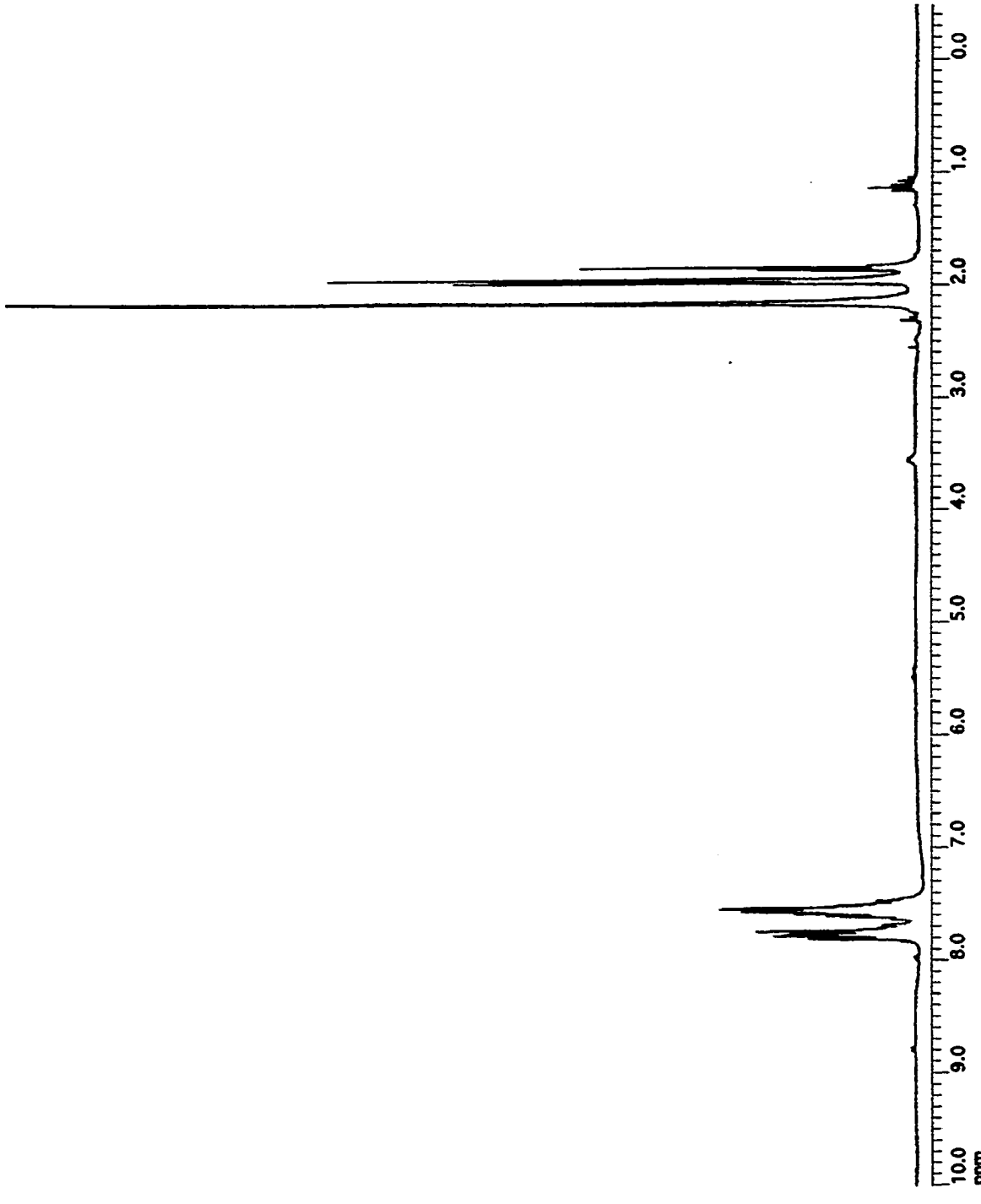

Figure D.2 ^{1}H-NMR spectra of Chloro-bridged-Pd complex in CD_3CN.

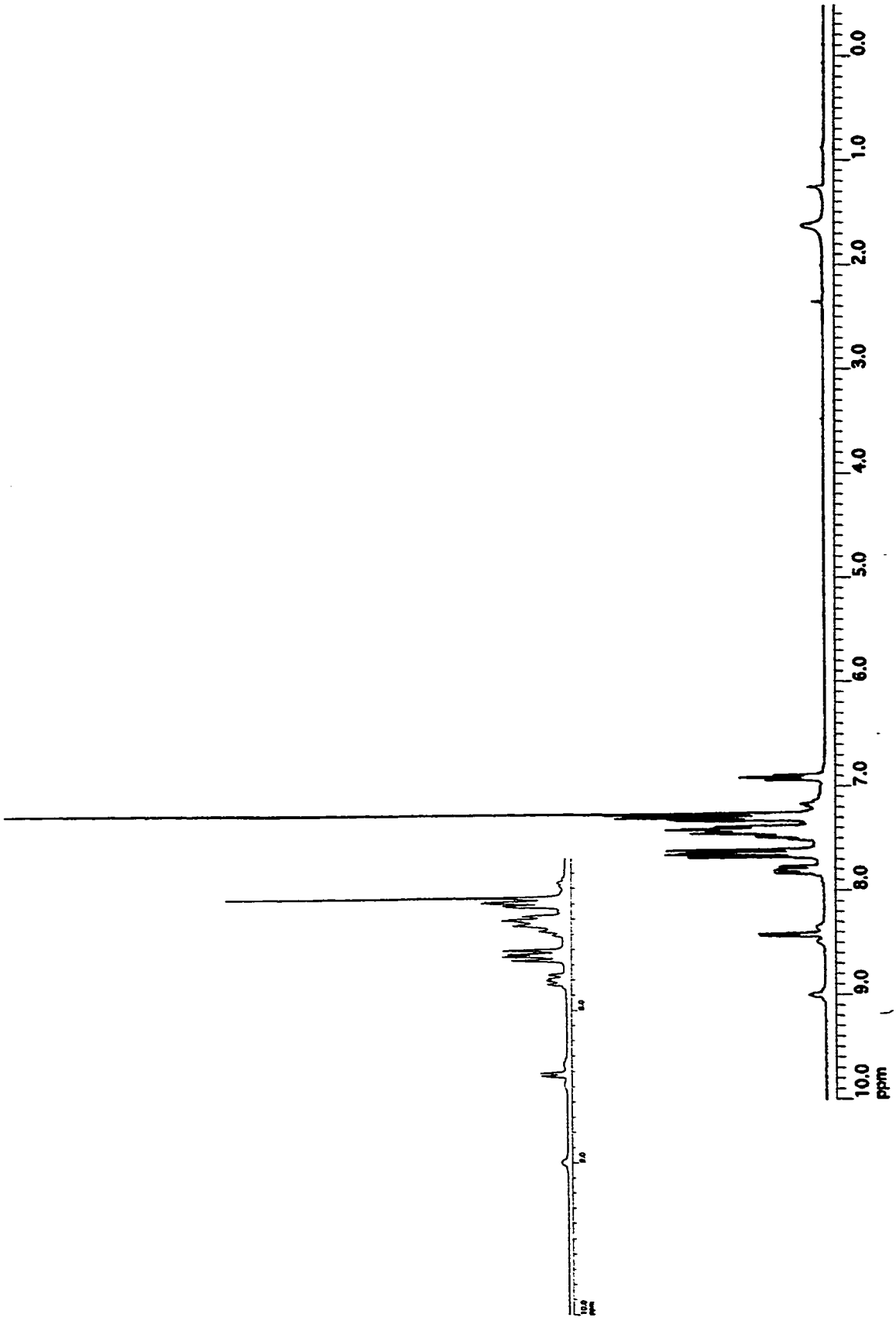

Figure D.3 ^{1}H-NMR spectra of Chloro-bridged-Pd complex with Pyridine in CD_3CN.

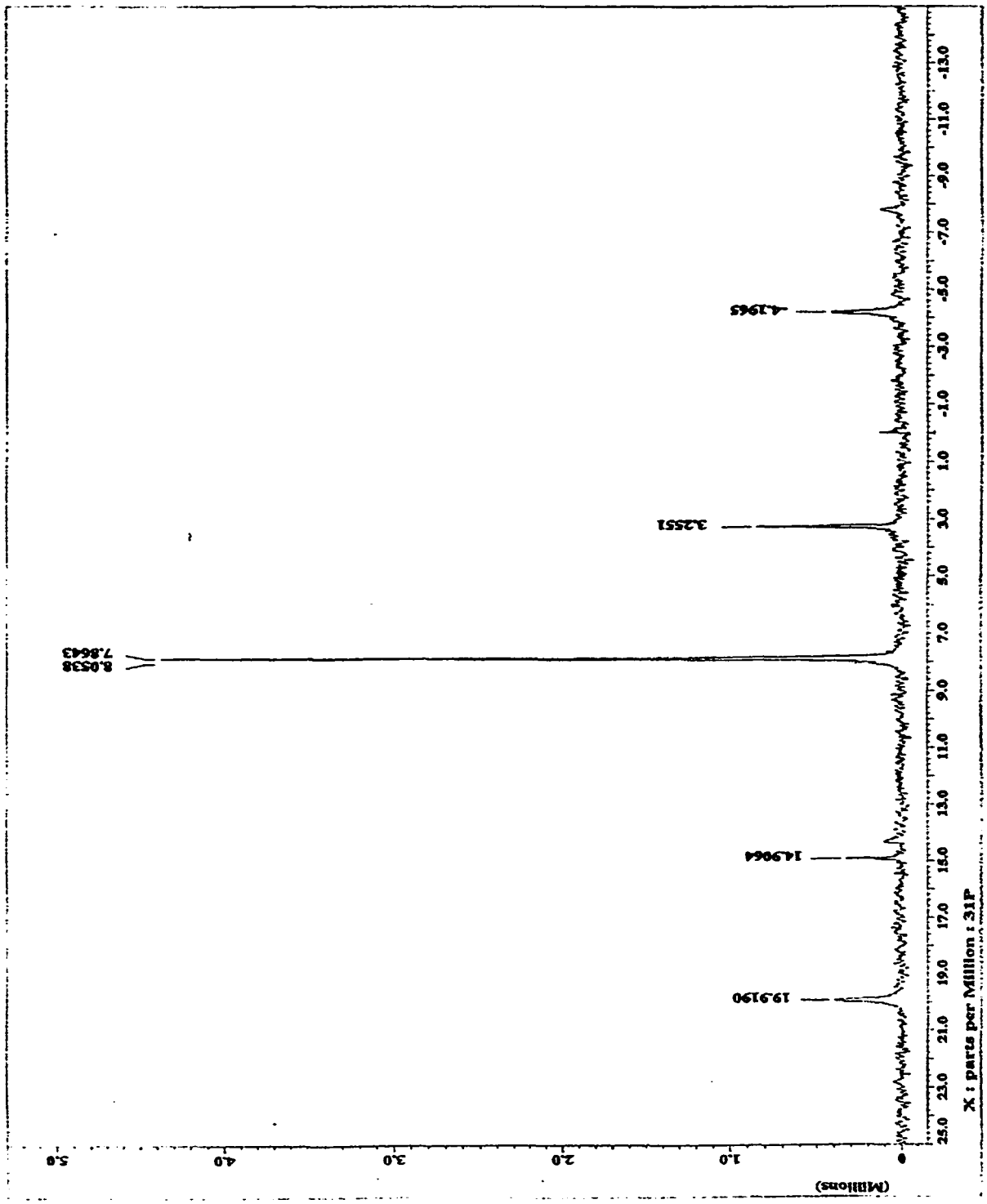

Figure D.4 ^{31}P*-NMR spectra of Chloro-bridged-Pd complex with Pyridine in* CD_3CN.

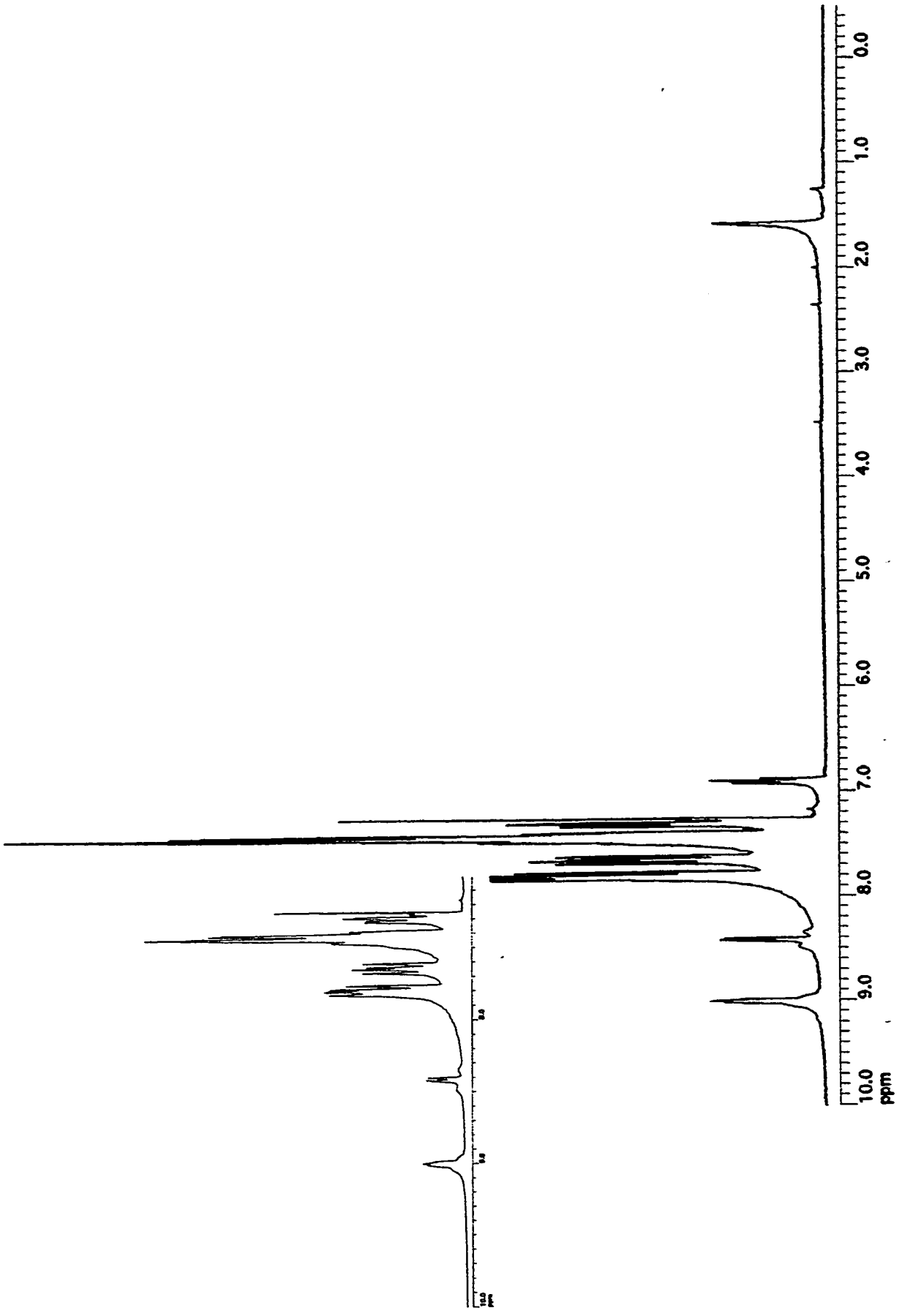

Figure D.5 ^{1}H-NMR spectra of Chloro-bridged-Pd complex with Pyridine 5%EtOH in CD_3CN.

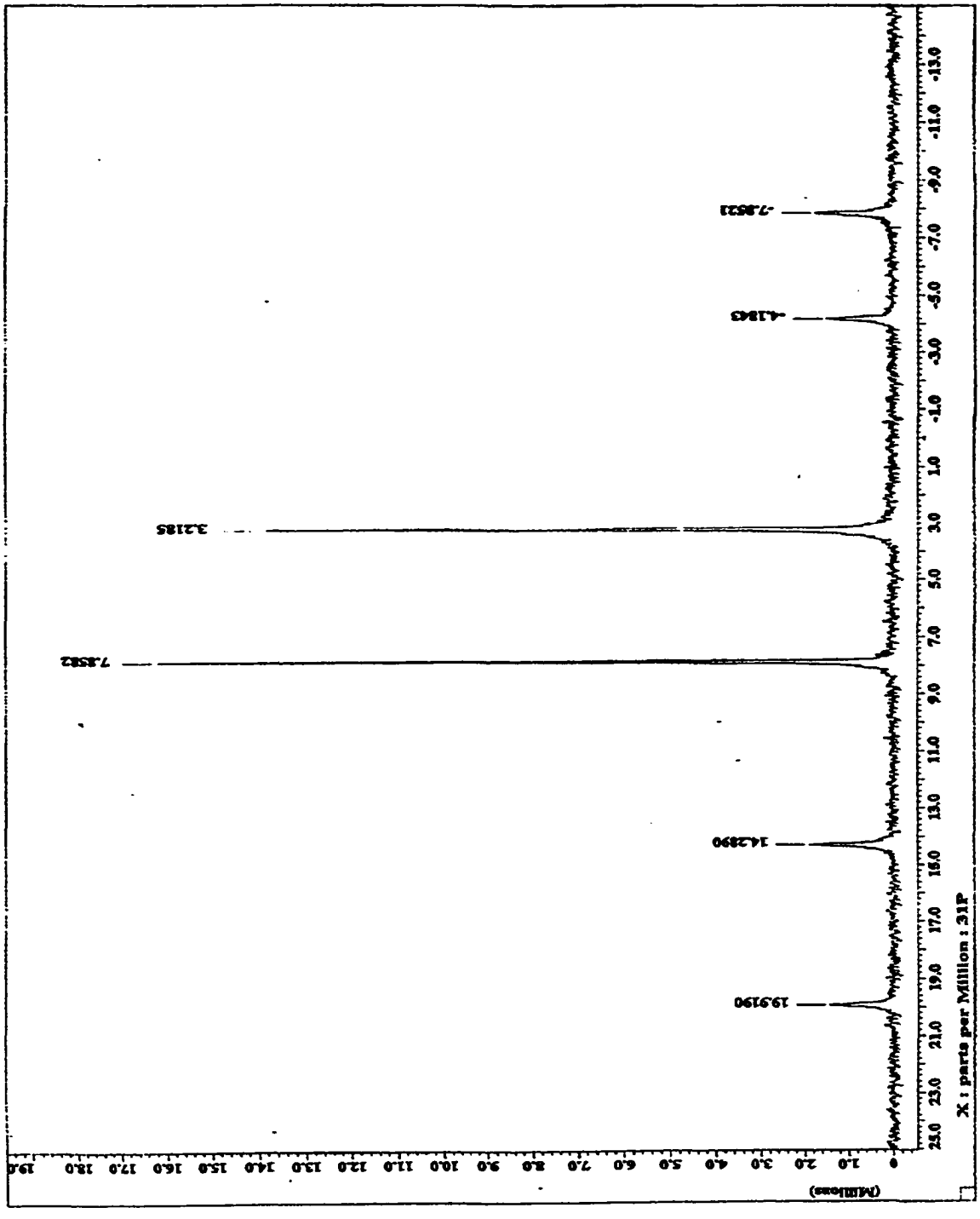

Figure D.6 ^{31}P-NMR spectra of Chloro-bridged-Pd complex with Pyridine 5%EtOH in CD_3CN.

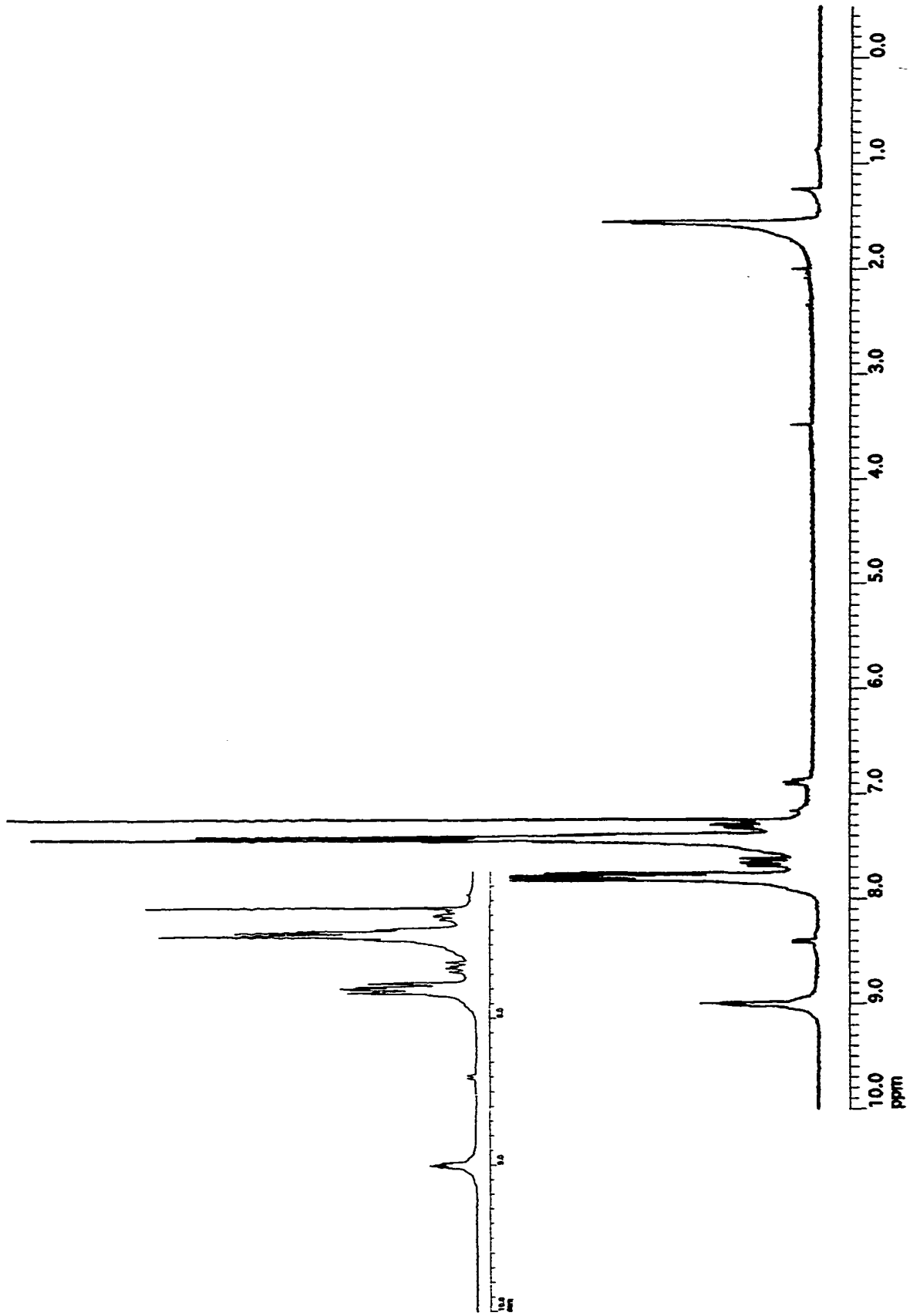

Figure D.7 ^{1}H-NMR spectra of Chloro-bridged-Pd complex with Pyridine 20%EtOH in CD_3CN.

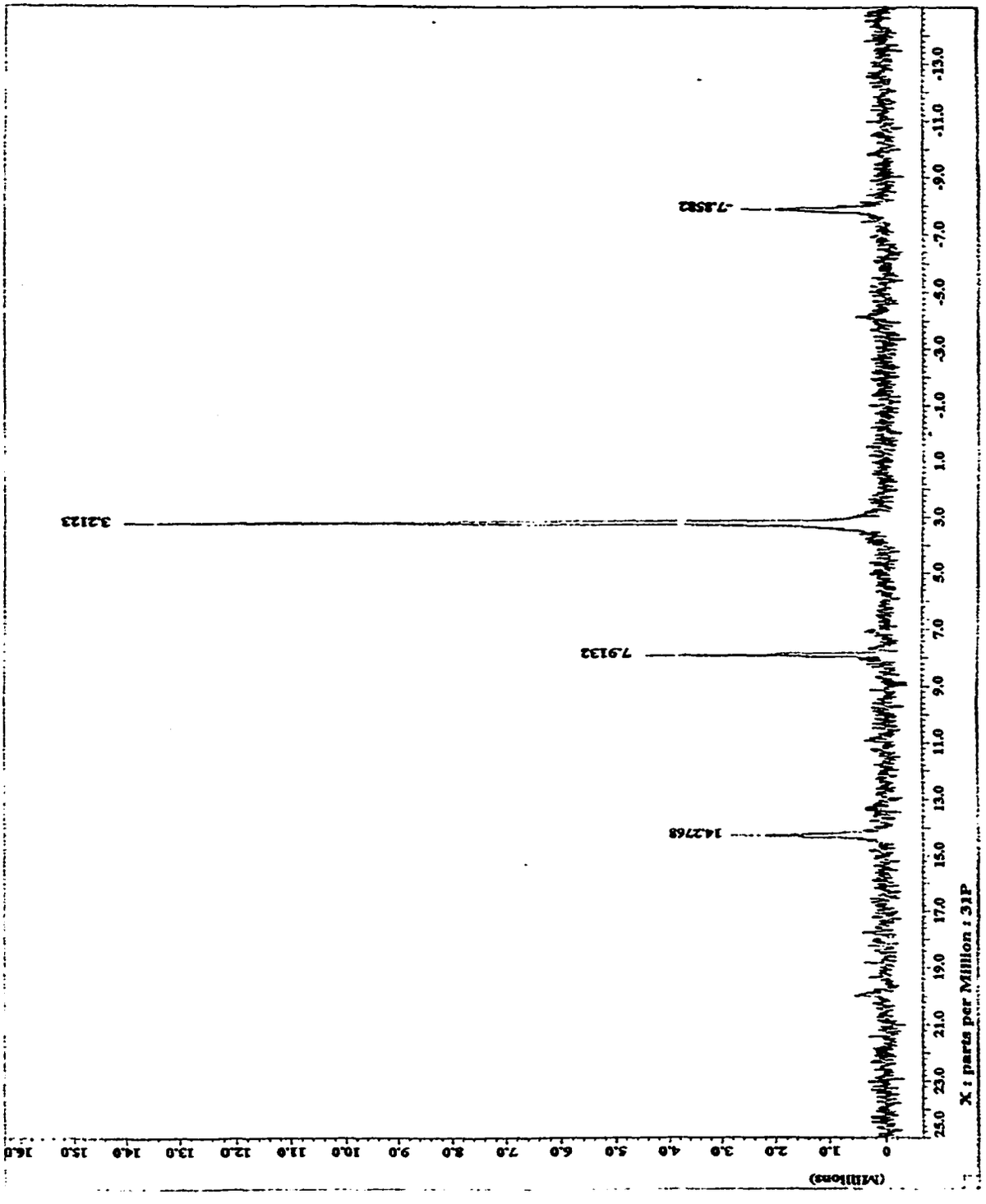

Figure D.8 ^{31}P-NMR spectra of Chloro-bridged-Pd complex with Pyridine 20%EtOH in CD_3CN.

Chapter 1: Introduction

1.1 F. Wohler, *Poggendorfs Ann. Physik*, **1828**, *12*, 253.

1.2 J.-M. Lehn, in *Supramolecular Chemistry: Concepts and Perspectives*, VHC, Weinheim, **1995.**

1.3 P. Ehrlich, in *Studies on Immunity*, Wiley, New York, **1906.**

1.4 E. Fischer, *Ber. Deutsch. Chem. Ges.*, **1894**, *27*, 2985.

1.5 A. Werner, *Zeitschr. Anorg. Chem.*, **1893**, *3*, 267.

1.6 a) M.M. Shemyakin, N.A. Aldanova, E.I. Vinogradova, and M. Y. Feigina, *Tetrahedron Lett.*, **1963**, 1921. b) Z. Stefanac, and W. Simon, *Microchem. J.*, **1967**, *12*, 125. c) Z. Stefanac, and W. Simon, *Chimia*, **1966**, *20*, 436.

1.7 a) C.J. Pedersen, *J. Am. Chem. Soc.*, **1967**, *89*, 7017. b) C.J. Pedersen, *Angew. Chem., Int. Ed. Engl.*, **1988**, *27*, 1053.

1.8 a) J.-M. Lehn, *Struct. Bonding*, **1973**, *16*, 1. b) B. Dietrich, J.-M. Lehn, and J.-P. Sauvage, *Tetrahedron Lett.*, **1969**, 2885. c) B. Dietrich, J.-M. Lehn, J.-P. Sauvage, and J. Blanzat, *Tetrahedron*, **1973**, *29*, 1629. d) B. Dietrich, J.-M. Lehn, and J.-P. Sauvage, *ibid.*, **1973**, *29*, 1647.

1.9 a) J.-M. Lehn, *Angew. Chem*, **1988**, *100*, 91. b) J.-M. Lehn, *Angew. Chem.*, **1990**, *102*, 1347.

1.10 a) *Non-linear Optical Properties of Organic Molecules and Crystals*, eds. D.S. Chemla, and J. Zyss, Academic Press, New York, Vol. 1, **1986** and Vol. 2, **1987**. b) D.J. Williams, *Angew. Chem.* **1984**, *96*, 637. c) A.M. Glass, *Science*, **1984**, *226*, 657. d) H.S. Nawla, *Adv. Mater.*, **1993**, 341.

1.11 a) J.-M. Lehn in *Non-linear Optical Properties of Organic Molecules and Crystals*, eds. D.S. Chemla, and J. Zyss, Academic Press, New York,Vol. 2, **1987**, 215.

1.12 C.-Y. Liu, H.L. Pan, M.A. Fox, and A.J. Bard, *Chem. Mater.*, **1997**, *9*, 1422.

1.13 N.A. Rakow, and K.S. Suslick, *Nature*, **2000**, *406*, 710.

1.14 Y. Shimizu, A. Ishikawa, and S. Kusabayashi, *Chem. Lett.*, **1986**, *7*, 1041.

1.15 a) H.S. Nalwa, in *Non Linear Optics of organic Molecular and polymeric Materials*, Eds: H.S. Nalwa, and S. Miyata, CRC Press: Boca Raton, FL, **1997**, pp. 89-350, 611-797. b) H.S. Nalwa, *Adv. Mater.*, **1993**, *5*, 341.

Chapter 2: *Individual Porphyrins*

2.1 a) E. Gross, Z. Malik, and B. Ehrenberg, *J. Membrane Biol.*, **1987**, *97*, 215. b) J. Moan, and T. Christensen, *Tumor Res.*, **1980**, *15*, 1. c) (review) D.P. Valenzeno, *J. Photochem. Photobiol. B: Biology*, **1987**, 147. d) J.C. Maziere, R. Santus, P. Morliere, J.-P. Reftmann, C. Candide, I. Mora, S. Salmon, C. Maziere, S. Gatt, and I. Dubertet, *J. Photochem. Photobiol., B: Biology*, **1990**, *6*, 61. e) J.T. Groves, and S.S. Marla, *J. Am. Chem. Soc.*, **1995**, *117*, 9578.

2.2 V.I. Yagodin, Y.K. Levental, A.I. Fragina, V.T. Kurnygina, V.T. Nikitina, *Klim. Drev.*, **1988**, *3*, 3.

2.3 a) C.M. Drain, and J.-M. Lehn, *J. Chem. Soc., Chem. Commun.*, **1994**, *19*, 2313. b) C.M. Drain, K.C. Rusell,, and J.-M. Lehn, *J. Chem. Soc., Chem. Com.*, **1996**, *3*, 337. c) R.C. Kwong, S. Sibley, T. Dubovoy, M. Baldo, S.R. Forrest, and M.E. Thompson, *Chem. Materials*, **1999**, *11*, 3709. d) C.V.K. Sharma, G.A. Broker, J.G. Huddleston, J.W. Baldwin, R.M. Metzger, and R.D. Rogers, *J. Am. Chem. Soc.*, **1999**, *121*, 1137. e) M.C.T. Fyfe, and J.F. Stoddart, *Acc. Chem. Res.*, **1997**, *30*, 393.

2.4 a) G. McDermott, S.M. Prince, A.A. Freer, A.M. Hawthornthwaite-Lawless, M.Z. Papiz, R.J.Cogdell, and N.W. Isaacs, *Nature*, **1995**, *374*, 517. b) A.M. Hawthornthwaite and R.J. Cogdell, in *The Chlorophylls*, ed. H. Scheer, CRC, Boca Raton, **1993**. c) A.T. Gardiner, R.J. Cogdell, and S. Takaichi, *Photosyn. Res.*, **1993**, *38*, 159. d) W. Kuhibrandt, D.N. Wang and Y. Fujiyoshi, *Nature*, **1994**, *367*, 614. e) A.T. Brunger, *Nature*, **1992**, 472.

2.5 a) (Review) T. Mlodnicka, *J. Mol. Catal.*, **1986**, 36, 205. b) L. Pauling, *Nature* (London), **1964**, 182. c) J.J. Weiss, *Nature* (London), **1964**, 183. d) M.M. Taqui Khan and A.E. Martell, in *Homogeneous Catalysis by Metal Complexes*, Academic Press, New York, **1974**. e) J. Sobczak and J.J. Ziolkowski, *J. Mol. Catal.*, **1981**, 11. f) L. Vaska, *Acc. Chem. Res.*, **1976**, *9*, 175. g) E. Ochiai, *J. Inorg. Nucl. Chem.*, **1973**, *35*, 3375.

2.6 G.L. Duveneck, K. Gulden, R.E. Kunz, and J. Sochtig, *PCT Int. Appl.*, WO 9808077, **1997**.

2.7 D. Dolphin, in *The Porphyrins*, Vol. I-VII, Academic Press, NY **1978**.

2.8 C.K. Chang, Proc. Natl. Acad. Sci. USA, **1981**, 2653.

2.9 K.M. Smith, in *Porphyrins and Metalloporphyrins*, Elsevier Scientific Publication, Amsterdam, **1975**.

2.10 H. Scheer, in *Chlorophylls*, CRC Press, Boca Raton, FL, **1991**. b) J. Deisenhofer, and H. Michel, *EMBO J.*, **1989**, *8*, 2149.

2.11 a) (review) R. Bonnett, *Chem. Soc. Rev.*, **1995**, *24*, 19. b) (review) T.J. Dougherty, *Photochem. Photobiol.*, **1987**, *46*, 569. c) (review) C.J. Byrne, L.V. Marshallsay, S.Y. Sek, and A.D. Ward, in *Photodynamic Therapy of Neoplastic Disease*, ed. D. Kessel, Vol.2 131-144, CRC Press, Boca Raton, **1990**. d) S. Bai, C. Liu, and Z. Guo, *Proc. SPIE*, **1993**, 1616, 275. e) C.S. Lok, A.J. MacRobert, J. Bedwell, J. Regula, N. Krasner, and S.G. Bown, *Br. J. Cancer*, **1993**, *68*, 41. f) R. Bonnett, R.J. Ridge, P.A. Scoulides, and M.C. Berenbaum, *J. Chem. Soc., Chem. Commun.*, **1980**, *24*, 1198. g) R. Bonnett, R.J. Ridge, P.A. Scoulides, and M.C. Berenbaum, *J. Chem. Soc., Perkins Trans 1*, **1981**, *12*, 3135.

2.12 a) A.D. Alder, F.R. Longo, and W. Shegalis, *J. Am. Chem. Soc.*, **1964**, 3145. b) A.D. Alder, F.R. Finarelli, J.Goldmacher, J. Assour, and L. Korasakoff, *J. Org. Chem.*, **1967**, *32*, 476.

2.13 a) J.S. Lindsey, I.C. Schreiman, H.C. Hsu, P.C. Kearney, and A.M. Marguerattaz, *J. Org. Chem.*, **1987**, *52*, 827. b) J.S. Lindsey, K.A. MacCrum, J.S. Tyhonas, and Y.-Y. Chuang, *J. Org. Chem.*, **1994**, *59*, 579.

2.14 Rothemund, *J. Ann. Chem. Soc.*, **1939**, 2912.

2.15 R.H. Ball, G.D. Dorough, and M. Calvin, *J. Am. Chem. Soc.*, **1946**, 2278.

2.16 a) G.P. Arsenault, E. Bullock, and S.F. MacDonald, *J. Am. Chem. Soc.*, **1960**, 4384. b) L.T. Nguyen, M.O. Senge, and K.M. Smith, *J. Org. Chem.*, **1996**, *61*, 998.

2.17 C.M. Drain, and X. Gong, *J. Chem. Soc., Chem. Commun.*, **1997**, *21*, 2117.

2.18 A. Treibs, and N. Haberle, Justus Liebigs Ann. Chem., **1968**, *718*, 183.

2.19 *The Porphyrin Handbook*, Eds. K.M. Kadish, K.M. Smith, R. Guilard, **2000.**

2.20 G.J. Medforth, in *The Porphyrin Handbook*, Eds. K.M. Kadish, K.M. Smith, R. Guilard, **2000**, Vol 5, Chapter 35, 4.

2.21 E.D Becker, in *High Resolution NMR*, Academic Press, Orlando, **1980**, 167.

2.22 C.B. Storm, T. Teklu, and E.A. Sokolski, *Ann. N.Y. Acad. Sci.*, **1973**, 206.

2.23 K.N. Solov'ev, V.A. Mashenkov, A.T. Gradyushko, A.E. Turkova, and U.P. Legina, *J. Appl. Spectrosc.*, **1970**, *14*, 1106.

2.24 M. Gouterman, G.H. Wagniere, and L.C. Snyder, *J. Mol. Spectroscopy*, **1963**, 108.

2.25 H. Budzikiewicz, in *The Porphyrins*, Vol. III, Edited by D. Dolphin, Academic Press, New York, **1978**, p395.

2.26 K.M. Smith, in *The Porphyrins and Metalloporphyrins*, Edited by H.E. Falk, Elsevier Scientific Publishing Co., Amsterdam, **1975**.

2.27 M. Gouterman, in *The Porphyrins*, Vol. III, Edited by D. Dolphin, Academic Press, New York, **1978**.

2.28 P.J. Spellane, M. Gouterman, A. Antipas, S. Kim, and Y.C. Lin, *Inorg. Chem.*, **1980**, *19*, 386.

2.29 P.G. Seybold, and M. Gouterman, *J. Mol. Spectrosc.*, **1969**, *31*, 1.

2.30 A.T. Gradyushko, and M.P. Tsvirko, *Opt. Spekrosc.*, **1971**, *31*, 548.

2.31 J.H. Brannon, and D. Magde, *J. Am. Chem. Soc.*, **1980**, *102*, 62.

2.32 A.T. Gradyushko, A.N. Sevchenko, K.N. Solovyov, and M.P. Tsvirko, *Photochem. Photobiol.*, **1970**, *11*, 387.

2.33 K.M. Smith, in *Laboratory Methods in Porphyrin and Metalloporphyrin Research*, Elsevier, New York, **1975**, 42.

Chapter 3: *Formation and Characterization of Multiporphyrin Arrays*

3.1 For recent review: a) M.R. Wasielewski, *Chem. Rev.*, **1992**, *92*, 435. b) D. Gust, T.A. Moore, and A.L. Moore, *Acc. Chem. Res.*, **1993**, *26*, 198. c) H. Kurreck, and M. Huber, *Angew. Chem., Int. Ed. Engl.*, **1995**, 849. d) A. Harriman, and J.-P. Sauvage, *Chem. Soc. Rev.*, **1996**, *34*, 41.

3.2 For recent review a) H. Imahori, and Y. Sakata, *Adv. Mater.*, **1997**, *9*, 537. b) D. Gust, T.A. Moore, and A.L. Moore, *Res. Chem. Intermed.*, **1997**, *23*, 621. c) A.P. de Silva, H.Q.N. Gunaratne, T. Gunnlaugsson, A.J.M. Huxley, C.P. McCoy, J.T. Rademacher, and T.E. Rice, *Chem. Rev.*, **1997**, *97*, 1515.

3.3 a) R.W. Wagner, T.E. Johnson, and J.S. Lindsey, *J. Am. Chem. Soc.*, **1996**, *118*, 11166. b) F. Li, S. Gentermann, W.A. Kalsbeck, J. Seth, J.S. Lindsey, D. Holten, and D.F. Bocian, *J. Mater. Chem.* **1997**, 7, 1245.

3.4 a) J.L. Sessler, B. Wang, and A. Harriman, *J. Am. Chem. Soc.*, **1993**, *115*, 10418. b) J.L. Sessler, B. Wang, and A. Harriman, *J. Am. Chem. Soc.*, **1995**, *117*, 704. c)

T. Arimura, C.T. Brown, S.L. Springs, and J.L. Sessler, *Chem. Soc., Chem. Commun.*, **1996**, *19*, 2293. d) C.A. Hunter, and R.K. Hyde, *Angew Chem., Int. Ed. Engl.*, **1996**, *35*, 1936. e) C.A. Hunter, and R.J. Shannon, *Chem. Soc., Chem. Commun.*, **1996**, *11*, 1361.

3.5 a) J.-S. Hsiao, B.P. Kreuger, R. W. Wagner, T. E. Johnson, J. K. Delaney, D. C. Mauzerall, G. R. Fleming, J. S. Lindsey, D. F. Bocian, and R. J. Donohoe, *J. Am. Chem. Soc.*, **1996**, *118*, 11181. b) A. M. Brun, A. Harriman, V. Heitz, and J.-P. Sauvage, *J. Am. Chem. Soc.*, **1991**, *113*, 8657. c) J.-P. Collin, A. Harriman, V. Heitz, F. Obodel, and J.-P. Sauvage, *J. Am. Chem. Soc.*, **1994**, *116*, 5679. d) A. Harriman, F. Odobel, and J.-P. Sauvage, *J. Am. Chem. Soc.*, **1995**, *117*, 9461. e) L. Flamigni, N. Armoroli, F. Bariegelletti, V. Balzani, J.-P. Collin, J.-P. Dalbavie, V. Heitz, and J._P. Sauvage, *J. Phys. Chem, B*, **1997**, 5936.

3.6 a) M.R. Wasielewski, *Chem. Rev.*, **1992**, *92*, 435. b) D. Gust; T.A. Moore, and A.L. Moore, *Acc. Chem. Res.*, **1993**, *26*, 198. c) A. Harriman, and J.-P. Sauvage, *Chem. Soc. Rev.*, **1996**, *25*, 41. d) P.G. Van Patten, A.P. Shreve, J.S. Lindsey, and R.J. Donohoe, *J. Phys. Chem.,:B*, **1998**, *101*, 4209.

3.7 D. Gosztola, M.P. Niemczyk, and M.R. Wasielewski, *J. Am. Chem. Soc.*, **1998**, *120*, 5118.

3.8 R.W. Wagner, J. S. Lindsey, J. Seth, V. Palaniappan, and F. Bocian, *J. Am. Chem. Soc.*, **1996**, *118*, 3996.

3.9 A.P. De Selva, H.Q.N. Gunaratne, T. Gunnlaugsson, A.J.M. Huxley; C.P. McCoy, J.T. Rademacher, and T.E. Rice, *Chem. Rev.*, **1997**, *97*, 1515 and references therein.

3.10 R.W. Wagner, and J.S. Lindsey, *J. Am. Chem. Soc.*, **1994**, *116*, 9759.

3.11 a) C. Sousa, C. Maziere, and J.C. Maziere, *Cancer Lett.*, **1998**, *128*, 177. b) W.J.A. deVree, M.C. Essers, and W. Sluiter, *Cancer Res.*, **1997**, *57*, 2555. c) A. Jasat, and D. Dolphin, *Chem. Rev.*, **1997**, *97*, 2267.

3.12 a) P.N. Taylor, A.P. Wylie, J. Huuskonen, and H.L. Anderson, *Angew. Chem., Int. Ed. Engl.*, *1998*, *37*, 986. b) N. Nishino, R.W. Wagner, and J.S. Lindsey, *Org. Chem.*, **1996**, *61*, 7534. c) R.W. Wagner, T.E. Johnson, and J.S. Lindsey, *J. Am. Chem. Soc.*, **1996**, *118*, 1166. d) A. Osuka, N. Tanabe, R.P. Zhang, and K. Maruyama, *Chem. Lett.*, **1993**, *9*, 1505. e) D. Hammel, P. Erk, B. Schuler, J. Heinze, and K. Müllen, *Adv. Mater.*, **1992**, 737.

3.13 a) A. Vidal-Ferran, Z. Clyde-Watson, N. Bampos, and J.K.M. Sanders, *J. Org. Chem.*, **1997**, *62*, 240. b) S. Anderson, H.L. Anderson, and J.K.M. Sanders, *J. Chem. Soc., Perkin Trans. 1*, **1995**, 2255.

3.14 a) C.M. Drain, and J.-M. Lehn, *Chem. Soc., Chem. Commun.*, **1994**, 2313. b) R.W. Wagner, J. Seth, S.I. Yang, D. Kim, D.F. Bocian, D. Holten, and J.S. Lindsey, *J. Org. Chem.*, **1998**, *63*, 5042. c) R.V. Slone, and J.T. Hupp, *Inorg.* Chem., **1997**, *36*, 5422.

3.15 C.M. Drain, F. Nifiatis, A. Vasenko, and J.D. Batteas, *Angew. Chem., Int. Ed. Engl.*, **1998**, *37*, 2344.

3.16 H. Yuan, L. Thomas, and L.K. Woo, *Inorg. Chem.*, **1996**, *35*, 2808.

3.17 M. Fujita, F. Ibukuro, K. Yamaguchi, and K. Ogura, *J. Am. Chem. Soc.*, **1995**, *117*, 4175.

3.18 P.J. Stang, J. Fan, and B. Olenyuk, *J. Chem. Soc., Chem. Commun.*, **1997**, 1453.

3.19 J. March, in *Advanced Organic Chemistry*, **1992**, 4rth Edition, A Wiley-Intersciense Publication.

3.20 C.E. Dykstra, *Acc. Chem. Res.*, **1998**, 355.

3.21 M. Craven, Trans. Am. Crystallogr. Assoc., **1988**, 71.

3.22 G.M. Whitesides, E.E. Simanek, J.P. Mathias, C.T. Seto, M. Mammen, and D.M. Gordon, *Acc. Chem. Res.*, **1995**, *28*, 37.

3.23 J.-M. Lehn, *Angew. Chem., Int. ed. Engl.*, **1990**, *29*, 1304. b) M.C. Etter, *Acc. Chem. Res.*, **1990**, 120.

3.24 C.T. Fyte, and J.F. Stoddard, *Acc. Chem. Res.*, **1997**, 393. b) C.M. Paleos, and D. Tsiourvas, *Angew. Chem. Int. ed. Engl.*, **1995**, *34*, 1839.

3.25 a) T.J. Murray, and S.C. Zimmerman, *J. Am. Chem. Soc.*, **1992**, *114*, 4010. b) F.H. Beijer, R.P. Sijbesma, J.A.J.M. Vekemans, E.W. Meijer, H. Kooijman, and A.L. Spek, *J. Org. Chem.*, **1996**, *61*, 6371.

3.26 X. Sun, G.P. Lovenzi, *Helv. Chim. Acta*, **1994**, *77*, 1520.

3.27 X.Shi, and C.M. Drain, *J. Org. Chem.*, **2000**, submitted.

3.28 a) C.M. Drain, X. Shi, T. Milic, and F. Nifiatis, *J. Chem. Soc., Chem. Commun.*, **2001**, 287. b) C.M. Drain, X. Shi, F. Nifiatis, and T. Milic, in preparation.

3.29 a) (Review) L. Fielding, *Tetrahedron*, **2000**, *56*, 6151. b) W.F. DeGrado, and J.D. Lear, *J. Am. Chem. Soc.*, **1985**, *107*, 7684. c) D.A. Deranleau, *J. Am. Chem. Soc.*, **1969**, *91*, 404. d) B.J. Whitlock, and H.W. Whitlock, *J. Am. Chem. Soc.*, **1990**, *112*, 3910.

Chapter 4: *Photophysical Properties of Multiporphyrin Arrays*

4.1 a) A. Harriman, and J.P. Sauvage, Chem. Soc. Rev., **1996**, *25*, 41. b) A. Harriman, and R. Ziessel, *J. Chem. Soc., Chem. Com.*, **1996**, 1707. c) C. Turro, C.K. Chang, G.E. Leroi, R.I. Cukier, D.G. Nocera, *J. Am. Chem. Soc.*, **1992**, *114*, 4013. d) A. Berman, E.S. Izraeli, H. Levanon, B. Wang, and J.L. Sessler, *J. Am. Chem. Soc.*, **1995**, *117*, 8252.

4.2 a) L.O. Bjorm, and J.F. Allen, *Nature*, **1995**, 25. b) S. Borman, *C&E News*, **1998**, 14.

4.3 a) F. Fungo, L.A. Otero, L. Sereno, J.J. Silber, and E.N. Durantin. *J. Mater. Chem.*, **2000**, *10*, 645. b) L.R. Milgrom, *J. Chem. Soc., Perkin Trans. 1*, **1984**, 1483.

4.4 a) M. Linke, J.-C. Chambron, V. Heitz, J.-P. Sauvage, *J. Am. Chem. Soc.*, **1997**, *119*, 11329. b) P.R. Ashton, V. Balzani, O. Kocian, L. Prodi, N. Spencer, and J.F. Stoddart, *J. Am. Chem. Soc.*, **1998**, *120*, 11190.

4.5 V. Balzani and F. Scandola, *Supramolecular Photochemistry*, Eliis Horwood, London, **1991**.

4.6 a) H Kuhn, and H.-D. Forsterling, in *Principles of Physical Chemistry*, **2000**, ed. John Wiley & Sons inc. b) K.N. Solovey, M.P. Tsvirko, A.T. Gradyushko, D.T. Kozhich, *Opt. Spektrosk.*, **1971**, 871.

4.7 a) J. Chatt, and L.M. Venanzi, *Inorg. Chem.*, **1951**, 2351. b) R.J. Goodfellow, and L.M. Venanzi, *Inorg. Chem.*, **1965**, 7533. c) G. Annibale, M. Bonivento, L. Canovese, L. Cattalini, G. Michelon, and M.L. Tobe, *Inorg. Chem.*, **1985**, *24*, 797.

Appendix

A.1 M. Gouterman, in the *Porphyrins*, Ed. D. Dolpin, Academic Press: New York, **1979**, Vol III p 1-165.

A.2 H.N. Fonda, J.V. Gilbert, R.A. Cormier, J.R. Sprague, K. kamioka, and J.S. Connoly, *J. Phys. Chem.*, **1993**, *97*, 7024.

A.3 a) M. Gouterman, *J. Mol. Spectr.*, **1961**, 138. b) M. Gouterman, *J. Chem. Phys.*, **1959**, *30*, 1139. c) M. Gouterman, G.H. Wagniere, and L.C. Snyder, *J. Mol. Spectr.*, **1963**, 108.

D.1 G. Annibale, M. Bonivento, L. Canovese, L. Cattalini, G. Michelon, and M.L. Tobe, *Inorg. Chem.*, **1985**, *24*, 797.

D.2 H.C. Clark, G. Ferguson, V.K. Jain, and M. Parvez, *Inorg. Chem.*, **1985**, *24*, 1477.

D.3 A. Pidcock, R.E. Richards, and L.M. Venanzi, *J. Chem. Soc. A*, **1966**, 1707.